CHEMICAL REVIEWS

pubs.acs.org/CR Review

Ionic Liquids for the Separation of Fluorocarbon Refrigerant Mixtures

Published as part of Chemical Reviews virtual special issue "Ionic Liquids for Diverse Applications".

Kalin R. Baca, Karim Al-Barghouti, Ning Wang, Madelyn G. Bennett, Lucia Matamoros Valenciano, Tessie L. May, Irene V. Xu, Max Cordry, Dorothy M. Haggard, Abigail G. Haas, Ashley Heimann, Abby N. Harders, Hannah G. Uhl, Diego T. Melfi, Andrew D. Yancey, Rajkumar Kore, Edward J. Maginn, Aaron M. Scurto, and Mark B. Shiflett*

Cite This: https://doi.org/10.1021/acs.chemrev.3c00276 Read Online

ACCESS | Metrics & More | Article Recommendations | Supporting Information

ABSTRACT: This review discusses the research being performed on ionic liquids for the separation of fluorocarbon refrigerant mixtures. Fluorocarbon refrigerants, invented in 1928 by Thomas Midgley Jr., are a unique class of working fluids that are used in a variety of applications including refrigeration. Fluorocarbon refrigerants can be categorized into four generations: chlorofluorocarbons, hydrochlorofluorocarbons, hydrofluorocarbons, and hydrofluoroolefins. Each generation of refrigerants solved a key problem from the previous generation; however, each new generation has relied on more complex mixtures that are often zeotropic, near azeotropic, or azeotropic. The complexity of the refrigerants used and the fact that many refrigerants form azeotropes when mixed makes handling the refrigerants at end of life extremely difficult. Today, less than 3% of refrigerants that enter the market are recycled. This is due to a lack of technology in the refrigerant reclaim market that would allow for these complex, azeotropic refrigerant mixtures to be separated into their components in order to be effectively reused, recycled, and if needed repurposed. As the market for recovering and reclaiming refrigerants continues to grow, there is a strong need for separation technology. Ionic liquids show promise for separating azeotropic refrigerant mixtures as an entrainer in extractive distillation process. Ionic liquids have been investigated with refrigerants for this application since the early 2000s. This review will provide a comprehensive summary of the physical property measurements, equations of state modeling, molecular simulations, separation techniques, and unique materials unitizing ionic liquids for the development of an ionic-liquid-based separation process for azeotropic refrigerant mixtures.

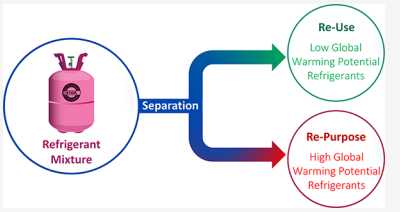

CONTENTS

Received: April 26, 2023
Revised: January 28, 2024
Accepted: February 13, 2024

1. INTRODUCTION

1.1. Refrigerant History

Refrigeration technology is imperative to everyday life, with current uses including transportation, building comfort, manufacturing processes, commercial cooling, and food and vaccine storage. Historically, temperature control technologies were used as early as 1200 BC. These early technologies were the basis for the research that led to the invention of modern refrigeration. The first cooling processes were reliant on ice and evaporative processes. In 1805, Oliver Evans first pitched the idea of a volatile fluid in a closed cycle.[1] In 1834, Jacob Perkins designed and patented a mechanical refrigeration machine with a vapor-compression cycle for water known as the Perkins Cycle.[2] This achievement marked the fundamental use of refrigerants as known today.[3] In 1860, Ferdinand Carré patented water−ammonia absorption refrigeration as one of the first artificial refrigeration systems.[2] However, these first refrigerants were volatile fluids including methyl formate ($C_2O_2H_4$), ammonia (NH_3), sulfur dioxide (SO_2), and methyl chloride (CH_3Cl). These refrigerants are flammable, toxic, or highly reactive, all major concerns that prompted the search for a safer refrigerant.

In 1920, Willis H. Carrier and R. W. Waterfill suggested dichloroethylene (R-1130(E), HCO-1130(E)) be the next refrigerant to be used in a cooling system.[4] This kickstarted the first generation of chlorocarbon (CC) refrigerants used on a commercial scale and the shift toward safer refrigerants.[5] In 1928, Thomas Midgley Jr. synthesized the first chlorofluorocarbon (CFC) refrigerant at the General Motors Research Lab with Albert Henne and Robert McNary.[2] Refrigerant R-12 (CFC-12, CF_2Cl_2), a CFC, became the first non-flammable, non-toxic refrigerant. In 1931, R-12 began to be commercially produced, followed by R-11 (CFC-11, $CFCl_3$) in 1932. CFCs became a staple in air conditioners, refrigerators, and other practical industrial and household applications because of low flammability and toxicity.[4]

The next major shift happened after the Vienna Convention for the Protection of the Ozone Layer in 1985. The convention brought awareness to ozone-depleting hazards and set a framework of protection into action. CFCs were linked to ozone depletion and were phased out of production with the Montreal Protocol in 1987.[6,7] Hydrochlorofluorocarbons (HCFCs), the second generation of fluorocarbon (FC) refrigerants, were used in the phase down of high ozone depletion potential (ODP) refrigerants because the lower amount of chlorine present in HCFCs compared to CFCs reduced the ODP compared to CFCs. In 1990, the Clean Air Act accepted the Significant New Alternatives Policy (SNAP) amendment to further monitor the phase out process of high ODP chemicals. Hydrofluorocarbons (HFCs), notable for having zero ODP, took the place of CFCs and HCFCs becoming the third generation of FC refrigerants. HFCs have properties comparable to CFCs such as low boiling point and high latent enthalpy of vaporization, while also having zero ODP. This was made possible by the mixing of different HFCs to get the right set of physical properties needed to effectively replace the CFCs and HCFCs.

Due to the high global warming potential (GWP) of HFCs, up to 12,400 times more GWP than CO_2 equivalence,[8] the Kigali Amendment to the Montreal Protocol Act in 2016 was enacted.[9] This legislation calls for the phase out of HFCs in favor of the next generation of refrigerants, hydrofluoroolefins (HFOs), which have zero ODP and much lower GWP. In 2020, the United States passed the American Innovation and Manufacturing (AIM) Act, which required the production and consumption of HFCs to decrease by at least 85% (in terms of million metric tons of CO_2 equivalent) before 2036.[10] In addition, legislation from the California Air Resources Board (CARB) and the European Parliament has been passed concerning HFC regulation.[4,11,12]

Since the first large scale commercial use of CFC refrigerants in the 1930s, refrigerant usage has increased rapidly. Today it is estimated that there are 850 million kilograms of refrigerant used in cooling applications.[13] This amount will only continue to increase due to global development and global temperature rise.[14] Besides increasing usage, the complexity of the refrigerants used also continues to increase with each transition to a new generation of refrigerants. CFC and HCFC refrigerants are simple, one-component refrigerants, the majority of HFC refrigerants are two- to three-component mixtures, and HFO refrigerants can be as many as four- to six-component mixtures. ASHRAE has designations for 94 unique zeotropic/azeotropic refrigerant blends and a total of 149 recognized zeotropic/azeotropic refrigerant blends including different compositions of the same mixture.[15] The complete list of approved refrigerant designations can be found in the latest ASHRAE Standard 34.[15] This large number of mixtures makes handling these refrigerants, especially at end of life, difficult. Figure 1 summarizes the key refrigerant generations and legislation seen since the 1830s, and Table 1 shows the prefix, atoms, and double bonds present for common refrigerant fluorocarbons.

https://doi.org/10.1021/acs.chemrev.3c00276
Chem. Rev. XXXX, XXX, XXX−XXX

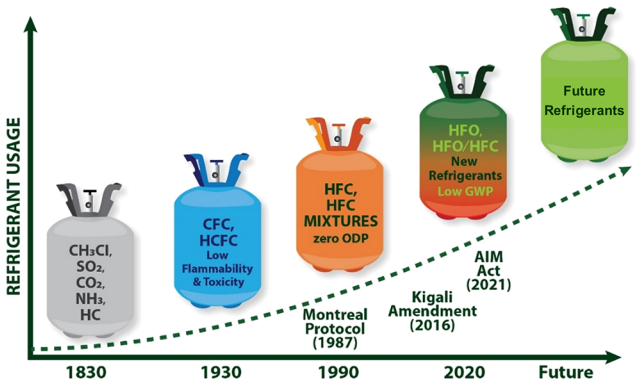

Figure 1. Visual representation of the transition of each refrigerant generation and the key legislation that was supporting the transition.

Table 1. Refrigerant Substances, the Prefixes Used, and the Atoms and Bonds Found in These Molecules[15]

Substance	Prefix	Atoms and Double Bonds
chlorofluorocarbon	CFC	Cl, F, C
hydrochlorofluorocarbon	HCFC	H, Cl, F, C
hydrofluorocarbon	HFC	H, F, C
hydrofluoroolefin	HFO	H, F, C, C═C
hydrochlorofluoroolefin	HCFO	H, Cl, F, C, C═C

For more information, Sicard and Baker give a detailed review of each FC refrigerant generation and syntheses used.[5]

1.2. Refrigerant Naming

A standardized nomenclature for fluorocarbons was created by DuPont and then implemented by the American Society of Heating, Refrigerating, and Air-Conditioning Engineers (ASHRAE). The refrigerants are named with an "R" and followed by a number assigned by ASHRAE.[16] The series numbers for different group designations are shown in Table 2. The R

Table 2. Series Designations for Commercial Refrigerant Naming[15]

Series	Group Designation
000	Methane-based compounds
100	Ethane-based compounds
200	Propane-based compounds
300	Cyclic organic compounds
400	Zeotropic mixtures
500	Azeotropic mixtures
600	Organic compounds
700	Inorganic compounds
1000	Unsaturated organic compounds

represents the type of fluorocarbon, which for the purposes of this review article are chlorofluorocarbons (CFCs), hydrochlorofluorocarbons (HCFCs), perfluorocarbons (PFCs), hydrofluorocarbons (HFCs), hydrochlorofluoroolefins (HCFOs), and hydrofluoroolefins (HFOs). The assigned number after the fluorocarbon code follows the "Plus 90 Rule", shown in Figure 2, where 90 is added to the number of the refrigerant, except if it is in the 400 or 500 series which define mixtures. The result of this addition is either a three- or four-digit number that should be read from left to right: (1) the first digit represents the number of double bonds, if any; (2) the second digit represents the number of carbon atoms; (3) the

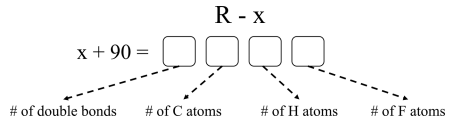

Figure 2. Visualization of the "Plus 90 Rule".

third digit represents the number of hydrogen atoms; and (4) the fourth digit represents the number of fluorine atoms. Any remaining bonds to the carbon are satisfied with the addition of chlorine. For example, for the refrigerant HCFC-22, 22 + 90 = 112, which means that there are no double bonds, and the molecule is composed of 1 carbon, 1 hydrogen, 2 fluorine, and 1 chlorine.

Refrigerant mixtures are assigned to the 400 and 500 level refrigerants, with the 400s being ordinary and zeotropic refrigerants and the 500s being azeotropic mixtures. ASHRAE defines zeotropic refrigerants as a two-or-more-component refrigerant mixture that has different compositions in the equilibrium vapor and liquid phase.[17] Azeotropic refrigerants are defined as two-or-more-component refrigerant mixtures that have the same compositions in the equilibrium vapor and liquid phase at a given pressure.[17] The numbers for the mixtures are assigned based on the order each were commercialized, and any capital letters (e.g., R-410A) define the mixture compositions. Lowercase letters after the number represent the next most symmetric isomer after the base version of the naming (e.g., HFC-134a vs HFC-134). If there is a bromine or iodine atom instead of a chlorine atom a B/I notation is used at the end of the name (e.g., CFC-13 vs CFC-13B1). Yancey et al. and Sicard et al. give a detailed breakdown of refrigerant naming,[5,18] and additional information about refrigerant nomenclature can be found in the ASHRAE handbook.[16]

1.3. Refrigerant Recycling

Considering that commonly used HFC refrigerants often have high global warming potentials and global legislation calls for the phase out of HFC production, recycling, and reusing these refrigerants is becoming increasingly important.[19] Currently, recycling HFC refrigerants in industry involves recovering and purifying refrigerants to AHRI 700 purity standards needed for refrigerant resale and reuse in refrigeration systems.[20] Typical impurities in recovered refrigerants include water, non-absorbable gases (NAG), and lubricants. Today these non-refrigerant impurities can be removed using traditional methods. For example, NAG (i.e., air) can be removed using a purge system, lubricants using a single plate flash unit, and water using molecular sieves. This means that, as long as the refrigerant mixture has remained in spec or is a single-component refrigerant and only has standard non-refrigerant contaminants, reclaimers are able to recycle that refrigerant back into the market. However, a majority of the refrigerants used today are azeotropic mixtures that are often mixed together at end of life meaning an increasing amount of the refrigerants recovered are unable to be separated and recycled by reclaimers today. Figure 3 shows the breakdown of refrigerants that are recyclable and non-recyclable today.

Because of this, even in countries managing refrigerant recycling well, such as Japan, the recycle rate is only 30% and shows little growth.[20] In order to truly recycle and reuse refrigerants, the individual components of a mixture must be separated using advanced separation technologies.[21] For example, the separation of refrigerant R-410A, which is a mixture of 50 wt % HFC-32 (difluoromethane, CH_2F_2) and 50

https://doi.org/10.1021/acs.chemrev.3c00276
Chem. Rev. XXXX, XXX, XXX−XXX

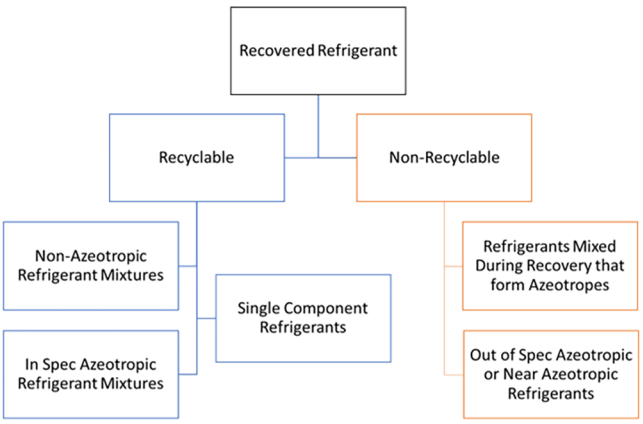

Figure 3. Breakdown of recyclable and non-recyclable refrigerants.

wt % HFC-125 (pentafluoroethane, CHF_2CF_3), would allow for (1) the HFC-32 to be blended into new HFO refrigerants such as R-454B (31.1 wt % HFO-1234yf ($CH_2{=}CFCF_3$) and 68.9 wt % HFC-32) and (2) the HFC-125 to be repurposed as a high-value, fluorinated feedstock for production of new low-GWP materials. Due to the near azeotropic nature of this mixture, the separation of R-410A cannot be achieved today using conventional methods such as fractional distillation.

This is true for any azeotropic refrigerant mixture whether it was designed as azeotropic or if it was mixed at end of life becoming azeotropic. Azeotropes can form between many common refrigerants including fluorocarbons, hydrocarbons, dimethyl ether, ammonia, etc. ASHRAE reports 20 azeotropic refrigerant mixtures with ASHRAE designations, but there are significantly more azeotropes that can be formed between the various combinations of refrigerants. Zhao et al. reports 42 binary mixtures of common refrigerants that form azeotropes using peng-robinson equation of state predictions.[22] Table 3 shows a visualization of all the azeotropes formed and the mole percent compositions. There are also a significant number of mixtures that are zeotropic or show near azeotropic behavior. Because of the large number of azeotropic mixtures, there is a significant amount of refrigerant that is unable to be effectively recycled today. Furthermore, traditional incineration processes consume large amounts of energy and can lead to hazardous emissions if not carefully monitored and the cost of disposal will lead to illegal venting and hazardous emissions to the environment. Separation processes that allow for the separation of complex refrigerant mixtures are in urgent need to recycle high GWP components and realize both environmental and economic benefits.

1.4. Ionic Liquids for Separating Fluorocarbons

Ionic liquids (ILs) are salts with melting temperatures below 100 °C, composed of an organic cation and an organic or inorganic anion. ILs are named using the cation and anion of the specific IL where the cation is stated first followed by the anion. Because ILs often have long names, abbreviations are commonly used in written work. For example, 1-hexyl-3-methylimidazolium chloride is often abbreviated as [hmim][Cl] or [C_6C_1im][Cl]. The abbreviations used throughout this work are structural-based (e.g., [C_6C_1im][Cl]) and are all defined in the Supporting Information.

There are nearly infinite possible combinations of cations and anions,[23] making ILs highly optimizable depending on the

Table 3. Azeotropes Formed by Common Refrigerants and the Mole Percent Compositions[15,22]

	HC-270	HC-290	HC-600	HC-600a	HC-1270	CFC-12	CFC-13	CFC-114	CFC-115	CFC-116	HCFC-22	HFC-32	HFC-125	HFC-134	HFC-134a	HFC-152a	HFC-227ea	HFO-1234ze(E)	R-717	R-1130(E)
HC-290																				
HC-600																				
HC-600a																				
HC-1270																				
CFC-12																				
CFC-13																				
CFC-114																				
CFC-115																				
CFC-116																				
HCFC-22						(0.808,0.192)			(0.63,0.37)											
HCFC-31						(0.332,0.668)		(0.754,0.246)												
HFC-23							(0.50,0.50)													
HFC-32		(0.64,0.36)	(0.95,0.05)	(0.88,0.22)					(0.734,0.266)	(0.558,0.442) (0.627,0.373)										
HFC-125	(0.76,0.24)	(0.80,0.20)		(0.90,0.10)	(0.535,0.465)							(0.302,0.698)								
HFC-134		(0.30,0.70)		(0.60,0.40)																
HFC-134a	(0.40,0.60)	(0.35,0.65)	(0.79,0.21)	(0.76,0.24)	(0.20,0.80)															
HFC-143a		(0.60,0.40)											(0.70,0.30) (0.588,0.412)							
HFC-152a		(0.27,0.73)	(0.83,0.17)	(0.76,0.24)	(0.20,0.80)	(0.394,0.606)								(0.15,0.85)	(0.967,0.033)					
HFC-227ea		(0.17,0.83)	(0.68,0.32)																	
HFC-245fa				(0.20,0.80)																
HFC-236ea		(0.08,0.92)																		
HFC-236fa		(0.10,0.90)		(0.40,0.60)																
HFO-1234yf		(0.36,0.64)		(0.84,0.16)										(0.532,0.468) (0.558,0.442)	(0.50,0.50)					
HFO-1234ze(E)		(0.15,0.85)		(0.63,0.37)										(0.37,0.63)			(0.916,0.084) (0.939,0.061)			
HFO-1336mzz(Z)																				(0.636,0.364)
CFC-13I1														(0.52,0.48)		(0.39,0.61)		(0.565,0.435)		
RE-170		(0.048,0.952)		(0.90,0.10)											(0.60,0.40)		(0.40,0.60)			
R-218											(0.369,0.631)									
R-717															(0.77,0.23)	(0.77,0.23)				
1-Butene																			(0.185,0.815)	

Positive azeotropes
Negative azeotropes
Series 500 Refrigerants
Composition: (left column, top row)

Commercially Mixed Refrigerant
HFC-32(0.381) + HFC-125(0.18) + HFC-134a(0.439)
HFC-125(0.358) + HFC-134a(0.038) + HFC-143a(0.604)
HFC-134a(0.085) + HFC-152a(0.217) + HFO-1234yf (0.697)

Ternary Saddle-Point Azeotropic
HFC-32 (0.925) + HFC-125(0.038) + HFC-143a(0.037)
HC-600a(0.337)+ HFC-134(0.188) + HFC-152a(0.475)
HFC-134a(0.033)+ RE-170(0.837) + HC600a(0.130)
HFC-152a(0.057) + HFC-134(0.577) + HFO-1234zeE(0.366)
CF3I(0.453) + HFC-134(0.073) + HFC-152a(0.474)
RE-170(0.036) + HFC-236fa(0.356) + HC600a(0.608)

Ternary Maximum-Point Azeotrope
CF3I(0.289) + HC-600a(0.222) + HFO-1234zeE(0.489)
R-717 (0.715) + HFC-134a(0.137) + HFC-152a(0.148)
R-717(0.818) + HC-600(0.139) + HFC-152a(0.043)
R-717(0.704) + HC-600(0.068) + HFC-125(0.228)

https://doi.org/10.1021/acs.chemrev.3c00276
Chem. Rev. XXXX, XXX, XXX−XXX

Table 4. Structure, Formula, Molecular Weight, Melting Point, Viscosity, and Density of Several ILs

Ionic Liquid	Formula	MW ($g \cdot mol^{-1}$)	Melting Point (K)	Density ($kg \cdot m^{-3}$)	Viscosity (Pa·s)
$[C_6C_1im][Cl]$	$C_{10}H_{19}ClN_2$	202.72	<RT[27]	1039.7 ± 2.7[28]	18.1 ± 2.4[28]
$[C_6C_1im][Br]$	$C_{10}H_{19}BrN_2$	247.18	<RT	1228.17 ± 0.69[29]	3.6 ± 0.8[30]
$[P_{6,6,6,14}][Cl]$	$C_{32}H_{68}ClP$	519.32	<RT	892.80 ± 6.2[31]	1.68 ± 0.25[31]
$[C_4C_1im][PF_6]$	$C_8H_{15}PF_6N_2$	284.19	265.15[32]	1367.6 ± 2.9[33]	0.274 ± 0.021[34]
$[C_2C_1im][Tf_2N]$	$C_8H_{11}F_6N_3O_4S_2$	391.31	270.15[35]	1519.1 ± 0.7[36]	0.033 ± 0.0017[37]

operational parameters. Properties that can be modified by changing the cation, anion, or alkyl chain length include solubility, melting points, thermal and electrical conductivity, and stability.[24] Additionally, many ILs demonstrate negligible vapor pressure, making them ideal solvents for a variety of processes. Detailed reviews of ILs, syntheses, and properties can be found in the literature, including those by Welton.[25,26] Table 4 shows the molecular weight, melting point, viscosity, and density of several ILs for some insight into the variation seen in physical properties with the variation of the cation and anion.

Particularly for use with gas absorption processes, IL properties such as the alkyl chain length, free volume, and intermolecular attractions can be modified to optimize an absorption process by varying the solubility of FC refrigerants. Despite ILs being studied for over a century,[38] the thermophysical properties of many ILs remain unexplored. With only two decades of research focused on ILs with FC there is also a significant need for more research regarding the thermophysical properties of IL−FC refrigerant systems. Gathering the data essential for process design is a large undertaking, and the literature within the field has only scratched the surface.

ILs have been proposed to serve as the entrainer in the separation processes as well as working pairs with refrigerants in absorption refrigeration technology. Understanding the thermophysical, dynamic, and structural properties of refrigerant/IL mixtures can help better design ILs to pair with and separate refrigerant mixtures. This review will discuss the research being performed to understand phase equilibria, thermodynamic properties, transport properties, and interactions between ILs and FC refrigerants including experimental measurements, modeling, and molecular simulations. This is essential information for accurately designing and building separation processes that can be commercialized and used in the refrigerant industry. Finally, the review will discuss the current efforts for designing and building an extractive distillation process that utilizes ILs as the entrainer. A complete nomenclature list of the ILs and refrigerants discussed in this work can be found in the Supporting Information.

2. PHASE EQUILIBRIUM

2.1. Vapor−Liquid Equilibrium

Vapor−liquid equilibrium (VLE) data is essential in the design process of many systems involving ILs and refrigerant gases. VLE data, coupled with other property data for the systems, is used to model the molecular interactions between ILs and refrigerant gases.[39] These models are essential to building simulations of an effective refrigerant/IL absorption system.[40] Applications of these systems include the use of ILs as entrainers in an extractive distillation process to separate refrigerant mixtures[41] and as an absorbent in an absorption refrigeration cycle.[42] In an isolated system, refrigerant gas molecules absorb into a sample of IL at a rate depending on the physical properties of both components, including IL fluorination or hydrogenation.[43] Measuring this process offers an insight into the compatibility of components and how the components operate within a system. VLE data is typically reported as a function of pressure and composition.

VLE data with ILs and refrigerants has been studied for almost two decades, spanning dozens of papers[8,14,24,39,40,42−92,95,97−100] and patents for both use of IL in HFC and HFO separation.[41,93,94] As a result of this time span, a variety of methods have been used, but two are most commonly used, as explained by Asensio-Delgado et al.[85] The gravimetric method uses a precise computer-controlled apparatus to measure equilibrium.[39] The gravimetric method accurately measures changes in weight, pressure, and temperature to form an automated system to find the adsorption−desorption of a gas in a system, first described by Shiflett and Yokozeki in 2005,[45] and applicable methodology by Asensio-Delgado et al.[95] A microbalance inside the apparatus operates using an electrobalance with a delicate scale inside a pressure- and temperature-controlled reactor. The sample weight is balanced by a controlled counterweight and carefully measured until system stabilization occurs. After data is collected, corrections must be made for the buoyancy and aerodynamic forces, shown in eq 1.[45,96]

$$C_b = \text{Buoyancy} = gV_i\rho_g(T, P) = g\frac{m_i}{\rho_i}\rho_g(T, P) \quad (1)$$

Since its first use with IL and refrigerant systems in 2005, the gravimetric method has been used in many studies in the field.[8,14,39,43,48,55,58,59,66,71,72,77,78,81,87] The uncertainties reported for solubility results using a gravimetric method are often in a range of 5−6 mol %; however, the specific uncertainty of all reported data should be gathered from the reporting source.

The isochoric saturation method is also commonly used, with the first reporting in 2006 by Yokozeki and Shiflett,[57] and is first described by Jacquemin et al.,[44] with an applicable methodology given by Asensio-Delgado et al.[95] This method begins with a known volume of gaseous solute, in this case refrigerant gas, added to a known quantity of degassed solvent, or an IL sample previously under vacuum purification. The constant-volume apparatus used in this method measures the pressure change as gas is added, determining when that pressure stabilizes, and equilibrium is reached. This pressure can then be related to the solubility of refrigerant gas in the IL sample, but it is important to take into account the volume change of the liquid (i.e., swelling) otherwise the method can underestimate the sorption capacity. The volumetric method used with refrigerant and IL systems is prevalent in the literature (refs 14, 40, 42, 51, 56, 60, 63−65, 68, 73−75, 80, 82, 83, 85, 86, 90−92, and 97−100).

Other methods that appear in the literature include the HPVC synthetic method,[56] synthetic isochoric method,[95] synthetic isobaric method,[95] static-type apparatus,[79,82] isobaric microbulliometer,[84] NMR,[61] pressure decay,[50] visual method,[95]

https://doi.org/10.1021/acs.chemrev.3c00276
Chem. Rev. XXXX, XXX, XXX−XXX

Table 5. FC Refrigerant and IL Combinations with Vapor−Liquid Equilibrium Data[a]

Refrigerant \ Ionic Liquid	$[C_2C_1im][Pf_2N]$	$[C_2C_1im][BF_4]$	$[C_2C_1im][N(CN)_2]$	$[C_2C_1im][OTf]$		$[C_2C_1im][PF_6]$	$[C_2C_1im][PFBS]$	$[C_2C_1im][PFP]$	$[C_2C_1im][SCN]$
PFC-14									
CFC-114									
CFC-114a									
HCFC-22									
HCFC-124									
HCFC-124a									
HFC-32	39,41,94	85	14	70,98	85		70	70	68
HFC-125		101	14	70			70	70	14
HFC-134a	41,59,94	85	14	70,73	85		70, 73	70,73	68
HFC-152a				98					
HFC-143a									
HFC-41									
HFC-23						90			
HFC-161									
HFC-134	93								
HFC-236fa									
HFC-227ea									
HFC-245fa									
HFO-1234yf		64,85	14		85	63			68
HFO-1234ze									
HFO-1234ze(E)		80	14		52				52
HCFO-1233zd(E)									
HFC-32+HFC-125									

https://doi.org/10.1021/acs.chemrev.3c00276
Chem. Rev. XXXX, XXX, XXX−XXX

Table 5. continued

Refrigerant \ Ionic Liquid	$[C_2C_1im][Tf_2N]$			$[C_2C_1im][TFES]$	$[C_2C_1im][C_1CO_2]$		$[C_2C_1im][Cl]$	$[C_2C_1py][PFBS]$	$[C_3C_1py][Tf_2N]$
PFC-14		73							
CFC-114	71								
CFC-114a	71								
HCFC-22	77			77					
HCFC-124	71								
HCFC-124a	71								
HFC-32	39	70,73	86	39	70	81	78	70	39
HFC-125	72	70,73			70	81	78	70	
HFC-134a	43,71,97	70,73			70			70,73	
HFC-152a		77							
HFC-143a	72								
HFC-41			86						
HFC-23		73	86						
HFC-161									
HFC-134	71								93
HFC-236fa									
HFC-227ea									
HFC-245fa									
HFO-1234yf						65			
HFO-1234ze									
HFO-1234ze(E)	52,80								
HCFO-1233zd(E)									
HFC-32+HFC-125									

https://doi.org/10.1021/acs.chemrev.3c00276
Chem. Rev. XXXX, XXX, XXX−XXX

Table 5. continued

Refrigerant \ Ionic Liquid	[C_3C_1im][Tf_2N]	[C_3C_1im][Cl]	[C_4C_1im][Cl]	[C_4C_1im][C_1CO_2]	[C_4C_1im][BF_4]		[C_4C_1im][$N(CN)_2$]	[C_4C_1im][FS]	[C_4C_1im][HFPS]	[C_4C_1im][C_1SO_4]
PFC-14										
CFC-114										
CFC-114a										
HCFC-22						77				
HCFC-124										
HCFC-124a										
HFC-32	94	78	78	39,81	94,24	81	14	39,41,94	39,41,94	39,41,94
HFC-125		78	78	81		81	14			
HFC-134a							14		41,59,94	
HFC-152a										
HFC-143a										
HFC-41										
HFC-23										
HFC-161										
HFC-134	94									
HFC-236fa										
HFC-227ea										
HFC-245fa										
HFO-1234yf				65		63	14			
HFO-1234ze										
HFO-1234ze(E)							14			
HCFO-1233zd(E)										
HFC-32+HFC-125					102					

https://doi.org/10.1021/acs.chemrev.3c00276
Chem. Rev. XXXX, XXX, XXX−XXX

Table 5. continued

Refrigerant \ Ionic Liquid	[C_4C_1im][OTf]	[C_4C_1im][PF_6]		[C_4C_1im][SCN]		[C_4C_1im][TFES]	[C_4C_1im][TPES]	[C_4C_1im][TTES]	[C_4C_1py][Tf_2N]	[C_6C_1im][BF_4]	
PFC-14											
CFC-114											
CFC-114a											
HCFC-22			40,77								
HCFC-124											
HCFC-124a											
HFC-32	98,24	94,24	40,81	39	81	39,41,94	39,41,94	39,41,94	39		100
HFC-125		94,24	40,81		81						100
HFC-134a		94,24	40,59				41,59,94	41,59,94		97	
HFC-152a	98	94,24									100
HFC-143a		94,24	40								100
HFC-41			58								
HFC-23		24	57								
HFC-161			58								100
HFC-134			58								
HFC-236fa										42	
HFC-227ea										42	
HFC-245fa										42	
HFO-1234yf			63,76							64	100
HFO-1234ze											
HFO-1234ze(E)			75						80		80
HCFO-1233zd(E)										64	
HFC-32+HFC-125		102									

https://doi.org/10.1021/acs.chemrev.3c00276
Chem. Rev. XXXX, XXX, XXX−XXX

Table 5. continued

Refrigerant / Ionic Liquid	[C_6C_1im][Cl]		[C_6C_1im][Br]	[C_6C_1im][I]	[C_6C_1im][FAP]		[C_6C_1im][OTf]		[C_6C_1im][PF_6]		[C_6C_1im][Tf_2N]		[C_6C_1im][TFES]
PFC-14													
CFC-114													
CFC-114a													
HCFC-22													
HCFC-124													
HCFC-124a													
HFC-32	81	78	78	78	81	50		100			67,99	100	39
HFC-125	81	78	78	78	81			100			67	100	
HFC-134a							97	99	97	99	99	61,97	
HFC-152a						50		100			67	100	
HFC-143a								100			100	51	
HFC-41												56	
HFC-23												55	
HFC-161						50		100			100	51	
HFC-134					93								
HFC-236fa												54	
HFC-227ea												54	
HFC-245fa												54	
HFO-1234yf								100	76		100	83	
HFO-1234ze												83	
HFO-1234ze(E)									75			83	
HCFO-1233zd(E)								91				91	
HFC-32+HFC-125													

https://doi.org/10.1021/acs.chemrev.3c00276
Chem. Rev. XXXX, XXX, XXX−XXX

Table 5. continued

Refrigerant \ Ionic Liquid	$[C_7C_1im][TFES]$	$[C_8C_1im][BF_4]$	$[C_8C_1im][I]$	$[C_8C_1im][PF_6]$	$[C_8C_1im][Tf_2N]$	$[C_8C_1im][TFES]$	$[(C_8)_2im][I]$	$[C_2H_4C_6F_{13}C_1im][Pf_2N]$	$[C_2H_4C_6F_{13}C_1im][Tf_2N]$	$[C_{12}C_1im][TFES]$	$[(C_1)_2C_3im][Tf_2N]$	$[(C_1)_2C_3im][TMeM]$	
PFC-14													
CFC-114													
CFC-114a													
HCFC-22													
HCFC-124													
HCFC-124a													
HFC-32	39,41,94		41,94				41,94			39,41,94	39	39,41,94	41,94
HFC-125													
HFC-134a					43			43	43				
HFC-152a													
HFC-143a													
HFC-41													
HFC-23						48							
HFC-161													
HFC-134												93	94
HFC-236fa													
HFC-227ea													
HFC-245fa													
HFO-1234yf		64		76									
HFO-1234ze													
HFO-1234ze(E)		80		75									
HCFO-1233zd(E)													
HFC-32+HFC-125													

https://doi.org/10.1021/acs.chemrev.3c00276
Chem. Rev. XXXX, XXX, XXX−XXX

Table 5. continued

Refrigerant \ Ionic Liquid	$[P_{4,4,4,1}][C_1SO_4]$	$[P_{4,4,4,2}][(C_2)_2PO_4]$		$[P_{6,6,6,14}][Cl]$		$[P_{6,6,6,14}][CNPyr]$	$[P_{6,6,6,14}][C_2NO_2]$	$[P_{6,6,6,14}][Tf_2N]$	$[P_{6,6,6,14}][TMP]$	$[P_{6,6,6,14}][TPES]$	$[P_{4,4,4,14}][HFPS]$	[m-2-HEA][C_2CO_2]	[m-2-HEA][C_4CO_2]
PFC-14													
CFC-114													
CFC-114a													
HCFC-22													
HCFC-124													
HCFC-124a													
HFC-32	92	92	53	78	92	53	53	86	66			86	86
HFC-125					78				46				
HFC-134a			53			53	53		46	59	41,59,94		
HFC-152a									46				
HFC-143a													
HFC-41	92	92			92			86				86	86
HFC-23	92	92			92			86				86	86
HFC-161									46				
HFC-134													
HFC-236fa									66				
HFC-227ea									66				
HFC-245fa									66				
HFO-1234yf					65								
HFO-1234ze													
HFO-1234ze(E)													
HCFO-1233zd(E)													
HFC-32+HFC-125													

[a]The data available is represented by different colors: single temperature isotherm (blue), multi-temperature isotherm (green), and single pressure isobar (orange).

weight method,[95] autoclave method,[90] and semi-infinite volume technique[100] for VLE data acquisition. Each of these methods have different levels of uncertainty; consult the original source for the reported uncertainty and methodology.

Much progress has been made in recent years regarding an in-depth study of the interactions between refrigerants and ILs. The most thoroughly surveyed IL−FC refrigerant combination is HFC-134a with $[C_2C_1im][Tf_2N]$ with six reports detailing information about the interaction of this pair.[43,70,71,73,97,99] HFC-32 with $[C_4C_1im][PF_6]$ and $[C_2C_1im][CF_3SO_2]$ are other well-characterized systems with four sets of data discussing the interactions.[40,70,81,85,94,98,99]

HFC-32 is the most studied FC refrigerant. Other FC refrigerants that were frequently studied were HFC-125 (CHF_2CF_3) and HFC-134a (CH_2FCF_3), both being components in many common refrigerant blends (e.g., R-410A, R-404A, R-407C). The ionic liquid $[C_2C_1im][Tf_2N]$ has been studied the most in the literature. Other common ionic liquids studied are $[C_4C_1im][PF_6]$ and $[C_6C_1im][Tf_2N]$. The cation that has been investigated the most is $[C_2C_1im]$, and the anion is $[Tf_2N]$. Table 5 and Table 6 show a summary of the systems investigated. Asensio-Delgado et al. provide the UC-RAIL excel database as Supporting Information, which compiles a majority of the phase behavior data for ILs and refrigerants.[8]

2.1.1. Temperature and Pressure. A common trend investigated is the effect of temperature and pressure on the solubility of various refrigerant + IL blends. Among the VLE data provided, temperatures ranged from 283 to 413 K and pressures from 0.03 to 33 MPa. Several studies showed that lower temperatures and higher pressures improve the gas solubility.

https://doi.org/10.1021/acs.chemrev.3c00276
Chem. Rev. XXXX, XXX, XXX−XXX

Table 6. Number of Times VLE Data Was Measured for Different Anion and Cation Combinations with Different FC Refrigerants

	Anion → / Cation ↓	[I]⁻	[Br]⁻	[Cl]⁻	[BF_4]⁻	[PF_6]⁻	[SCN]⁻	[C_1CO_2]⁻	[Tf_2N]⁻	[Pf_2N]⁻	[$N(CN)_2$]⁻	[OTf]⁻	[PFBS]⁻	[PFP]⁻	[TFES]⁻	[FS]⁻	[HFPS]⁻	[TPES]⁻	[TTES]⁻	[FAP]⁻	[TMeM]⁻	[C_1SO_4]⁻	[$(C_2)_2PO_4$]⁻	[CNPyr]⁻	[C_2NO_2]⁻	[TMPP]⁻	[C_2CO_2]⁻	[C_4CO_2]⁻
		6	2	16	28	36	8	10	63	8	10	22	8	4	13	3	9	7	6	6	7	6	5	2	2	8	3	3
80	[C_2C_1im]⁺			2	6	2	5	6	27	7	5	10	4	4	2													
4	[C_3C_1im]⁺			2					2																			
79	[C_4C_1im]⁺			2	7	28	3	4			5	3			3	3	6	6	6			3						
65	[C_6C_1im]⁺	2	2	4	13	4			24			9			1					6								
3	[C_7C_1im]⁺														3													
8	[C_8C_1im]⁺	2			2	2			1						1													
3	[$C_{12}C_1im$]⁺														3													
8	[$(C_1)_2C_3im$]⁺								1												7							
2	[$(C_8)_2im$]⁺	2																										
4	[C_2C_1py]⁺												4															
2	[C_3C_1py]⁺								2																			
2	[C_4C_1py]⁺								2																			
2	[$C_8H_4F_{13}mim$]⁺								1	1																		
3	[$P_{4,4,4,1}$]⁺																					3						
5	[$P_{4,4,4,2}$]⁺																						5					
3	[$P_{4,4,4,14}$]⁺																3											
22	[$P_{6,6,6,14}$]⁺			6					3									1						2	2	8		
6	[m-2-HEA]⁺																										3	3

Sun et al. came to this conclusion when examining HFO-1234ze(E) ($CF_3CH{=}CHF$) with imidazolium-based ionic liquids. The solubility was as follows: [C_8C_1im][PF_6] > [C_6C_1im][PF_6] > [C_4C_1im][PF_6]. This trend is also linked to alkyl chain length, which is discussed in a later section.[75]

Liu et al. (2015) further supported this temperature solubility trend in a handful of different blends. When providing new experimental data for HFC-32, HFC-152a (CH_3CHF_2), and HFC-125 with [C_6C_1im][Tf_2N], the solubility was found to be HFC-152a > HFC-32 > HFC-125 that increased at lower temperatures.[67]

Shariati et al. collected VLE data for HFC-23 (CHF_3) in [C_2C_1im][PF_6] at multiple temperatures and pressures. From the data, it was concluded that at lower concentrations of HFC-23 and lower pressures the equilibrium pressure increases in an almost linear fashion with HFC-23 concentration. However, increasing the HFC-23 concentration further would significantly increase the equilibrium pressure. The group also found that, as pressure decreases, the solubility of the ionic liquid in HFC-23 decreased drastically.[90]

The Liu et al. (2016) group compared the solubilities of HFO-1234yf, HFO-1234ze(E), and HFCs in [C_6C_1im][Tf_2N] and found that the solubilities of HFO-1234yf and HFO-1234ze(E) are more sensitive to temperature but are comparable to HFCs.[83] Furthermore, the solubility of HFO-1234ze(E) was higher than that of HFO-1234yf. Because of this, it was concluded that both blends show potential for the absorption refrigeration cycle.[83]

He et al. (2017) determined that temperature had a positive effect on the absorption rate but a negative effect on the absorption capacity for the refrigerants HFC-32, HFC-125, HFC-161 (CH_3CH_2F), HFC-143a (CH_3CF_3), HFO-1234yf, and HFC-152a in the room temperature ILs [C_6C_1im][Tf_2N], [C_6C_1im][OTf], and [C_6C_1im][BF_4].[83,100] In a later work, He et al. (2018) collected VLE data of HCFO-1233zd(E) ($CHCl{=}CHCF_3$) in [C_6C_1im][Tf_2N], [C_6C_1im][OTf], and [C_6C_1im][BF_4]. Hydrochlorofluoroolefins (HCFOs) are a class of refrigerants that are similar to HFOs but do contain chlorine and have a very low ODP that may be considered acceptable for future refrigerants. The group determined that the solubility of HCFO-1233zd(E) tended to increase with increasing pressure and decrease with increasing temperature. Of the ILs, HCFO-1233zd(E) was most soluble in [C_6C_1im][Tf_2N], but its diffusion coefficient in this IL was also the lowest.[91]

Esaki et al. further supported this conclusion. The solubility of refrigerant HFO-1234yf with ILs [C_4C_1im][Tf_2N], [C_4C_1im][BF_4], and [C_2C_1im][PF_6] was determined via an isochoric saturation method. It was found that the solubility of HFO-1234yf increased in the following order: [C_4C_1im][Tf2N] > [C_4C_1im][BF_4] > [C_2C_1im][PF_6].[63] This was calculated through the NRTL model and evaluated from the Duhring diagram that allows for comparison of respective vapor pressure and temperature of solution.[103] Because of its absorption capacity, the group focused on the HFO-1234yf and [C_4C_1im][Tf_2N] blend. Equilibrium solubility decreased according to [C_4C_1im][Tf_2N] > [C_4C_1im][BF_4] > [C_2C_1im][PF_6].[63]

Shiflett et al. (2013) measured the adsorption of HFC-23 on three different zeolites and studied the solubility of HFC-23 in [C_8C_1im][TFES]. The group found that the solubility capacity of HFC-23 in the IL and zeolites were equal when the system pressure was 2.5 MPa for the IL and 0.25 MPa for the zeolite, indicating that the same solubility that could be achieved with the IL could be reached using a zeolite and much lower pressure.[48]

Trends between mole fraction, temperature, and pressure have also been noted. Sun et al. examined the refrigerant HFO-

https://doi.org/10.1021/acs.chemrev.3c00276
Chem. Rev. XXXX, XXX, XXX−XXX

1234yf and noted that increasing temperature and decreasing pressure decreased the mole fraction of HFO-1234yf. Under isothermal and isobaric conditions, HFO-1234yf was found to be most soluble in $[C_8C_1im][PF_6]$ and least soluble in $[C_4C_1im][PF_6]$.[75]

Liu et al. (2019) also noted that, for HFC-227ea (CF_3CHFCF_3), HFC-236fa ($CF_3CH_2CF_3$), and HFC-245fa ($CF_3CH_2CHF_2$) in $[C_6C_1im][BF_4]$, HFC-245fa was the most soluble in this IL, followed by HFC-236fa, and then HFC-227ea.[42] At lower temperatures, the mole fractions of all three refrigerants increased in the liquid phase, though the interdiffusion coefficients decreased. The liquid phase mole fractions were also found to increase when the pressure was increased.[42]

2.1.2. Alkyl Chain. Varying the length of the alkyl chain in the cation significantly impacts the solubility of an FC in an IL. Many authors have concluded that increasing the cation alkyl chain increases solubility. Figure 4 shows the structures of an imidazolium-based cation with varying alkyl chain length.

Dong et al. came to this conclusion when conducting gas solubility measurements in an isothermal synthetic apparatus. Measurements were made on HFC-32 and HFC-152a with

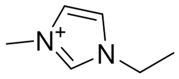

1-ethyl-3-methylimidazolium

$[C_2C_1im]^+$

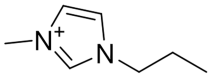

1-propyl-3-methylimidazolium

$[C_3C_1im]^+$

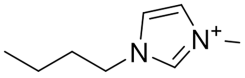

1-butyl-3-methylimidazolium

$[C_4C_1im]^+$

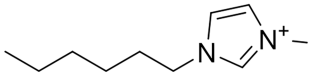

1-hexyl-3-methylimidazolium

$[C_6C_1im]^+$

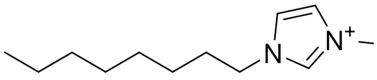

1-octyl-3-methylimidazolium

$[C_8C_1im]^+$

Figure 4. Imidazolium-based cations with increasing alkyl chain lengths.

$[C_2C_1im][CF_3SO_2]$ and $[C_4C_1im][CF_3SO_2]$ due to good miscibility with HFCs. It was determined that the solubility of HFC-32 is larger than that of HFC-152a for the same IL. Additionally, the solubility of $[C_4C_1im][CF_3SO_2]$ is larger than that of $[C_2C_1im][CF_3SO_2]$ for the same HFC.[98]

Wang et al. (2017) investigated this effect with HFO-1234ze(E) and $[C_2C_1im][BF_4]$, $[C_6C_1im][BF_4]$, and $[C_8C_1im][BF_4]$. Results indicated that increasing solubility was linked to an increase in the cation alkyl group length.[80] Additionally, Sun et al. (2017) presented absorption data of HFO-1234yf with $[C_2C_1im][BF_4]$, $[C_6C_1im][BF_4]$, and $[C_8C_1im][BF_4]$ and found that solubility increases with the length of the alkyl chain due to an increase in van der Waals interactions. Solubilities of HFO-1234yf decrease in the order $[C_8C_1im][BF_4] > [C_6C_1im][BF_4] > [C_2C_1im][BF_4]$.[64]

Lepre et al. (2019) collected solubility data of HFC-134a in $[C_2C_1im][Tf_2N]$, $[C_8C_1im][Tf_2N]$, $[C_8C_1im][Pf_2N]$, $[C_2H_4C_6F_{13}C_1im][Tf_2N]$, and $[C_2H_4C_6F_{13}C_1im][Pf_2N]$. The refrigerant was found to be most soluble in $[C_2H_4C_6F_{13}C_1im]$-$[Pf_2N]$, followed by $[C_2H_4C_6F_{13}C_1im][Tf_2N]$, $[C_8C_1im]$-$[Pf_2N]$, $[C_8C_1im][Tf_2N]$, and $[C_2C_1im][Tf_2N]$.[43] The group noted that HFC-134a solubility increased when the alkyl side chain of the cation is fluorinated (the solubility of HFC-134a still increased when the anion was fluorinated, though the increase was not as significant). It was also observed that ILs with fluorinated side chains in the cations were more selective in separating HFC-134a from ethane, while ILs with hydrogenated cations were better able to separate HFC-134a from perfluoromethane.[43] The group hypothesized that the non-polar regions of the polar HFC-134a contributed significantly to its solubility in ILs, using thermodynamic properties of solvation and molecular dynamics simulations to determine that an entropic effect was responsible for HFC-134a's greater solubility in fluorinated ILs.[43]

Sosa et al. (2019) utilized a gravimetric method for single-component absorption isotherms of HFC-32, HFC-125, and HFC-134a in various ILs.[70] The group found that the absorption of these HFCs increased significantly in ILs with a fluorinated alkyl side chain with four carbon atoms. The group determined that, in separating mixtures of HFC-134a/HFC-125 and HFC-32/HFC-125, the selectivity was increased by using fluoro-containing ILs lacking the alkyl fluorinated chain, but ILs with the alkyl fluorinated chain were more selective in separating HFC-134a/HFC-32.[70]

Baca et al. (2022) demonstrated using HFC-32 and HFC-125 in six ILs with halogen anions [I]−, [Br]−, [Cl]− and cations $[C_xC_1im]+$ (x = 2, 3, 4, and 6) and $[P_{6,6,6,14}][Cl]$ that the solubility of HFC-32 did not change appreciably with increasing alkyl chain length in the imidazolium cation.[78] However, HFC-125's solubility increased with increasing alkyl chain length, due to van der Waals forces. The phosphonium-containing ILs had higher solubilities of both refrigerants at lower pressures than the imidazolium ion with the same chloride ions. Of the ILs studied, $[C_6C_1im][Cl]$ and $[P_{6,6,6,14}][Cl]$ were the most selective in separating R-410A.[78]

2.1.3. Anion and Cation. The type of anion and cation in an IL largely impacts refrigerant solubility. Figure 5 shows the structures of common cations and anions investigated. Wang et al. (2017) produced VLE data on refrigerant HFO-1234ze(E) with $[C_2C_1im][BF_4]$, $[C_6C_1im][BF_4]$, and $[C_8C_1im][BF_4]$. When comparing with previous work, it was determined that the anion's diameter or charge density led to the solubility of

https://doi.org/10.1021/acs.chemrev.3c00276
Chem. Rev. XXXX, XXX, XXX−XXX

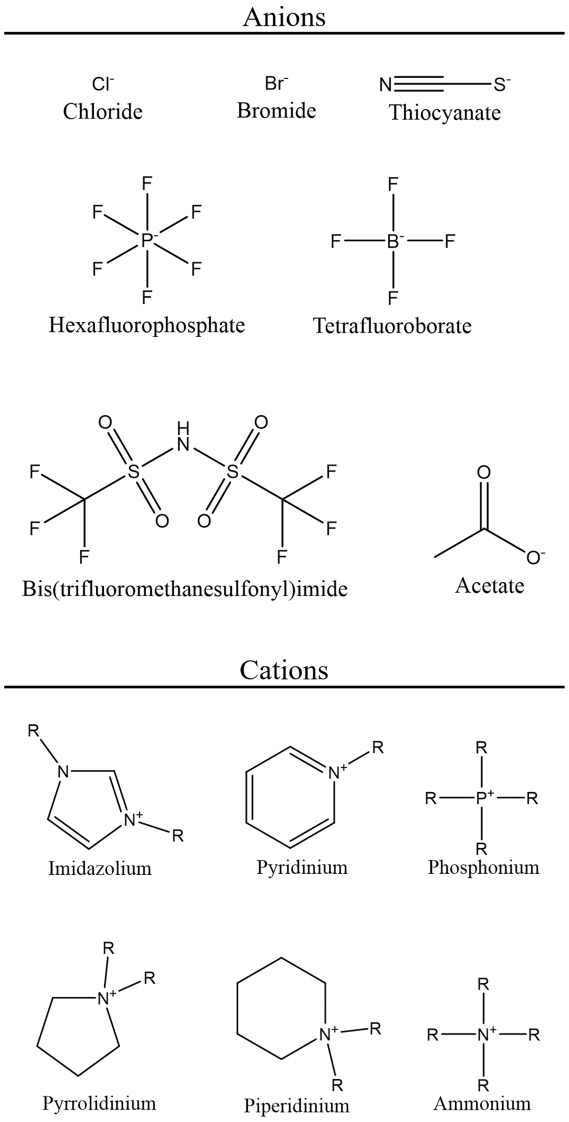

Figure 5. Structures of common anions and cation bases found in ILs.

HFO-1234ze(E) being lower with $[C_6C_1im][BF_4]$ than with $[C_6C_1im][Tf_2N]$.[80]

Asensio-Delgado et al. (2021) collected VLE data and diffusion coefficients at infinite dilution for HFC-32, HFC-125, HFC-134a, HFO-1234yf, and HFO-1234ze(E) with two cyanide-based ionic liquids $[C_2C_1im][N(CN)_2]$ and $[C_4C_1im][N(CN)_2]$.[14] The ILs were selected as other ILs with cyanide moieties in the anion, such as a thiocyanate anion, have had improved selectivity of the separation of HFC and HFO mixtures, and their low viscosities are helpful for improving mass transfer.[14] It was found that HFC-125 and HFO-1234yf are less soluble in the ILs used than the other refrigerants, which could be beneficial in the separation of common refrigerant mixtures R-410A and R-454B.[14]

Baca et al. (2022) found that the solubility of HFC-32 was not affected by the anion used, but the solubility of HFC-125 increased as the size of the anion decreased and the Lewis basicity strength and electronegativity of the anion increased for ILs $[C_6C_1im][I] > [C_6C_1im][Br] > [C_6C_1im][Cl]$.[78] Baca et al. also found that the solubility of HFC-32 and HFC-125 was significantly higher at lower pressures in $[P_{6,6,6,14}][Cl]$ than $[C_6C_1im][Cl]$. This shows phosphonium-based ILs have strong potential for FC refrigerant separation.

Liu et al. (2016) examined the solubility data of HFC-32, HFC-245fa, HFC-227ea, and HFC-236fa with $[P_{6,6,6,14}]$-[TMPP]. This showed HFCs are more soluble in $[P_{6,6,6,14}]$-[TMPP] than in the corresponding alkanes.[66] Liu et al. (2015) investigated HFC-161 and HFC-143a in $[C_6C_1im][Tf_2N]$ showing that $[C_6C_1im][Tf_2N]$ has higher solubilities for the refrigerant than for smaller hydrocarbons.[51]

Sousa et al. (2014) studied the gas solubility of HFC-23, HFC-32, and HFC-41 in three ionic liquids, $[P_{6,6,6,14}][Cl]$, $[P_{4,4,4,1}][C_1SO_4]$, and $[P_{4,4,4,2}][(C_2)_2PO_4]$. It was found that HFC-23 and HFC-32 had higher solubility in $[P_{4,4,4,2}]$-$[(C_2)_2PO_4]$, whereas HFC-41 had higher solubility in $[P_{6,6,6,14}][Cl]$. The group also found that the solubilities were higher than other ammonium cation room temperature ionic liquids (RTILs) studied in other sources.[92]

2.1.4. Fluorinated and Non-Fluorinated Anions. The degree of anion fluorination has also been found to affect the solubility of refrigerants. For example, Shiflett et al. (2006) collected data for the solubility and diffusivity of HFC-32 in 19 ionic liquids.[39] Five of the ionic liquids contained novel fluorocarbon sulfonate anions. Results showed that the choice of cation and anion had a significant effect on the solubility of the HFC-32. HFC-32 exhibited higher solubility in ionic liquids with fluorinated anions in comparison to non-fluorinated anions. The group hypothesized that hydrogen bonding may explain the increased solubility of HFC-32 relative to non-fluorinated anions.[39]

Shiflett et al. (2006) also investigated the solubility of HFC-134a in seven different ionic liquids, three of which contained novel fluorocarbon sulfonate anions and another two that were commercially available.[59] The group found that, of the three ILs with novel anions, $[P_{6,6,6,14}][TPES]$ and $[P_{4,4,4,14}][HFPS]$ had the largest deviations (negative) from Raoult's law in HFC-134a. It was hypothesized that hydrogen−fluorine interactions between HFC-134a and the ionic liquids were primarily responsible.[59]

In addition to these studies, Jovell et al. (2020) compared HFC-134a solubility in various ionic liquids, finding that it was more soluble in those with a greater number of fluorine atoms in the anion.[73] Similarly, Liu et al. showed that the solubility of refrigerants was improved when hydrogen atoms in the alkane were replaced by fluorine atoms.[50]

Asensio-Delgado et al. (2020) investigated ionic liquids containing fluorinated and non-fluorinated anions and found that the low viscosity $[C_2C_1im][SCN]$ was best suited for separating refrigerant mixtures containing HFC-32, HFC-134a, and HFO-1234yf.[68] Results showed that ionic liquids with small, non-fluorinated anions are better able to separate HFC/HFO mixtures than ionic liquids with larger molar volume and fluorinated anions.[68]

Morais et al. (2020) collected isothermal VLE data for HFC-32 and HFC-125 in various ionic liquids containing fluorinated and non-fluorinated anions.[81] The group collected the data using a gravimetric microbalance and the van der Waals equation of state to correlate the solubility data. HFC-32 was found to be more soluble in ionic liquids with fluorinated anions, likely due to hydrogen bonding between the refrigerant and the anion.[81] Similarly, HFC-125 was found to be more soluble in ionic liquids with non-fluorinated anions. Of the ionic liquids used, $[C_4C_1im][SCN]$ had the lowest solubility for both refrigerants, suggesting that the choice of anion greatly

https://doi.org/10.1021/acs.chemrev.3c00276
Chem. Rev. XXXX, XXX, XXX−XXX

determines the solubility of the refrigerants. The predicted data and experimental data aligned well, and the group found that $[C_6C_1im][Cl]$ and $[C_4C_1im][C_1CO_2]$ were most effective at separating R-410A.[81]

2.1.5. Hydrogen Bonding. As previously described, refrigerant gases and ionic liquids can undergo hydrogen bonding and impact refrigerant solubility. Jovell et al. (2020) found that, for HFC-134a, HFC-125, HFC-23, HFC-32, and PFC-14 (CF_4) in $[C_2C_1im][Tf_2N]$, refrigerants with more hydrogen had higher absorption due to hydrogen bonding between refrigerant molecules. Of the FCs studied, HFC-134a had the highest solubility.[73] The group also noted that the carboxylate anion provided slightly higher solubility for HFC-134a. The group also noted that HFC-134a solubility was lower in deep eutectic solvents than in fluorinated ionic liquids, but higher proportions of the acid in deep eutectic solvents did increase HFC-134a solubility.[73]

Sosa et al. (2022) determined that the hydrogen bond acceptor character of the ionic liquid greatly affected the effectiveness of the ionic liquid in separating refrigerants.[53] This was supported by Liu et al. (2016) who stated that HFCs are more soluble than the corresponding alkanes based off the consideration that dispersive forces, dipole−dipole interactions, and hydrogen bond interactions exist between HFCs and $[P_{6,6,6,14}][TMPP]$.[66]

Shiflett et al. (2007) looked at how hydrogen substitution of refrigerants impacted solubility.[71] It was found that perhalogenated compounds and isomers had close to identical solubility behavior with large immiscibility gaps. Thus, it was concluded that ionic liquids are not suited for this separation. With monohydrogen substituted halocarbons, a difference was seen with a liquid−liquid immiscibility gap. Testing revealed that hydrogen substitution increased solubility.[71]

Furthermore, Yu et al. (2018) examined the ability of $[C_2C_1im][BF_4]$ to absorb HFC-125. VLE data for a mixture of $[C_2C_1im][BF_4]$ with HFC-125 and $[C_2C_1im][BF_4]$ with HFC-125 and H_2O was measured.[101] Using both the COSMO-RS model and quantum chemistry calculations, the group determined that the anion $[BF_4]^-$ dictated the HFC-125 dehydration, as this anion formed strong hydrogen bonds with H_2O. The group also found that the solubility of HFC-125 in $[C_2C_1im][BF_4]$ decreased with low amounts of H_2O present.[101]

2.2. Phase Behavior

The full global phase behavior is necessary to know the practical limits of an ionic liquid with refrigerants. For an extractive distillation column, it is important to know where vapor−liquid equilibrium no longer exists or where vapor−liquid−liquid equilibrium (VLLE) begins. In order to avoid the VLLE region when designing a process, the full phase behavior must be measured and understood.[40,104] According to the Gibbs phase rule for a binary system, four phases can be present at the same time; however, only two or three phases are more likely to occur.[105]

The global phase behavior of ionic liquids with refrigerants is commonly characterized by the Scott−van Konynenburg scheme.[106] The classification system was developed for binary systems of liquids and gases with six different types labeled I through VI. Most ionic liquid and refrigerant binary systems have been classified as Type V.[8,57,71,72,74,97,107−110] Type V behavior has a lower critical end-point (LCEP) and an upper critical end-point (UCEP). Above the LCEP, either another liquid phase forms or VLLE is observed. Two liquid phases exist until the UCEP, where the liquid phases become miscible. Type III is also a common classification[72,108,109] and differs from Type V by not having a LCEP. Thus, the VLLE region does not have a lower limit. Systems without VLLE are Type I. $[C_4C_1im][PF_6]$ with HFC-134a and HFC-152a[109] as well as with HFC-125[110] were predicted to be Type IV meaning another VLLE region at lower temperatures. This region is likely to interfere with solid phases, so the systems are classified as Type V. Bolz et al. designed a newer classification system for the International Union of Pure and Applied Chemistry (IUPAC) that provides a more descriptive way to represent the curvature and connectivity of the critical curves. Type V would be 2^P, and Type III would be 1^P1 using the new system.[111]

Three main experimental methods have been used for the determination of VLLE: the volumetric, cloud-point, and view cell methods. These methods use the theory of Gibb's phase rule, such that, when three phases and two components are present, the system is univariant. If one intensive variable such as temperature is changed, all other intensive variables are set.

The volumetric method apparatus uses two tubes for a given binary ionic liquid and refrigerant mixture to solve for the composition of the liquid phases. The vapor phase is known by assuming it consists only of refrigerant, since ionic liquids have negligible vapor pressure. Mass-and-volume methods are used for the determination of the liquid phases. Each tube is filled with a known amount of ionic liquid and refrigerant at a different overall composition. The tubes are allowed to come to equilibrium in terms of composition. The height of the tubes, the total weight of the tubes, and the volume of each phase is used to determine the weight fraction of the liquid phases. This simple method allows for composition measurements of all three phases without the need for any analytical equipment.[109,110]

Another method used to measure the VLLE is the cloud-point method. With this approach, multiple tubes are prepared with an overall composition that is in the VLLE region. The temperature of the tubes is then lowered until one liquid phase forms. The temperature is slowly raised until a cloud layer becomes visible at the cloud-point temperature. At this temperature, the liquid level is measured and the amount of refrigerant gas in the vapor phase is accounted for. Equation of states can then be used to determine the amount of refrigerant gas in the liquid phase or the cloud-point composition.[71]

The view cell method has the same theory as the cloud-point method but utilizes a different apparatus design. Ren and Scurto described a static equilibrium apparatus composed of a high-pressure view cell, water bath, high-pressure syringe pump, high-precision temperature measurement, and a high-precision pressure gauge. A set amount of ionic liquid is loaded into the system, and refrigerant gas is fed until a small second layer appears. This second layer is assumed to be negligible in mass. Mass balances are then used to solve for the composition of the first liquid phase.[112]

2.2.1. Phase Behavior Trends. The amount of research dedicated to the global phase behavior of refrigerants and ionic liquids is drastically smaller than studies dedicated to vapor−liquid equilibrium. Table 8 shows the systems with VLLE data reported in the literature; only nine imidazolium-based ILs and one pyridinium IL have data reported. For practical applications, all phase regions should be known, and additional research should be conducted to inform separation processes. Table 7 shows the number of times a specific anion and cation has been used for VLLE measurements. The $[C_4C_1im][PF_6]$ and $[C_6C_1im][Tf_2N]$ are the most studied ionic liquids with 14

https://doi.org/10.1021/acs.chemrev.3c00276
Chem. Rev. XXXX, XXX, XXX−XXX

Table 7. Number of Times VLLE Data Was Measured for Different Anion and Cation Combinations with Different FC Refrigerants

		7	16	16	1	1	1
	Cation \ Anion	$[BF_4]^-$	$[PF_6]^-$	$[Tf_2N]^-$	$[HFPS]^-$	$[N(CN)_2]^-$	$[TFES]^-$
3	$[C_2C_1im]^+$			3			
18	$[C_4C_1im]^+$	2	14		1	1	
19	$[C_6C_1im]^+$	4	2	13			
1	$[C_8C_1im]^+$						1
1	$[C_4C_1py]^+$	1					

and 13 refrigerant gases tested, respectively. Not shown in the figures, the supercritical HFC-23 solubility was also measured with various ionic liquids.[90,113]

In terms of trends in VLLE data, the effect of replacing hydrogen with deuterium in HCFC-22 to make HCFC-22-d has been reported.[107] This substitution had little effect on the immiscible VLLE region with $[C_4C_1im][PF_6]$. When hydrogen or deuterium is substituted with fluorine in the refrigerant such as HCFC-22 and HCFC-22-d to CFC-11, CFC-113, and HCFC-123, the miscible region increases.[107] Hydrogen bonding with the fluorine may be an explanation for this effect. Interestingly, the substitution has a drastic impact on the VLLE region despite minimal differences in VLE behavior.

Ren and Scurto found that increasing the imidazolium alkyl chain length causes an increase in the miscibility region.[74] The longer chain length is thought to induce dipole moments and yield favorable interactions with HFC-134a. Ren and Scurto also found that increasing fluorination of the anion caused the miscible region to increase.[74] The hydrogen bonding increases with anion fluorination, allowing for the liquid phase to be miscible over a larger region.

Table 8. FC Refrigerant and IL Combinations with Vapor−Liquid−Liquid Equilibrium Data[a]

Refrigerant \ Ionic Liquid	$[C_2C_1im][Tf_2N]$	$[C_4C_1im][BF_4]$	$[C_4C_1im][HFPS]$	$[C_4C_1im][PF_6]$	$[C_4C_1im][N(CN)_2]$	$[C_6C_1im][BF_4]$	$[C_6C_1im][PF_6]$	$[C_6C_1im][Tf_2N]$	$[C_8C_1im][TFES]$	$[C_4C_1py][BF_4]$
CFC-11				107						
CFC-113				107				71		
CFC-113a								71		
CFC-114								71		
CFC-114a								71		
HCFC-22				107						
HCFC-22-*d*				107						
HCFC-123				107				71		
HCFC-123a								71		
HCFC-124								71		
HCFC-124a								71		
HFO-1132a			108		108			108	108	108
HFC-32										
HFC-125	72			110						
HFC-134a	74			109		74,97	74,97	71,74,97		
HFC-152a				109						
HFC-143a	72			109						
HFC-41				109						
HFC-23				57						
HFC-161				109						
HFC-134								71		
HFC-4310mee *erythro*		60		60		60				
HFC-4310mee *threo*		60		60		60				

View cell
Volumetric
Volumetric and cloud-point
Predicted
Volumetric, cloud-point, and View cell

[a]The experimental methods are represented by different colors: view cell (blue), volumetric (green), volumetric and cloud-point (orange), predicted (purple), and volumetric, cloud-point, and view cell (yellow).

https://doi.org/10.1021/acs.chemrev.3c00276
Chem. Rev. XXXX, XXX, XXX−XXX

Table 9. FC Refrigerant and IL Combinations with Diffusion Coefficients[a]

Refrigerant \ Ionic Liquid	[C_2C_1im][PF_2N]	[C_2C_1im][BF_4]	[C_2C_1im][$N(CN)_2$]	[C_2C_1im][OTf]	[C_2C_1im][PF_6]	[C_2C_1im][SCN]	[C_2C_1im][Tf_2N]		[C_2C_1im][TFES]		[C_3C_{1im}][Cl]	[C_4C_1im][BF_4]		[C_4C_1im][Cl]	[C_4C_1im][C_1CO_2]		[C_4C_1im][FS]
HFC-23					41,94												
HCFC-22								77		77			77				
HFC-32	39,41,94	85	14			68		39,41,94	39,41,94		78	81	24,41,94	78	39,41,94	81	39,41,94
HFC-125			14								78	81		78		81	
HFC-134a	41,59,94	85	14	85		68											
HFC-152a																	
HFC-245fa																	
HFC-143a																	
HFC-227ea																	
HFC-41																	
HFC-161																	
HFC-134																	
HFC-236fa																	
HFO-1234yf			14	85		68	85										
HFO-1234ze			14	52		52	52										
HCFO-1233zd(E)																	
HBFC-22B1								87					87				

Refrigerant \ Ionic Liquid	[C_4C_1im][HFPS]		[C_4C_1im][C_1SO_4]	[C_4C_1im][PF_6]		[C_4C_1im][$N(CN)_2$]	[C_4C_1im][SCN]	[C_4C_1im][TFES]	[C_4C_1im][TPES]		[C_4C_1im][TTES]		[C_6C_1im][BF_4]	[C_6C_1im][Br]	[C_6C_1im][Cl]	[C_6C_1im][FAP]	
HFC-23					24,41,94												
HCFC-22					77,94												
HFC-32	39,41,94		39,41,94	81	24,41,94	14	39,41,94	39,41,94	39,41,94		39,41,94		100	78	81	50	81
HFC-125				81	24,41,94	14							100	78	81		81
HFC-134a		41,59,94			24,41,94	14				41,59,94		41,59,94					
HFC-152a					24,41,94								100			50	
HFC-245fa													42				
HFC-143a					24,41,94								100				
HFC-227ea													42				
HFC-41					94												
HFC-161					94								100			50	
HFC-134					94												
HFC-236fa													42				
HFO-1234yf						14							100				
HFO-1234ze						14											
HCFO-1233zd(E)													91				
HBFC-22B1					87												

https://doi.org/10.1021/acs.chemrev.3c00276
Chem. Rev. XXXX, XXX, XXX−XXX

Table 9. continued

Ionic Liquid / Refrigerant	[C_6C_1im][I]	[C_6C_1im][OTf]	[C_6C_1im][Tf_2N]			[C_7C_1im][TFES]	[C_8C_1im][I]	[$(C_8)_2$im][I]	[$C_{12}C_1$im][TFES]	[$P_{4,4,4,14}$][HFPS]	[$P_{6,6,6,14}$][Cl]	[$P_{6,6,6,14}$][TPES]	[C_4C_1py][Tf_2N]	[$(C_1)_2C_3$im][Tf_2N]	[$(C_1)_2C_3$im][TMeM]	[C_3C_1py][Tf_2N]
HFC-23																
HCFC-22																
HFC-32	78	100		100		39,41,94	41,94	41,94	39,41,94		78		39,41,94	39,41,94	39,41,94	39,41,94
HFC-125	78	100		100							78					
HFC-134a			61							41,59,94		41,59,94				
HFC-152a		100		100												
HFC-245fa					54											
HFC-143a		100		100												
HFC-227ea					54											
HFC-41																
HFC-161		100		100												
HFC-134																
HFC-236fa					54											
HFO-1234yf		100		100												
HFO-1234ze																
HCFO-1233zd(E)		91		91												
HBFC-22B1																

[a]The diffusion coefficients are represented by different colors: single T, single P (blue), single T, multi P (green), multi P, single T (orange), and multi T, multi P (yellow).

Another study by Shiflett et al. (2008) looked at how chirality affects the phase equilibria with various ionic liquids.[60] HFC-4310mee *Erythro*-isomer and HFC-4310mee *Threo*-isomer were used with [C_4C_1im][PF_6], [C_4C_1im][BF_4], and [C_2C_1im]-[BF_4]. It was found that the VLLE region was larger for the *Erthro*-isomer for all three of the ionic liquids. The presence of fluorine and the orientation of the hydrogen atom in the refrigerants can dramatically impact phase behavior in ionic liquids.

2.3. Phase Equilibrium General Trends

All VLE data reported is of FC refrigerant and IL combinations. HFC-32 is the most reported refrigerant, whereas [C_2C_1im]-[Tf_2N] is the most reported IL. VLE data was collected in single temperature isotherm, multitemperature isotherm, and single pressure isobar. The majority of the VLE data consisted of single temperature and multitemperature isotherms. Of the VLE data for FC refrigerants and IL combinations, [C_2C_1im]+ is the most recorded cation while [Tf_2N]− is the most reported anion. For the VLE data, lower temperatures and higher pressures generally improved gas solubility. Increased cation alkyl chain length was found to increase the solubility of a FC in an IL. The anion and cation of the IL had a large impact on the refrigerant solubility due to factors including anion size, electronegativity, and Lewis basicity strength. Experiments with [$P_{6,6,6,14}$][Cl] showed strong potential for FC separation. ILs with fluorinated anions showed higher solubility for HFC-32 compared to non-fluorinated anions, which could be due to hydrogen bonding and fluorine−hydrogen interactions. Hydrogen bonding can also greatly impact FC solubility in an IL, and in some FCs, hydrogen bonding between refrigerant molecules led to higher absorption. Hydrogen substitution was also found to have increased solubility.

VLE data is often the first data collected when a new FC refrigerant/IL system is being investigated. It acts as both a screening process and a vital base for the separation process modeling. There is still significant work to be performed on ILs with greater variation in the cation and anion to better understand which ILs are the best for FC refrigerant separations. There is also a need for faster screening methods and more binary gas sorption experiments.

The refrigerant reported in the most papers was HFC-134a, and the most common IL is [C_4C_1im][PF_6]. For the determination of the VLLE region, the three main experimental methods used were the volumetric, cloud-point, and view cell methods. Substitution of a hydrogen or deuterium with fluorine increased the miscible region and had a drastic impact on the VLLE region. The miscible region was also found to increase with increasing imidazolium alkyl chain length due to induced dipole moments. Chirality heavily affects the phase behavior of an IL as well as the presence of fluorine, and the orientation of the hydrogen atom. More studies on VLLE phase regions need to be completed for systems intended for separation applications.

3. THERMODYNAMIC AND TRANSPORT PROPERTIES

Thermodynamic and transport properties of pure component ILs, pure component refrigerants, and mixtures of ILs and refrigerants are imperative for optimal design and sizing of engineering equipment utilizing such systems. For instance, pumping duty is heavily dependent on the viscosity of such systems; furthermore, viscosity and surface tension play a crucial

https://doi.org/10.1021/acs.chemrev.3c00276
Chem. Rev. XXXX, XXX, XXX−XXX

Table 10. Number of Times Diffusion Coefficients Have Been Calculated for Different Anion and Cation Combinations with Different FC Refrigerants

		6	2	8	19	28	5	7	5	27	9	13	5	10	3	3	8	6	10	3
	Anion / Cation	[I]$^-$	[Br]$^-$	[Cl]$^-$	[BF_4]$^-$	[PF_6]$^-$	[FAP]$^-$	[SCN]$^-$	[C_1CO_2]$^-$	[Tf_2N]$^-$	[TPES]$^-$	[TFES]$^-$	[Pf_2N]$^-$	[OTf]$^-$	[TMeM]$^-$	[C_1SO_4]$^-$	[HFPS]$^-$	[TTES]$^-$	[$N(CN)_2$]$^-$	[FS]$^-$
32	[C_2C_1im]$^+$				2	2		4		7		4	6	3					5	
2	[C_3C_1im]$^+$			2																
74	[C_4C_1im]$^+$			2	7	26		3	5		6	3				3	6	6	5	3
39	[C_6C_1im]$^+$	2	2	2	10		5			11				7						
2	[C_8C_1im]$^+$	2																		
3	[C_7C_1im]$^+$											3								
2	[$(C_8)_2$im]$^+$	2																		
3	[$C_{12}C_1$im]$^+$											3								
3	[$P_{4,4,4,14}$]$^+$																3			
5	[$P_{6,6,6,14}$]$^+$			2							3									
3	[C_3C_1pyr]$^+$									3										
3	[C_4C_1pyr]$^+$									3										
6	[$(C_1)_2C_3$im]$^+$									3					3					

role in mass transfer limitations as the time to reach equilibrium in such mixtures would be a function of the respective viscosity/diffusivity. Sizing heat exchangers in applications utilizing IL−FC refrigerant systems would require proper knowledge of the heat capacity, density, and thermal conductivity of the mixtures. Enthalpy data would further aid in predicting heating duty and molecular interactions in the mixtures. Thermodynamic and transport properties may also assist in understanding molecular mechanisms and/or reaction mechanisms in reactions engineering or media utilizing IL systems.

Various studies on the transport properties of binary mixtures of ILs and refrigerants have illustrated that certain thermodynamic and transport properties of ILs are altered significantly by the addition of fluorinated refrigerants while others are less affected by considerable amounts of added refrigerants. For instance, the viscosity of most IL−FC refrigerant systems decreases to more than 50% of the pure IL viscosity with the addition of moderate amounts of refrigerant (<50 mol %). However, that might not be the case with properties such as thermal conductivity and/or density in which pronounced decreases/increases with molar compositions are not evident at low to moderate compositions.[114−116] Therefore, accurate data on the thermodynamic and transport properties of the mixtures is essential for the proper design of engineering applications utilizing IL−FC refrigerant mixtures.

Diffusion coefficients are essential to understanding mass transfer and selectivity. In the literature, there is data on the diffusion coefficients calculated using Fick's law and on the infinite dilution diffusion coefficients calculated using the semi-infinite volume model. Table 9 and Table 10 present the quantities and respective sources for diffusion coefficients for FC refrigerants and IL mixtures found in the literature.

In addition to diffusion, density and viscosity data are the most abundant of the thermodynamic and transport properties highlighted in this section for FC refrigerant + IL systems. Thermal conductivity, interfacial/surface tension, enthalpy of absorption, and speed of sound each have one respective source that reports data for FC refrigerant/IL mixtures in the open literature while self-diffusivity data is reported in two literature sources. Table 11 and Table 12 present the quantities and respective sources of thermodynamic and transport properties of FC refrigerants and IL mixtures found in the literature. It is worth noting that 26% of the mixture thermodynamic and transport properties (other than Fickian diffusion) reported in the literature are on systems utilizing TFE as a refrigerant. Separation of conventional refrigerant blends would require further knowledge of mixture transport and thermodynamic properties utilizing conventional refrigerants (with boiling points lower than standard temperature). Furthermore, there exists a need to better understand the governing interaction phenomena in IL/gas mixtures so that ILs can be better tailored to meet specific tasks in different mixtures. Assessment of IL/gas interactions requires a multicomponent approach involving physical measured data/properties and molecular simulations.

3.1. Diffusion

Different trends were found after analyzing the diffusion coefficients for different refrigerant−ionic liquid systems. Overall, the diffusion coefficients of the hydrofluorocarbons in the ionic liquids increase with increasing temperature.[50,100] Systems with low-viscosity ionic liquids had a higher diffusivity

https://doi.org/10.1021/acs.chemrev.3c00276
Chem. Rev. XXXX, XXX, XXX−XXX

Table 11. FC Refrigerant and IL Combinations with Thermodynamic and Transport Properties Excluding Diffusion Coefficients[a]

Refrigerant \ Ionic Liquid	[C_2C_1im][BF_4]	[C_2C_1im][Tf_2N]	[C_2C_1im][$N(CN)_2$]	[C_4C_1im][BF_4]	[C_4C_1im][PF_6]	[C_4C_1im][Tf_2N]	[C_6C_1im][BF_4]	[C_6C_1im][PF_6]	[C_6C_1im][Tf_2N]
HCFC-124		71							
HFC-32				117, 117, 117					
HFC-125		72		117, 117, 117	110				
HFC-134a	71	114					97	97	114, 61,97, 61, 61,116
HFC-152a									116
HFC-143a		72			109				
HFC-41					109				
HFC-23					57				
HFO-1234yf									118
HFO-1234ze(E)									118
TFE	115,119		120, 120, 120	121, 121,122	121, 121,123	121, 119,121			
PFC-5114								124, 124	
HFE-125		72							
HFE-143a		72							

Viscosity		Single Temperature Isotherm
		Multiple Temperature Isotherms
Density		Multiple Temperature Isotherms
Thermal Conductivity		Multiple Temperature Isotherms
Surface Tension		Multiple Temperature Isotherms
Speed of Sound		Multiple Temperature Isotherms
Self Diffusivity		Single Temperature Isotherm

[a]The data type is represented by different colors: viscosity (grey), density (orange), thermal conductivity (green), surface tension (blue), speed of sound (pink), and self-diffusivity (yellow).

Table 12. Number of Times Thermodynamic and Transport Properties Have Been Measured for Different Anion and Cation Combinations with Different FC Refrigerants Excluding Diffusion Coefficients

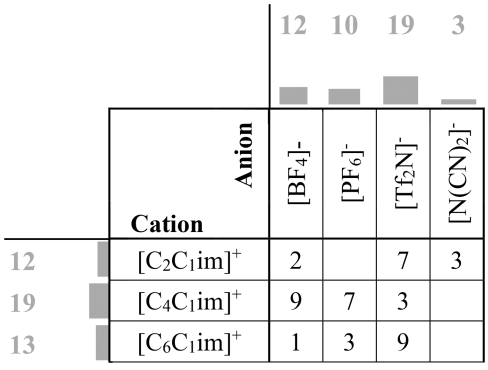

than systems with viscous ionic liquids.[14,68,85] The size of molecules plays an important role in the magnitude of diffusion, as refrigerants with smaller molecules, such as HFC-32, showed a greater diffusivity than systems with larger molecules, such as HFC-125.[78,81] The diffusion coefficients for refrigerants with comparable molecular size, such as HFC-134a and HFO-1234yf, were similar.[85] With HCFC-22, the diffusivity increased exponentially with pressure. Even though some conclusions can be made from trends observed in different systems, there is limited data on diffusion of ionic liquid and refrigerant systems. Collecting this data to better understand diffusivity trends and the impact of different ionic liquid properties on diffusion coefficients is still a work in progress.[8]

3.1.1. Temperature and Pressure. Many studies revealed that the diffusion coefficients of HFCs in ionic liquids increased with increasing temperature and pressure.[50,100]

This was first supported by Liu et al. (2018) who gathered solubility and diffusion data for HFC-32 and HFC-152a in [C_6C_1im][FAP]. Data was gathered at temperatures ranging from 293 to 343 K and at pressures up to 0.5 MPa. The researchers found that increasing the temperature resulted in increasing diffusion coefficients and the solubility order was opposite of the diffusion coefficients. Furthermore, the group found that the data corelated well with the NRTL equation and the Wilke−Chang equation.[50] Liu et al. (2019) continued to support the relationship of temperature and pressure with diffusion coefficients when studying the fluorinated propanes HFC-227ea, HFC-236fa, and HFC-245fa with [C_6C_1im]-[BF_4].[42] Data was measured from 303 to 343 K and at 332 kPa. The authors highlighted the importance of the interdiffusion parameter. The researchers found that these coefficients increased with increasing temperature. Additionally, the interdiffusion data correlated well with the Arrhenius, Litovitz, and Vogel−Fulcher−Tammann equations. The group found that HFC-236fa in [C_6C_1im][BF_4] exhibited the highest interdiffusion coefficients.[42]

He et al. also noted the effect of temperature and pressure on diffusion coefficients. The group measured the diffusion coefficients for refrigerants HFC-32, HFC-125, HFC-161, HFC-143a, HFO-1234yf, and HFC-152a with ionic liquids

https://doi.org/10.1021/acs.chemrev.3c00276
Chem. Rev. XXXX, XXX, XXX−XXX

$[C_6C_1im][Tf_2N]$, $[C_6C_1im][OTf]$, and $[C_6C_1im][BF_4]$. The data correlated well with the Wilke−Chang equation. The authors concluded that increasing temperature increases diffusion coefficients.[100] He et al. continued to support this statement when examining HCFO-1233zd(E) in $[C_6C_1im][Tf_2N]$, $[C_6C_1im][OTf]$, and $[C_6C_1im][BF_4]$. Data was taken at temperatures ranging from 303.1 to 343.2 K and pressures up to 0.14 MPa. The data furthered proved that increasing temperature increased the diffusion coefficients.[91]

3.1.2. Viscosity. Many studies in the literature report that systems with low-viscosity ionic liquids exhibit higher refrigerant diffusivity than systems with viscous ionic liquids.[14,68,85]

Asensio-Delgado et al. made this correlation when collecting the solubility and diffusivity data of HFC-32, HFC-134a, and HFO-1234yf with ionic liquids $[C_2C_1im][BF_4]$, $[C_2C_1im][OTf]$, and $[C_2C_1im][Tf_2N]$.[85] Data was taken via an isochoric saturation method in a temperature range of 283.15 to 323.15 K and at pressures up to 0.9 MPa. The group was successful in correlating the data to the NRTL method. The researchers found that using low-viscosity ionic liquids yielded higher diffusion coefficients ranging from 10^{-10} to 10^{-9} m^2 s^{-1}. Because of this, it was stated that low-viscosity ILs would be viable options to achieve separation.[85] Further studies were conducted with mixtures of HFC-134a, HFC-32, and HFC-1234yf with $[C_2C_1im][SCN]$. The IL $[C_2C_1im][SCN]$ was selected for the study due to its low viscosity resulting in enhancement of diffusivity.[68] It has also been reported that HFC-32, HFC-125, HFC-134a, HFO-1234yf, and HFO-1234ze(E) diffusivities were higher in $[C_2C_1im][N(CN)_2]$ than in $[C_4C_1im][N(CN)_2]$. This result is directly related to the lower viscosity of $[C_2C_1im][N(CN)_2]$.[14]

Morais et al. found this trend to be true when looking at VLE data for HFC-32 and HFC-125 in $[C_4C_1im][BF_4]$, $[C_4C_1im][PF_6]$, and $[C_6C_1im][FAP]$.[81] Data was taken at 298.15 K and at a pressure range of 0.05 to 1.0 MPa. It was noted that HFC-32 and HFC-125 had higher diffusion coefficients in $[C_6C_1im][FAP]$ compared to the other ILs because of the lower viscosity.[81]

Baca et al. conducted measurements on HFC-32 and HFC-125 with six different ILs.[78] It was noted that HFC-32 and HFC-125 had the highest diffusion coefficient in the ionic liquid $[P_{6,6,6,14}][Cl]$ that had the lowest viscosity. This finding further supports the connection between high diffusion coefficients and low viscosity ILs.[78]

He et al. came to a similar conclusion after using the semi-infinite volume technique to measure diffusion coefficients of refrigerants HFC-32, HFC-125, HFC-161, HFC-143a, HFO-1234yf, and HFC-152a with ionic liquids $[C_6C_1im][Tf_2N]$, $[C_6C_1im][CF_3SO_2]$, and $[C_6C_1im][BF_4]$.[100] Data was taken from 303.2 to 343.2 K. The group concluded that the diffusion of HFCs in ionic liquids is smaller than in traditional solvents due to IL higher viscosity. However, it was noted that the diffusivities of HFCs in $[C_6C_1im][Tf_2N]$ were lower than those in $[C_6C_1im][CF_3SO_2]$ even though the viscosity of $[C_6C_1im][CF_3SO_2]$ is higher than the viscosity of $[C_6C_1im][Tf_2N]$. This oddity was attributed to the gas dissolving in the ionic liquid and changing the viscosity.[100]

3.1.3. Size of Molecules. Different investigations have found that the size of the refrigerant molecule has a significant impact on the diffusivity of refrigerants in ionic liquids.[78,81,85]

Morais et al. collected isothermal vapor−liquid equilibrium data using a gravimetric microbalance for systems composed of HFC-32 and HFC-125 with $[C_4C_1im][C_1CO_2]$, $[C_4C_1im][BF_4]$, $[C_4C_1im][PF_6]$, $[C_6C_1im][FAP]$, $[C_6C_1im][Cl]$, and $[C_4C_1im][SCN]$. HFC-32 had a higher diffusivity in $[C_4C_1im][BF_4]$, $[C_4C_1im][PF_6]$, $[C_6C_1im][FAP]$, and $[C_6C_1im][Cl]$. HFC-125 had a higher diffusivity in $[C_4C_1im][C_1CO_2]$. The higher diffusivity of HFC-32 in most ionic liquids is due to the smaller size of the molecule when compared to HFC-125.[81]

Baca et al. found a similar trend to what was observed by Morais et al. The group collected isothermal VLE data of refrigerant−ionic liquid systems with a gravimetric microbalance at a temperature of 298.15 K and pressures ranging from 0.05 to 1.0 MPa. The diffusion coefficients were estimated for $[C_6C_1im][I]$, $[C_6C_1im][Br]$, $[C_6C_1im][Cl]$, $[C_4C_1im][Cl]$, $[C_3C_1im][Cl]$, and $[P_{6,6,6,14}][Cl]$ with HFC-32 and HFC-125. Both refrigerants showed equal diffusions in $[C_3C_1im][Cl]$, while HFC-32 had a greater diffusion in the rest of the ionic liquids.[78]

Asensio-Delgado et al. used an isochoric saturation method to collect vapor−liquid equilibria data and calculate diffusion coefficients for systems composed of HFC-32, HFC-134a, and HFO-1234yf with ionic liquids $[C_2C_1im][BF4]$, $[C_2C_1im][CF_3SO_2]$, and $[C_2C_1im][Tf_2N]$. Absorption data for $[C_2C_1im][BF4]$ was collected with HFC-32 and HFC-134a. HFC-32 showed a greater diffusivity than HFC-134a at most of the temperatures due to its smaller molecular size. HFC-134a and HFO-1234yf diffusivity was also determined in $[C_2C_1im][CF_3SO_2]$. The diffusivity of HFC-134a in $[C_2C_1im][CF_3SO_2]$ was greater at 283.15 and 293.15 K, but the diffusivity of the FC in HFO-1234yf was higher at greater temperatures such as 303.15, 313.15, and 323.15 K.[85]

3.2. Density

In several studies, Shiflett and Yokozeki report molar volume data for several HFCs in $[C_4C_1im][PF_6]$ in the VLLE regime with uncertainties ranging between ±0.3 and ±5.0 cm^3/mol.[57,109,110] The HFCs reported on by Shiflett and Yokozeki include HFC-125, HFC-41, HFC-134a, HFC-143a, HFC-152a, HFC-161, and HFC-23. Shiflett and Yokozeki utilized a volumetric method based on physically measured volumes and masses of the system. Furthermore, Shiflett and Yokozeki utilize the same aforementioned volumetric method to measure the molar volumes of binary mixtures of CFC-113 (CCl_2FCClF_2), CFC-113a (CF_3CCl_3), CFC-114 ($CClF_2CClF_2$), CFC-114a (CCl_2FCF_3), HCFC-123 ($CHCl_2CF_3$), HCFC-123a ($CHClFCClF_2$), HCFC-124 (CF_3CHClF), HCFC-124a (CHF_2CClF_2), and HFC-134a in the ionic liquid $[C_2C_1im][Tf_2N]$ in the VLE and LLE regimes.[71] In another study, Shiflett and Yokozeki utilize the same volumetric method to report molar volumes of binary mixtures of different hydrofluorocarbons and hydrofluoroethers in $[C_2C_1im][Tf_2N]$.[72] The HFCs and HFEs investigated are HFC-125 and HFC-143a and hydrofluoroethers (HFEs) HFE-125 (CHF_2-O-CF_3) and HFE-143a (CH_3-O-CF_3). In all HFC/IL and HFE/IL mixtures investigated by Shiflett et al., negative molar volumes are observed throughout the composition regimes investigated.

Ren and Scurto measured the molar volume of HFC-134a saturated ionic liquids at temperatures of 298.15, 323.15, and 348.15 K and various pressures/compositions in the VLE and VLLE regimes with uncertainties less than ±0.5 cm^3/mol.[97,105] The ILs investigated are $[C_2C_1im][Tf_2N]$, $[C_6C_1im][Tf_2N]$, $[C_6C_1im][BF_4]$, and $[C_6C_1im][PF_6]$. Ren and Scurto utilize a high-pressure static equilibrium apparatus that employs a mass balance and measurement of the actual volume of the phases in

https://doi.org/10.1021/acs.chemrev.3c00276
Chem. Rev. XXXX, XXX, XXX−XXX

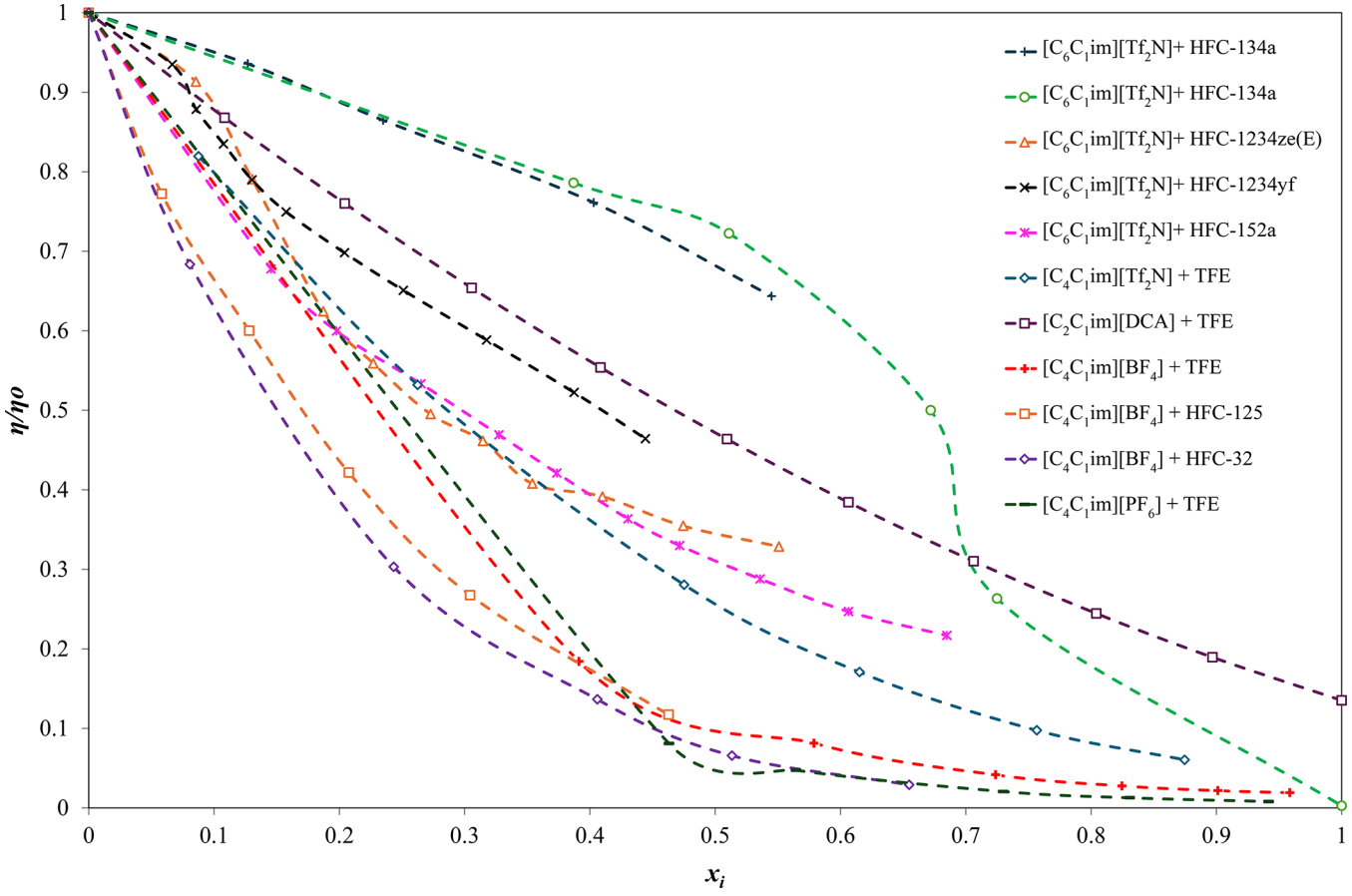

Figure 6. Normalized viscosity of fluorinated refrigerants and IL mixtures at 298.15 K. $[C_6C_1im][Tf_2N]$ + HFO-1234ze(E), $[C_6C_1im][Tf_2N]$ + HFO-1234yf, and $[C_6C_1im][Tf_2N]$ + HFC-152a at 303.15 K.

the system to determine the solubility and molar volumes of the mixture.[112]

More recently, the densities of $[C_4C_1im][BF_4]$ saturated with HFC-125 and $[C_4C_1im][BF_4]$ saturated with HFC-32 have been measured and reported at 298.15 K and molar compositions up to $x_{HFC\text{-}32} \approx 0.7$ and $x_{HFC\text{-}125} \approx 0.5$ utilizing a high-pressure oscillating U-tube densimeter.[117] The mass density of the $[C_4C_1im][BF_4]$/HFC-125 system exhibits an increase with increasing molar composition of the HFC. In contrast, the IL/HFC-32 system exhibits a gradual decrease in mass density with increasing molar composition of HFC-32 in the mixture. Both systems exhibit negative excess molar volumes across the composition range investigated. The density data is reported accurate to ±0.15%.

The fluorinated alcohol, 2,2,2-trifluorethanol (CF_3CH_2OH, TFE), has been proposed as a potential working refrigerant to be coupled with ionic liquids in absorption cycles operating at subambient pressure conditions.[125] Currás et al. measured the density of $[C_4C_1im][BF_4]$ with TFE as well as $[C_2C_1im][BF_4]$ with TFE at atmospheric pressure and temperatures ranging from 283.15 to 323.15 K for the $[C_4C_1im][BF_4]$ system and 293.15 to 323.15 K for the $[C_2C_1im][BF_4]$ system.[115] Currás et al. utilized an oscillating U-tube densimeter in which the fluid is filled into a U-shaped tube and the period of vibration is correlated to density.[14] At all temperatures investigated TFE has a higher pure component density than either of the ILs, $[C_4C_1im][BF_4]$ and $[C_2C_1im][BF_4]$. Densities measured by Currás et al. reflect a diluent effect in which the density increases with increasing molar composition of TFE in the mixture. Interestingly, the data illustrates that the system with the longer alkyl chain on the cation generally exhibits positive trends in excess molar volume with the exception of the values obtained at 333.15 K; however, the $[C_2C_1im][BF_4]$ + TFE system generally exhibits negative excess molar volumes at all temperatures investigated. Another study by Currás et al.[122] reports data on the density of mixtures of $[C_4C_1im][BF_4]$ + TFE with temperatures ranging between 283.15 and 333.15 K and pressures up to 40 MPa. Across all of the isotherms and isobars investigated, TFE exhibits a higher pure component density than the IL and the mixture exhibits a general increase in mass density with increasing molar composition of TFE. Both studies by Currás and co-workers report overall uncertainties of $\pm 4 \times 10^{-4}$ g/cm^3.

In a subsequent study, Currás et al. utilized a high-pressure U-tube densimeter to measure the densities of $[C_2C_1im][BF_4]$ + TFE mixtures and $[C_4C_1im][Tf_2N]$ + TFE mixtures at temperatures ranging between 283.15 and 333.15 K for the $[C_2C_1im][BF_4]$ + TFE system and 293.15−333.15 K for the ($[C_4C_1im][Tf_2N]$) + TFE system and pressures up to 40 MPa.[123] $[C_2C_1im][BF_4]$ has a pure component density lower than that of TFE under all conditions investigated, and the mixture exhibits an increase in density with increasing molar composition of TFE. In contrast, $[C_4C_1im][Tf_2N]$ has a higher pure component density than TFE under all conditions investigated and the $[C_4C_1im][Tf_2N]$ + TFE system exhibits a decrease in density with increasing molar composition of TFE. Their density data is reported with an expanded uncertainty of $\pm 2 \times 10^{-3}$ g/cm^3.

https://doi.org/10.1021/acs.chemrev.3c00276
Chem. Rev. XXXX, XXX, XXX−XXX

Currás et al. also measured the density of mixtures of $[C_4C_1im][PF_6]$ and TFE at temperatures between 288.15 and 333.15 K and pressures up to 40 MPa.[123] At temperatures up to 293.15 K, the density of pure TFE is higher than that of the IL and the difference between the two pure component densities is relatively high compared to subsequent temperatures. Hence, at 288.15 and 293.15 K, the density generally increases with increasing TFE composition. However, at 303.15 K, the pure component densities are relatively closer in value and the trends among the pressures investigated for the mixture are generally increasing toward the pure component density of TFE with increasing TFE molar composition with some isobars exhibiting a slight increase above the pure component TFE density at higher compositions of TFE (>0.90 mol_{TFE}). It is worth noting that any increase above the pure component density at this isotherm is observed to be equal to or less than 2 kg/m^3 which is the reported uncertainty of the density measurements in the study. At subsequent temperatures, the densities of the two components alternate order in terms of higher density at different isobars and the trends differ drastically among the pressures investigated in three general cases: (1) The IL has a lower pure component density, and the density increases toward the pure component TFE density with increasing molar composition of TFE. (2) The density increases above the density of either pure component density. (3) The density of the mixture increases or plateaus below the density of TFE and rises above either component's density at higher TFE compositions (>0.90 mol_{TFE}). Excess molar volumes reported in the study alternate between negative values and positive values with varying curvatures among the isotherms and isobars.

Salgado et al. also utilized an oscillating U-tube densimeter to measure the densities of $[C_4C_1im][BF_4]$, $[C_4C_1im][PF_6]$, and $[C_4C_1im][Tf_2N]$ and TFE binary mixtures at temperatures ranging from 278.15 and 333.15 K with a standard uncertainty of ±0.05% (68% confidence interval).[121] The results of Salgado et al. are in good agreement with those of Currás et al.[115,119,122,123] It is to be noted that the reported mole fractions of the two data sets are not synchronized and some error in the comparison might be attributed to the interpolation of the data (<2%).

Fatima et al. utilized an oscillating U-tube densimeter to measure the density of mixtures of 1-ethyl-3-methylimidazolium dicyanamide $[C_2C_1im][N(CN)_2]$ + TFE at atmospheric pressure and temperatures ranging between 298.15 and 323.15 K.[120] Similar to some of the aforementioned studies of Currás et al., TFE has a higher pure component density than the investigated IL across the temperature regimes investigated and the mixture exhibits an increase in density with increasing molar composition of TFE. The data of Fatima and co-workers is reported with an expanded uncertainty of $\pm 5 \times 10^{-4}$ g/cm^3 at a 95% confidence interval.

3.3. Dynamic Viscosity

Many common pure ionic liquids have relatively high viscosities in comparison to typical organic and inorganic solvents. Some ILs tend to have pure component viscosities that are an order of magnitude greater than those of pure refrigerants under the same conditions (or as saturated liquids at the same temperature). Only a few literature studies exist on the viscosities of ionic liquids and fluorinated refrigerant mixtures. Figure 6 illustrates the normalized viscosities relative to the pure component IL viscosity (η_o = pure component IL viscosity at T) for systems of fluorinated refrigerants and IL mixtures found in the literature.

In 2017, Ahosseini et al. reported the first study on the liquid dynamic viscosity of a biphasic IL and HFC mixture.[61] The authors utilized a high-pressure oscillating-piston viscometer to measure the viscosity of $[C_6C_1im][Tf_2N]$ and HFC-134a at 298.15, 323.15, and 343.15 K and pressures up to 2.03 MPa with an estimated nominal uncertainty of less than 1%. The findings show a large decrease in viscosity with increasing molar composition of the HFC in the liquid mixture. However, contrary to the observed behavior of the IL + TFE systems investigated by Salgado et al.[121] and Fatima et al.[120] to follow, the "excess" viscosity or viscosity deviation from ideality is positive under all of the probed conditions for the $[C_6C_1im][Tf_2N]$/HFC-134a system.

Zhang et al. confirmed the data of Ahosseini et al.[61] that utilized a modified dual-capillary viscometer to measure the liquid phase viscosity of HFC-134a saturated $[C_6C_1im][Tf_2N]$ under similar conditions.[116] The average relative deviation between the data of Ahosseini et al. and that of Zhang et al. is 2.28% with a maximum deviation of 7.23%. Furthermore, Zhang et al. measured the dynamic viscosity of binary mixtures of $[C_6C_1im][Tf_2N]$ saturated with HFC-152a, HFO-1234ze(E), and HFO-1234yf.[116,118] At all temperatures (283.15−343.15 K) and mole fractions (up to 0.70 mol of HFC-152a) investigated, the IL/HFC-152a system exhibits a relatively linear decrease in viscosity with increasing mole fraction of HFC with an increase in the slope of viscosity with composition as temperature decreases. The viscosity deviation from an idealized solution is negative for all conditions investigated in the study for the $[C_6C_1im][Tf_2N]$/HFC-152a system. The data reported by Zhang et al. for the viscosity of $[C_6C_1im][Tf_2N]$/HFO-1234ze(E) and $[C_6C_1im][Tf_2N]$/ HFO-1234yf at temperatures ranging from 283.15 to 343.15 K is the only available literature source on the viscosities of HFO-saturated ILs. Similar to the behavior of investigated IL/HFC mixtures, the viscosity decreases with increasing HFO mole fraction for both IL/HFO systems. The observed decrease is of a relatively linear form. The linearity increases with temperature. Interestingly, the viscosity deviation for the $[C_6C_1im][Tf_2N]$/HFO-1234ze(E) system is negative across the conditions investigated at the lower temperatures (>333.15K); however, at 333.15 K and an HFO-1234ze(E) mole fraction of 0.491, the viscosity deviation is positive (negative at all lower compositions at the same isotherm). At the highest isotherm investigated, 343.15 K, the viscosity deviation takes a sigmoidal curvature in which the viscosity deviation has a positive value at the first mole fraction reported ($x_{HFO\text{-}1234ze(E)} = 0.03$) followed by negative values for all subsequent mole fractions until $x_{HFO\text{-}1234ze(E)} \approx 0.26$ after which the viscosity deviation is positive and increasing for all data points reported. It is important to note that the data reported does not exceed a HFO mole percent of 56%. The $[C_6C_1im][Tf_2N]$/HFO-1234yf exhibits positive deviations at 283.15 K across the limited composition regime investigated ($x_{HFO\text{-}1234yf} < 0.38$). At 293.15, 303.15, 313.15, and 323.15 K, the viscosity deviations are negative across the composition regimes considered ($x_{HFO\text{-}1234yf} < 0.5$). At 333.15 and 343.15 K, the viscosity deviation is negative until a HFO molar composition of ∼0.18 and ∼0.17, respectively, after which the deviation is positive and increasing for all subsequent composition points ($x_{HFO\text{-}1234yf} < 0.5$). The data of Zhang is reported to be accurate to ±0.1 cP.

The viscosities of $[C_4C_1im][BF_4]$ saturated with HFC-125 and $[C_4C_1im][BF_4]$ saturated with HFC-32 have been measured and reported at 298.15 K and pressures up to 1.23

https://doi.org/10.1021/acs.chemrev.3c00276
Chem. Rev. XXXX, XXX, XXX−XXX

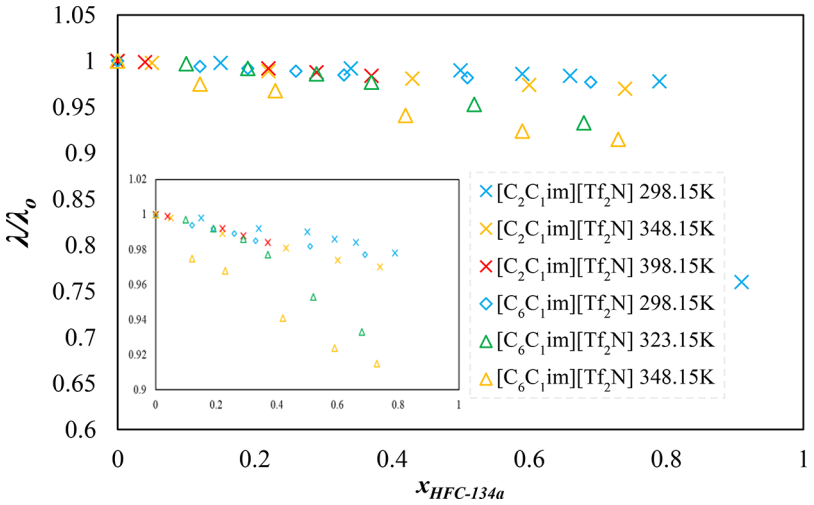

Figure 7. Normalized thermal conductivity of fluorinated refrigerants and IL mixtures. Inset: enlarged region between λ/λ_o = 0.9 and 1.0.

MPa with a nominal uncertainty of ±1 cP.[117] Both systems exhibit drastic decreases in viscosity with increasing mole fraction of the HFC. The IL/HFC-125 exhibits positive viscosity deviations across the composition ranges reported ($x_{HFC-125}$ < 0.5), while the IL/HFC-32 system exhibits negative deviations for all compositions investigated (x_{HFC-32} < 0.7).

Salgado et al. measured the dynamic viscosity of $[C_4C_1im][BF_4]$, $[C_4C_1im][PF_6]$, and $[C_4C_1im][Tf_2N]$ and TFE binary mixtures at atmospheric pressure and temperatures ranging from 278.15 and 333.15 K utilizing a rotational viscometer with an uncertainty of 2% (95% confidence interval).[121] For reference, pure component ILs $[C_4C_1im][BF_4]$, $[C_4C_1im][PF_6]$, and $[C_4C_1im][Tf_2N]$ at 298.15 K have viscosities of 106, 274, and 51.6 cP, respectively. Pure component TFE has a reported viscosity value of 1.84 cP at 298.15 K and atmospheric pressure. A general diluent effect is observed across the temperature ranges investigated in which the viscosity drastically decreases with increasing molar composition of TFE. The "excess" viscosity or viscosity deviation from an idealized solution for all of the systems investigated is negative. $[C_2C_1im][N(CN)_2]$ is a hydrophilic IL with relatively low viscosity which increases its potential feasibility in various engineering applications. Fatima et al. employed a falling-ball viscometer to measure the viscosity of $[C_2C_1im][N(CN)_2]$ + TFE mixtures at temperatures ranging from 298.15 to 323.15 K and atmospheric pressure with expanded uncertainties ranging between 0.20 and 0.80 cP.[120] While $[C_2C_1im][N(CN)_2]$ has a lower pure component viscosity than any of the ILs investigated by Salgado et al., a general diluent effect is still observed throughout the temperature ranges investigated. The viscosity of the mixture decreases with increasing TFE mole fraction. Similar to the aforementioned binary systems investigated by Salgado et al., the viscosity deviation from ideality is negative at all temperatures and compositions investigated.

3.4. Thermal Conductivity

A single publication exists on IL−FC refrigerant mixtures that reports the thermal conductivity of $[C_2C_1im][Tf_2N]$ saturated with HFC-134a and $[C_6C_1im][Tf_2N]$ saturated with HFC-134a.[114] The study utilizes the transient hot-wire technique to measure the thermal conductivity of the biphasic systems $[C_2C_1im][Tf_2N]$/HFC-134a and $[C_6C_1im][Tf_2N]$/HFC-134a at temperatures up to 398.15 and 348.15 K, respectively. The thermal conductivity of both systems decreases linearly with increasing HFC composition. Nevertheless, the thermal conductivity of the mixture at low and moderate HFC composition regimes is continuously dominated by the pure IL thermal conductivity rather than an equal contribution of both components. The thermal conductivity does not exhibit a significant decrease until very high molar compositions of the HFC in $[C_2C_1im][Tf_2N]$ are attained ($x_{hfc-134a}$ > 0.90). The IL with the longer alkyl chain on the cation ($[C_6C_1im][Tf_2N]$) exhibits a larger decrease in thermal conductivity with increasing molar composition of the HFC. This behavior is in contrast to what is observed for a system of an IL ($[C_6C_1im][Tf_2N]$) saturated with carbon dioxide. In this case, the thermal conductivity passes through a minimum at lower compositions of CO_2 followed by a gradual increase with increasing composition of dissolved CO_2 as a result of the higher pressures required for dissolution.[126] The lower pressures required for HFC-134a dissolution result in a diluent effect generally outweighing potential hydrostatic pressure effects on the thermal conductivity. The reported thermal conductivity values have a nominal uncertainty of less than 3 mW/m-K. The normalized thermal conductivities (λ/λ_o) of the $[C_6C_1im][Tf_2N]$/HFC-134a and $[C_2C_1im][Tf_2N]$/HFC-134a systems as a function of dissolved HFC mole composition are illustrated in Figure 7.

3.5. Self-Diffusivity

Applications coupling refrigerant and ILs are inherently multicomponent mass transfer problems. For multicomponent systems, the Maxwell−Stefan formulation is often preferred over the Fickian approach and has been adopted in commercial simulation software such as Aspen Plus.[127] While Fickian diffusion coefficients present a rather complex composition dependence, Maxwell−Stefan diffusion coefficients are more well behaved.[128] Maxwell−Stefan diffusion coefficients can be obtained using physically sound relations from self-diffusion coefficient data.[129−131]

Self-diffusion coefficients provide a measure of the average squared displacement of a molecule that is caused by Brownian motion in the absence of external driving forces.[132] Besides being used to obtain mutual diffusion coefficients, self-diffusion coefficients also provide insight into molecular structure. Other applications include, but are not limited to, the characterization and screening of membranes for gas separations[133] and correlations for the glass transition temperature in polymers.[134]

https://doi.org/10.1021/acs.chemrev.3c00276
Chem. Rev. XXXX, XXX, XXX−XXX

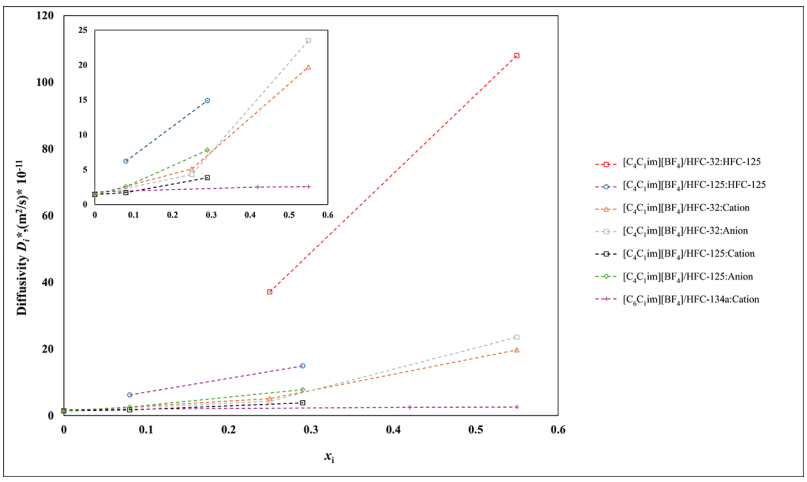

Figure 8. Self-diffusivity of fluorinated refrigerants and IL mixtures. Inset: enlarged region between $D_i^* = 0$ and 25×10^{-11} m^2/s.

Experimental self-diffusion coefficients are obtained using tracer methods, neutron scattering, or pulsed field gradient nuclear magnetic resonance (PFG-NMR) techniques.[135] The latter methodology is preferred having been adopted to quantify the vast majority of self-diffusion coefficient data reported in the literature.[136] To our knowledge, pulsed field gradient NMR is the only approach ever used in the determination of self-diffusion coefficients in ionic liquids + refrigerant mixtures.[61,117]

Pulsed field gradient NMR involves applying pulsed field gradients with different intensities to the sample. The signal is weakened as the gradient intensity increases, and the self-diffusion coefficient D is obtained from the slope of the diffusion decay, according to eq 2

$$\ln\left(\frac{I}{I_0}\right) = \left[-\gamma^2\delta^2G^2\left(\Delta - \frac{\delta}{3} - \frac{\tau}{2}\right)\right]D \tag{2}$$

where I and I_0 are the signal intensity in the presence and absence of the applied gradient, γ is the gyromagnetic ratio, δ is the length of the gradient pulse, G is the gradient strength, Δ is the diffusion time, and τ is the delay for refocusing.

Experimental self-diffusion coefficient data for mixtures of ionic liquid + refrigerant is rather scarce in the open literature. In fact, only two studies have been found for this review, as summarized in Table 11. Figure 8 illustrates trends in self-diffusion coefficients of respective constituents in mixture at 298.15 K.

In the first study, Ahosseini et al. reported the cation and refrigerant self-diffusion coefficients in $[C_6C_1im][Tf_2N]$ + HFC-134a mixtures.[61] The authors found that, as the refrigerant composition increases, the self-diffusion coefficient of the cation sharply increases and the self-diffusion coefficient of the refrigerant decreases. Besides, the authors verified that the cation self-diffusion coefficient follows a Stokes−Einstein type relation with the mixture viscosity. The authors report a general uncertainty in self-diffusion coefficients of less than 5%.

In the second study, Wang et al.[117] reported experimental measurements of the cation, anion, and refrigerant self-diffusion coefficients in $[C_4C_1im][BF_4]$ + HFC-32 or HFC-125. The authors observed a similar trend, with the cation and anion self-diffusion coefficients increasing as the refrigerant content increases as well as the refrigerant self-diffusion increasing with increasing refrigerant content in the mixture. In the study, the experimental results were compared with molecular dynamics predictions and excellent agreement was demonstrated between the experimental measurements and the simulations.

Overall, despite the importance of self-diffusion coefficients in process design and in the understanding of molecular structure, the literature for self-diffusion coefficients in systems of interest for hydrofluorocarbon separations using ionic liquids is very limited. Only two types of imidazolium-based ionic liquids and only three types of refrigerants have been studied so far. Given the potential that ionic liquids have demonstrated as entrainers for extractive distillation of HFC mixtures, more studies dedicated to self-diffusion coefficients should be carried out to build a comprehensive database for robust process design.

3.6. Speed of Sound

A single study exists on the speed of sound of an IL/fluorinated refrigerant mixture.[120] A single path-length method is used to measure the speed of sound of mixtures of $[C_2C_1im][N(CN)_2]$ and TFE at atmospheric pressure and temperatures between 298.15 and 323.15 K. The study reports pure component speed of sound for the IL more than two times that of pure TFE at all of the temperatures investigated. The mixture speed of sound decreases somewhat linearly ($R^2 > 0.96$) with increasing mole fraction of TFE in the mixture for all temperatures investigated. The reported uncertainty in sound velocity is ±0.5 m/s at a 95% confidence interval.

3.7. Interfacial and Surface Tension

Perfluorohexane or tetradecafluorohexane ($CF_3-CF_2-CF_2-CF_2-CF_2-CF_3$, PFC-5114) has been utilized as a coolant in electronics and has previously been proposed as a coolant for space-based applications.[137] Matsuda et al. measured the surface tension of $[C_6C_1im][PF_6]$ saturated with perfluorohexane in air as well as the interfacial tension of the IL saturated with perfluorohexane (under LLE conditions).[124] The interfacial tension of $[C_6C_1im][PF_6]$/perfluorohexane in air stays relatively constant with increasing temperature, while the interfacial tension of the IL saturated with perfluorohexane decreases linearly with increasing temperature. The reported uncertainty is ±0.05 mN/m.

3.8. Heat Capacity and Excess Heat

A single study reports on the excess heat of an IL and a refrigerant mixture.[115] Currás et al. report on the excess heat of binary mixtures of the ILs $[C_2C_1im][BF_4]$ and $[C_4C_1im][BF_4]$

https://doi.org/10.1021/acs.chemrev.3c00276
Chem. Rev. XXXX, XXX, XXX−XXX

with the refrigerant TFE at 293.15 and 333.15 K and atmospheric pressure. The total uncertainty reported is less than 1%. The findings illustrate that the mixing for both systems is endothermic and the heat of mixing is higher for the $[C_4C_1im][BF_4]$/TFE system.

Despite the importance of heat capacity data for mixtures of fluorinated refrigerants and ILs, such data is not present in the open literature. Heat capacity values for the mixtures are imperative for proper design and scaling of engineering applications employing such mixtures and for proper understanding and characterization of these systems, and this offers a new opportunity for researchers to measure and model the heat effects of fluorocarbons in ILs.

3.9. Thermodynamic and Transport Properties General Trends

Diffusion coefficients were calculated for FC refrigerant and IL combinations. The most common refrigerant was HFC-32, while the most frequent IL was $[C_4C_1im][PF_6]$. Diffusion coefficients were calculated at single and multiple temperatures and pressures. The most common cation for diffusion coefficient calculations was $[C_4C_1im]^+$, and the most common anion was $[Tf_2N]^-$.

All reported data on transport properties of fluorinated refrigerant/IL mixtures involves imidazolium-based ILs. After diffusion, viscosity and density are the most reported properties followed by thermal conductivity and self-diffusivity. From these properties, refrigerant TFE and IL $[C_2C_1im][Tf_2N]$ were reported most frequently. Additionally, the cation $[C_4C_1im]^+$ and the anion $[Tf_2N]^-$ appeared in the most studies. Density trends are non-uniform such that an increase, decrease, or no change in mass density is possible with addition of refrigerant, while viscosity always decreases sharply with increasing dissolved refrigerant content. The thermal conductivity of HFC/IL mixtures remains similar to that of the pure IL thermal conductivity at low-to-moderate mole fractions of dissolved HFC. The self-diffusivities of all constituents (HFC, cation, anion) increase with increasing dissolved HFC composition as illustrated in a single study, while another study illustrates the increase in the cation self-diffusivity with increasing HFC composition. Speed of sound and excess heats of FC-refrigerant/IL mixtures are reported only for systems involving TFE. The past decade has experienced a general increase in studies probing thermodynamic and transport properties of fluorinated refrigerant/IL mixtures. However, there still exists a paucity in reported data on calorimetric properties as well as surface/interfacial tension. Surface tension, heat capacity, and excess heats can have large contributions on unit design involving two-phase flow. Additionally, such properties can provide vital insight on molecular interactions of refrigerant/IL mixtures. More studies on the thermophysical properties of the mixtures are required for proper feasibility assessment and unit design.

4. MOLECULAR SIMULATION AND EQUATION OF STATE MODELING

4.1. Molecular Simulation of Refrigerants and Their Mixtures

Molecular simulation has long been used as an important tool to bridge theory and experiments. Simulations have been used to validate new theories, provide an atomic-level understanding and explanation for experiments, and guide experiments by making predictions. Not surprisingly, molecular simulations have played an important role in the development of refrigerants. For example, molecular simulation can be used to study the physical behavior of a refrigerant under extreme conditions such as high temperature and high pressure, where experiments may be very difficult. Molecular simulations can also be used to test the validity of equations of state used to model refrigerants.[138,139] Molecular simulations provide insight into the behavior of uncommercialized refrigerants such as most hydrofluoro-olefins (HFOs).[140] Promisingly, a molecular simulation can be used to systematically screen thousands of potential compounds to identify new refrigerants or search for solvents that might be effective in separating azeotropic refrigerant mixtures.

Some of the first refrigerants to be investigated by molecular simulation were the chlorofluorocarbons (CFCs). In 1988, Mountain et al.[141] developed pair potentials comprised of 12−6 Lennard-Jones (LJ) and Coulombic interactions for liquid CFC-12 (CF_2Cl_2) and HCFC-22 (CHF_2Cl). The LJ size and energy parameters (σ and ϵ) were tuned using experimental pressure and energy. Further estimation of heat capacity and diffusivity suggested that the model was satisfactory for that time. Based on the work done by Lísal et al.[142] on modeling ethane-like refrigerant derivatives, Stoll et al.[143] proposed a two-center Lennard-Jones plus point dipole (2CLJD) or quadrupole (2CLJQ) model for 54 different types of molecules, including carbon monoxide and halogenated derivatives of methane, ethane, and ethene. Parameters were obtained by fitting experimental critical temperature, vapor pressure, and saturated liquid density data. Molecular dynamics (MD) and Monte Carlo (MC) simulations were performed to calculate vapor−liquid equilibrium (VLE) properties like saturated liquid density, vapor pressure, and the enthalpy of vaporization. The models were found to be quite accurate, yielding mean deviations relative to experiments of less than 5% for all properties. Fernández et al.[144] used the same 2CLJD pair potential as Stoll et al.[143] to calculate dynamic properties such as shear viscosity and thermal conductivity of ten refrigerants, including CFC-11 ($CFCl_3$), CFC-12, HCFC-22, HFC-23, HFC-41 (CH_3F), HCFC-123, HFC-134a, HCFC-142b (CH_3CF_2Cl), HFC-143a, and HFC-152a. Equilibrium MD simulations with the Green−Kubo method were conducted to calculate viscosity and thermal conductivity. Although internal degrees of freedom were neglected in this model, the average deviation of these two properties from experiments for all refrigerants was less than 25%, suggesting a high degree of transferability of the 2CLJD model to other properties.

Classical force fields with fixed partial charges neglect electronic polarization, which can make it difficult to capture some properties of refrigerants. To address this, Lin et al.[145] developed a polarizable force field based on the classical Drude oscillator model which is a simplified theoretical model to mimic the effects of electronic polarizability for hydrochlorocarbons (HCCs), including HCC-140a (CH_3CCl_3), HCC-150a (CH_3CHCl_2), and HCC-160 (C_2H_5Cl). The model was based on the additive CHARMM general force field, incorporated Drude particles into carbon and chlorine, and turned on the LJ interactions between halogen Drude particles and hydrogen. Also, a pair-specific LJ parameter was utilized instead of standard combining rules. Lin et al. conducted MD simulations to reproduce the enthalpy of vaporization, molecular volume, static dielectric constant, and hydration free energy. Quantum calculations were used to examine the dipole moment and polarizability. The transferability of the developed parameters

https://doi.org/10.1021/acs.chemrev.3c00276
Chem. Rev. XXXX, XXX, XXX−XXX

was validated by comparing the pure solvent properties of 20 other halogenated aromatic and aliphatic derivatives with experiments.

Lísal and Vacek[146] introduced a semirigid all-atom model for HFC-125 and HFC-134a, which used Halgren's Buf 14−7 function and the Coulombic potential to describe the repulsion−dispersion and electrostatic interactions, respectively. Halgren's Buf 14−7 function and the Coulombic potential were applied to describe the repulsion−dispersion and electrostatic interactions, respectively. Radial distribution functions (RDFs) showed the existence of F−H hydrogen bonding interactions. The following negative part after the rapid initial decay of angular velocity autocorrelation functions versus time demonstrated the cage effect; i.e., most molecules reverse their velocity due to the rebound from neighboring molecules. Overall, the model was able to predict thermodynamic properties well and provided a promising model for ethane-type refrigerants for later studies. The same authors later applied the 2CLJD model to study the vapor−liquid equilibrium of binary mixtures, HFC-125 with HFC-134a and HFC-134a with HFC-32.[147] The researchers proposed the reaction Gibbs ensemble Monte Carlo (RGEMC) method to evaluate the VLE properties of binary mixtures, which combines Gibbs ensemble Monte Carlo (GEMC) and the reaction ensemble Monte Carlo method. This RGEMC method does not require information on mixtures and only uses an intermolecular potential and the vapor pressures of pure components. Excellent agreement was achieved on the pressure composition diagram of these two binary systems at different temperatures relative to REFPROP data, and comparable accuracy was found between the RGEMC method and the Wilson or UNIFAC approaches.

Potter et al.[148] developed a transferable semirigid all-atom force field with a 12−6 LJ potential and point charge Coulombic interactions for fluoromethanes, including HFC-32, HFC-23, and PFC-14. The mean absolute percent errors (MAPEs) of latent enthalpy of HFC-32, HFC-23, and PFC-14 relative to experiments were 11%, 3%, and 12%, respectively, while the MAPEs of the vapor pressure of HFC-32, HFC-23, and PFC-14 were 122%, 75%, and 32%, respectively. The uncertainties of latent enthalpy and liquid density of these refrigerants at different temperatures were on the order of 0.1 kJ/mol and 0.01 g/cm^3, and the relative uncertainties of vapor pressure varied from 1% to 22% depending on the temperature and refrigerant. The model does a good job matching orthobaric densities for all three refrigerants but fails to reproduce the structure of HFC-32, presumably due to the neglect of polarization. MD simulations were also applied to study the difference in thermophysical properties of three isomeric pairs of fluoroethanes: HFC-134 (CHF_2CHF_2) and HFC-134a, HFC-143 (CHF_2CH_2F) and HFC-143a, and HFC-152 (CH_2FCH_2F) and HFC-152a using the semirigid all-atom model.[149] The results of this work agreed with experimental molar volume and potential energy quite well. HFC-152 presented the greatest intramolecular rotational contribution to total potential energy among these fluorinated ethanes. Larger normal boiling points and larger heats of vaporization were observed in HFC-134 and HFC-143 compared to their isomers because of the relatively larger repulsion−dispersion interactions. At the same time, HFC-134 and HFC-143 have smaller gas-phase dipole moments and smaller Coulombic interaction energy than their isomers, HFC-134a and HFC-143a. HFC-152 had a higher normal boiling point, lower critical temperature, smaller heat of vaporization, larger gas-phase dipole moment, and weaker Coulombic interaction than its isomer, HFC-152a. RDFs demonstrated the existence of hydrogen bonding between F and H atoms. It was suggested that stronger F−H repulsion−dispersion interactions lead to higher normal boiling points for HFC-134, HFC-143, and HFC-152 compared to their corresponding isomers. ***SAFETY NOTE: Unlike many HFCs described in this review, it should be noted that HFC-143 (CHF_2CH_2F) and HFC-152 (CH_2FCH_2F) are highly toxic compounds and any attempt to synthesize or use the compounds in experimental research should be avoided.***

MD simulations were employed to study the liquid structure of HFC-32 using all-atom 12-6 LJ and Coulumbic pair potentials.[150] Higashi and Takada characterized site-to-site RDFs, coordination numbers (CNs), pair potential energy distribution functions, and the lifetime of clusters. Strong attractive interactions were found between H and F atoms, discovering that the interaction energy of F−H is the same as that of H_2O-CH_3F, and revealed that there are three bonding patterns: single F−H, double F−H, and triple F−H, where the single and double patterns contribute the most to thermodynamic properties of liquid HFC-32. Lísal and co-workers[151] then employed Higashi and Takada's model[150] to study the Joule−Thomson expansion process of HFC-32 using the constant enthalpy−constant pressure (NPH) MC simulation. The simulations covered a wide range of thermodynamic states and predicted the final temperatures of an expansion and the Joule−Thomson coefficient; the results agreed with those from an equation of state (EOS)[152] quite well.

Fermeglia et al.[153] developed a semirigid all-atom force field from quantum calculations with a 9−6 LJ potential and standard Coulombic interaction with partial charges for HFC-32, HFC-161, HFC-152a, HFC-134, HFC-134a, HFC-143, HFC-143a, and HFC-125. Good agreement was found between simulations and experiments for intramolecular energetic and geometric properties (i.e., bond lengths and angles) of isolated molecules. Since the results from the vibrational spectrum are highly tied to dynamic properties, the normal modes of HFCs were measured and compared with experimental data. Reasonably good agreement between experiment and simulation justified that the force field can account for dynamic properties. MD simulations were performed under the constant-temperature, constant-pressure (NPT) ensemble to compute liquid density, which agreed with experiments quite well. GEMC simulations were applied to study the properties of VLE. The average deviation between experimental and simulated saturated liquid and vapor densities was around 2%.

Peguin et al.[154] proposed an all-atom force field for HFC-134a based on the OPLS-AA model. Four potential models were provided with different partial charges and 12−6 LJ parameters and conducted molecular simulations to validate these models. The best force field had average deviations of 0.7%, 4.4%, 3.2%, 0.2%, 0.1%, 6.2%, 0%, and 2.2% compared with experimental liquid density, vapor density, vapor pressure, critical density, critical temperature, critical pressure, boiling temperature, and heat of vaporization, respectively. The uncertainties of predicted critical density, critical temperature, critical pressure, normal boiling point, heat of vaporization at 298 K, and surface tension were 0.2 kg/m^3, 0.1 K, 6.2 bar, 0 K, 2.2 kJ/mol, and 2.9 mN/m, respectively. The simulated surface tension also fell within the experimental range, and the deviation of the interfacial tension against water was 21.5% relative to experiments. The larger difference was explained by the fact that the SPC/E water model that was used cannot accurately reproduce the surface tension of

https://doi.org/10.1021/acs.chemrev.3c00276
Chem. Rev. XXXX, XXX, XXX−XXX

water. The model is considered the first all-atom force field of HFC-134a that uses the common 12−6 LJ potential.

Smith et al.[155] employed a series of MC simulations to calculate the isoenthalps of HFC-134a and HFC-143a and the vapor-compression refrigeration cycle of the binary mixture of HFC-134a and HFC-32 using the rigid 2CLJD model. The force fields from Lísal et al.[142] and Stoll et al.[143] were compared for performance, and it was found that Stoll's force field more accurately predicted the VLE properties of pure HFCs because the parameters were fitted on a larger experimental data set. The multistage molecular simulations require less experimental data than traditional macroscopic methods and can achieve a similar level of accuracy to the EOS approach in the REFPROP package. Inspired by Lísal et al.,[151] Figueroa-Gerstenmaier et al.[156] applied NPH MC simulations to compute the isoenthalps, Joule−Thomson coefficients, and Joule−Thomson inversion curves of HFC-125, HFC-134a, and HFC-152a. The rigid 2CLJD force field was used and accurately incorporated the specific heat of the ideal gas. It was found that molecular simulations can span a wider range of thermodynamic conditions than the EOS and were in excellent agreement with REFPROP. Compared with simple cubic EOSs, molecular simulations provide more quantitatively accurate estimations of Joule−Thomson related properties.

Yang et al.[157] proposed two newly developed all-atom force fields for HFC-152a with the AMBER functional form. These two models have the same intramolecular parameters but used different 12−6 LJ parameters and different partial charges. GEMC simulations were applied to study VLE properties of pure HFC-152a and the binary mixture of HFC-152a and HFC-32. The best force field had mean absolute deviations of 0.89%, 2.32%, and 2.84% relative to experiments from 250 to 360 K for saturated liquid density, saturated vapor density, and vapor pressure of pure HFC-152a, respectively. The average deviations of critical density, critical temperature, critical pressure, boiling temperature, and heat of vaporization of pure HFC-152a at 308.15 K were 0.49%, 0.38%, 3.80%, 0.34%, and 0.45%, respectively. The relative uncertainties of liquid density, vapor density, vapor pressure, and heat of vaporization of HFC-152a from 258.15 to 358.15 K for the best force field ranged from 1% to 4%, from 2% to 14%, from 4% to 9%, and from 2% to 10%, respectively. It was found vapor pressure and heat of vaporization are largely dependent on the dipole moment and also justified the ability of these force fields to precisely predict the phase equilibrium properties of the HFC-152a and HFC-32 binary mixture. MD simulations were employed to calculate the liquid density, thermal expansivity, shear viscosity, and self-diffusivity of HFC-152a. Good agreement between simulation and experiment demonstrated that the proposed force fields are capable of comprehensively and accurately describing the thermophysical behavior of HFC-152a. Partial RDFs showed the existence of weak hydrogen bonding between F and H atoms.

Befort et al.[158] developed a new workflow that utilizes machine learning methods to optimize the 12−6 LJ parameters of HFC-32 and HFC-125 while retaining the partial charges and intramolecular parameters of GAFF. MD simulations were employed to obtain liquid density and GEMC simulations to compute liquid density, vapor density, vapor pressure, and enthalpy of vaporization. A Gaussian process surrogate model was used to reduce the number of simulations required to efficiently search and screen promising parameter sets from half a million sets generated from Latin hypercube sampling. Multiple high-quality parameter sets were found for each HFC, and each had improved performance relative to the original GAFF model as well as Raabe's hand-tuned HFC-32 model.[159,160] The workflow has been applied to other refrigerants including HFC-143a (CF_3CH_3), HFC-134a (CH_2FCF_3), HC-50 (CH_4), HC-170 (C_2H_6), and PFC-14 (CF_4)[161] and can be generalized to more complex molecules. The recommended models have the transferability to accurately predict other properties that were not used during force field optimization.

Raabe and Maginn[162] developed the first available force field for 2,3,3,3-tetrafluoro-1-propene (HFO-1234yf) based on the AMBER force field functional form. The intramolecular parameters and partial charges were derived from quantum calculations and fine-tuned the LJ parameters against experimental data. GEMC simulations were conducted to compute the VLE properties, and MD simulations were utilized to study the structural properties. The overall agreement between simulated densities, vapor pressure, and normal boiling point and experiments was excellent, and the averaged deviations of critical temperature and critical density were 0.4% and 1.7%, respectively. Critical pressure was in the experimental range, and the difference between the simulated heat of vaporization and the reported value in the literature was only 1 kJ/mol. Partial RDFs indicated hydrogen bonding interactions between the F atom of the $-CF_3$ site and the H atoms. The same authors[163] then extended that work to more HFO molecules and developed a transferable force field for 3,3,3-trifluoro-1-propene (HFO-1243zf, $CF_3CH{=}CH_2$), HFO-1234yf, and hexafluoro-1-propene (PFO-1216, $CF_3CF{=}CF_2$) based on AMBER. The VLE properties of HFO-1234zf computed from GEMC simulations, including vapor pressure, heat of vaporization, critical temperature, and normal boiling point, agreed well with the available experimental values. Although experimental data on PFO-1216 is limited, the force field can be validated on reasonable predictions of properties that were available in experiments, including vapor pressure, liquid density, and critical temperature. Based on previous VLE simulations of HFO-1234yf,[162] further MD simulations were performed to compute density, isobaric heat capacity, thermal expansivity, shear viscosity, and self-diffusivity of pure liquid HFO-1234yf. Good agreement between simulation and available experimental data further validated the accuracy of the force fields. Skarmoutsos and Hunt[252] also employed the model from Raabe and Maginn[162] to study the dynamic and structural properties of weakly hydrogen-bonding liquid HFO-1234yf using MD and ab initio quantum simulations. Studied properties include center of mass (COM) and partial RDFs, residence and reorientational dynamics, diffusivity, spectral densities, etc. Paulechka et al.[164] also developed a force field for HFO-1234yf based on the OPLS-AA functional form and validated the model by VLE simulations. Deviations were observed in simulated liquid density and saturated pressure compared with experiments.

Raabe further extended the transferable force field[163] to describe additional HFO molecules, including trans-1,3,3,3-tetrafluoropropene (HFO-1234ze(E)), cis-1,3,3,3-tetrafluoropropene (HFO-1234ze), and cis-1,2,3,3,3-pentafluoropropene (HFO-1225ye(Z), $CHF{=}CFCF_3$).[165] Raabe updated the force field parameters of F atoms of the −CHF site of HFO-1225ye(Z) and the $-CF_2$ site of HFO-1216. GEMC simulations were carried out and achieved good estimations of the VLE properties of these compounds. The prediction of normal

https://doi.org/10.1021/acs.chemrev.3c00276
Chem. Rev. XXXX, XXX, XXX−XXX

boiling point can distinguish the cis- and trans-isomers, like HFO-1234ze and HFO-1234ze(E). MD simulations were conducted to investigate RDFs of HFO-1234ze and HFO-1234ze(E) and illustrated small differences in the local ordering structure between isomers. The same author used the force field developed in Raabe (2012)[165] to conduct GEMC simulations to study the VLE behavior of the binary mixtures of HFO-1234yf or HFO-1234ze(E) with HFC-32 or CO_2 from 273.15 to 313.15 K.[159] A new all-atom force field was developed for HFC-32, and the TraPPE force field was used to describe CO_2. VLE results from GEMC simulations agreed well with experiments and the PC-SAFT equation of state for HFO-1234yf or HFO-1234ze(E) with HFC-32 binary mixtures, and simulations provided predictions of HFO-1234yf or HFO-1234ze(E) with CO_2 mixtures which is consistent with the PC-SAFT correlation. Raabe's model for HFOs shows excellent potential in accurately predicting properties of mixtures. Later, Raabe performed MD simulations to study the density, diffusivity, viscosity, and structural properties of pure liquid HFO-1234yf, HFO-1234ze, HFO-1234ze(E), and HFO-1216 and the binary mixtures with HFC-32 or CO_2.[160] HFO-1234ze and HFO-1234ze(E) had higher density and viscosity than HFO-1234yf due to the stronger Coulombic interactions caused by the larger dipole or quadrupole moment. Different charge distributions also lead to different local ordering of these HFO compounds, as characterized by RDFs and spatial distribution functions (SDFs). HFC-32 prefers to associate with HFO-1234ze, while CO_2 favors HFO-1216, which is consistent with the observation that HFC-32 and CO_2 present the lowest diffusivity in HFO-1234ze and HFO-1216 among all studied mixtures, respectively.

To better model HCFO molecules, Raabe fine-tuned the LJ parameters of the Cl atom by fitting to experimental saturated densities and vapor pressure of trans-1-chloro-3,3,3trifluoropropene HCFO-1233zd(E).[166] GEMC simulations were performed to compare the VLE properties of HCFO-1233zd(E), cis-1-chloro-3,3,3-trifluoropropene (HCFO-1233zd(Z), CHCl=$CHCF_3$), cis-1,1,1,4,4,4-hexafluorobutene (HFO-1336mzz(Z), CF_3CH=$CHCF_3$), and trans-1,1,1,4,4,4-hexafluorobutene (HFO-1336mzz(E)). The cis-isomer with a higher dipole moment showed a higher normal boiling point than the trans-isomer. Simulations also predicted that HCFO-1233zd(E) and HFO-1336mzz(Z) have lower vapor pressure than 1,1,1,3,3-pentafluoropropane (HFC-245fa), a widely used working fluid in organic Rankine cycles. HFO-1336mzz(Z) had higher liquid density and heat of vaporization than HFC-245fa, while HCFO-1233zd(E) had lower liquid density and similar heat of vaporization relative to HFC-245fa. Raabe employed GEMC simulations to study the VLE properties of the ternary mixture R-445A, which consists of CO_2, HFC-134a, and HFO-1234ze(E) with a molar composition of 0.141, 0.091, and 0.768, respectively.[167] Raabe also studied the phase behavior of binary mixtures of CO_2/HFC-134a, HFC134a/HFO-1234ze-(E), and CO_2/HFO-1234ze(E) and conducted MD simulations to compute the density and viscosity of R-445A in the liquid phase. Good agreement was observed between simulations and REFPROP. Raabe developed force field parameters for HFO-1123 (CF_2≡CHF) and studied the density, viscosity, and VLE properties of HFC-134a/HFO1234ze(E) and HFO-1234yf/HFO-1234ze(E) binary mixtures.[168] GEMC simulations were also applied to investigate the VLE properties of HFO-1123/HFC-32, HFO-1123/HFO-1234yf, HFO-1123/HFO-1234ze-(E), HFO-1123/HFC-134a, and HFO-1123/CO_2 mixtures.[169] The binary mixture of HFO-1123/HFC-32 was found to be azeotropic, while other mixtures are zeotropic. Similar phase behavior was found between HFO-1123/HFO-1234yf and HFO-1123/HFC-134a because HFO-1234yf and HFC-134a present similar vapor pressure curves; thus, HFO-1234yf is considered as a promising alternative for HFC-134a.

Paulechka et al.[170] proposed a systematic workflow to optimize the LJ parameters based on the functional form of the OPLS-AA force field using the response surface mapping methodology. The model is capable of estimating the VLE properties of alkanes, alkenes, and their fluorinated derivatives. Although the accuracy of predicting VLE results of HFO-1234yf and HFO-1234ze(E) is lower than that of Raabe and Maginn,[162,165] the model presents a broader scope on describing alkanes and perfluoroalkanes. Zhang et al.[171] developed an all-atom force field for HFC-161 based on the Amber force field. GEMC simulations were performed to investigate VLE properties of pure HFC-161 and its binary mixture with HFO-1234yf. Deviations of simulated vapor pressure, liquid density, vapor density, critical temperature, critical pressure, and critical density of pure HFC-161 were 1.37%, 3.87%, 1.86%, 0.40%, 1.86%, and 1.47%, respectively.

Jovell Hidalgo studied the density, viscosity, vapor−liquid coexistence curve, vapor pressure, and surface tension of HFO-1234yf, HCFO-1233zd(E), HFC-32, HFC-125, HFC-134a, and the blends R-407F, R-513A, R-452B, and R-454B using molecular simulations.[21] Alam et al.[140] utilized the transferable COMPASS force field to yield the density, saturation pressure, vapor−liquid coexistence curve, critical point, internal energy, and enthalpy of pure HFO-1123, HFC-32, HFC-134a, and the binary blends of HFO-1123/HFC-32 and HFO-1123/HFC-134a. The Liu group performed ReaxFF MD simulations to study the thermal decomposition of HFO-1234yf with oxygen[172] and the pyrolysis mechanism of HFO-1336mzz(Z),[173] which provided a way to examine the chemical and thermal stability of organic working fluid from the molecular level.

4.2. Molecular Simulation on Refrigerant/IL Mixtures

Extensive molecular simulation studies[174−178] have been conducted on ILs. However, to the authors' knowledge, only a few papers have focused on refrigerant/IL mixtures using molecular simulations. Lepre et al.[43] examined the effect of the HFC polarity and the fluorination of ILs on the solubility of HFC in ILs with a combination of experiment and simulation. In the computational work, MD simulations were employed to calculate the RDFs of HFC-134a in $[C_2C_1im][Tf_2N]$, $[C_8C_1im][Tf_2N]$, $[C_2H_4C_6F_{13}C_1im][Tf_2N]$, and $[C_8C_1im]$-$[Pf_2N]$ to understand the liquid solvation environment of HFC-134a in fluorinated ILs from a microscopic perspective. It was found that anions tend to gather around the $-CH_2F$ site rather than the $-CF_3$ site of HFC-134a and the $-CH_2F$ site shows strong interactions with the negatively charged oxygen atom site of anions. The terminal carbon of the alkyl chain of cation attracts more HFCs than the headgroup of the cation for the studied ILs, except for $[C_2C_1im][Tf_2N]$, and shows greater interaction with the non-polar $-CF_3$ site of solute HFC-134a. It was concluded that a more favorable entropy of solvation leads to the increased solubility of HFC-134a in fluorinated ILs, and the non-polar site of HFC-134a plays a vital role in the solvation, although HFC-134a is a polar molecule. The same authors[47] also applied MD simulations to compute the structure factor of pure $[C_8C_1im][Tf_2N]$, $[C_2H_4C_6F_{13}C_1im][Tf_2N]$, $[C_8C_1im]$-$[Pf_2N]$, and $[C_2H_4C_6F_{13}C_1im][Pf_2N]$, the site-to-site RDFs of tetrafluoromethane (PFC-14, CF_4), hexafluoroethane (PFC-

https://doi.org/10.1021/acs.chemrev.3c00276
Chem. Rev. XXXX, XXX, XXX−XXX

Table 13. FC Refrigerant and IL Combinations with Molecular Simulations[a]

Refrigerant \ Ionic Liquid	$[C_2C_1im][Tf_2N]$	$[C_4C_1im][BF_4]$	$[C_4C_1im][PF_6]$	$[C_4C_1im][SCN]$	$[C_4C_1im][Tf_2N]$	$[C_6C_1im][Cl]$	$[C_6C_1im][BF_4]$	$[C_8C_1im][Pf_2N]$	$[C_8C_1im][Tf_2N]$	$[C_2H_4C_6F_{13}C_1im][Pf_2N]$	$[C_2H_4C_6F_{13}C_1im][Tf_2N]$	$[C_2C_1im][TCM]$	$[C_4C_1im][TCM]$	$[C_6C_1im][TCM]$	$[C_8C_1im][TCM]$
HFC-32		181	117	117	181	117	181		117	181							
HFC-125		181	117	117	181	117	181		117	181							
HFC-134a	43										43	43	43	43	180	180	180	180
HFO-1234yf								179							180	180	180	180
HFO-1234ze(E)															180	180	180	180
PFC-14											47	47	47	47				
PFC-116											47	47	47	47				
PFC-218											47	47	47	47				
R-410A			117	117		117			117									

Structure
Thermophysical, dynamic, and structural properties
Henry's law constant and structure
Solubility Isotherm

[a]The type is represented by different colors: structure (red), thermophysical, dynamic, and structural properties (grey), Henry's law constant and structure (blue), and solubility isotherm (green).

116, C_2F_6), and octafluoropropane (PFC-218, C_3F_8) in $[C_8C_1im][Tf_2N]$ and $[C_2H_4C_6F_{13}C_1im][Tf_2N]$, and the corresponding CNs. The peaks of interactions between the terminal carbon of the side chain of the cation and perfluorinated gases were the highest among cation−gas interactions, while peaks of interactions between the terminal carbon of the anion $[Tf_2N]^-$ and gases were the highest among anion−gas interactions. The CN of the terminal carbon of the side chain of $[C_2H_4C_6F_{13}C_1im]^+$ around perfluorinated gases was higher than that of $[C_8C_1im]^+$, which demonstrated that these perfluorinated gases favor the non-polar domains of ILs. Broader peaks were observed in the interactions of the terminal carbon of fluorinated cations and gases than those of hydrogenated cations. This phenomenon was consistent with the enhanced mobility of the solute in fluorinated ILs, which can be explained by the relatively larger free volumes because of lower cohesion.

Wang et al.[117] utilized MD simulations to investigate the thermophysical properties of HFC-32, HFC-125, and the near-azeotropic mixture R-410A in $[C_4C_1im][BF_4]$, $[C_4C_1im][PF_6]$, $[C_4C_1im][SCN]$, and $[C_6C_1im][Cl]$. The comprehensive investigation involved density, excess volume, diffusivity, viscosity, and structural properties including COM RDFs, partial RDFs, CNs, and SDFs. The computational results agree reasonably well with available experiments conducted both in this work and in the literature. The standard deviations of density and shear viscosity were on the order of 0.0001 g/cm^3 and of 1 to 10 mPa·s, respectively. The relative uncertainties of self-diffusivity of cation, anion, and HFCs were 0.07, 0.06, and 0.25, respectively. It was recognized that the mixing of HFC and IL is not ideal, and a smaller volume change was observed relative to the ideal mixing law. RDFs and SDFs justified the unaffected IL packing structure when adding HFCs. HFCs were found to present much faster dynamics than cations and anions, and increasing HFC concentration resulted in faster dynamics of mixtures. The molecular mechanism provided by partial RDFs and CNs demonstrated that both cations and anions play an important role in the solubility differences of HFCs in ILs: HFC-125 prefers the non-polar domain of ILs, while HFC-32 favors the more polar region.

MD simulations have also been conducted on the HFO-1234yf/$[C_4C_1im][Tf_2N]$ mixture.[179] Force fields of HFO-1234yf and $[C_4C_1im][Tf_2N]$ were validated on density and dynamics against experiments. The density of the liquid mixtures was reported to be lower than pure components, indicating the volume expansion of the IL. The potential energy gradually decreased (more negative) over time, reflecting that the dissolution process is exothermic. The cation diffused faster than the anion, and the diffusivity of HFO is larger than both cation and anion, which is similar to what was observed in HFC/IL mixtures.[117] The solvation structure was characterized by COM RDFs, showing a more intense interaction between the cation $[C_4C_1im]^+$ and the anion $[Tf_2N]^-$ than those between HFO-1234yf and cation or anion.

Recently, Pádua et al.[180] carried out MD simulations to explore the liquid structure of HFC-134a, HFO-1234yf, and HFO-1234ze(E) in $[C_nC_1im][TCM]$. The newly developed polarizable force field, CL&Pol, was applied on both IL and refrigerant, which were validated on Henry's law constants obtained from the free energy perturbation method. The simulated solubility agreed qualitatively with experimental data. Considering polarization in molecular description advances the accuracy of the computational model and helps garner a deeper understanding of how HFC and HFO distribute around ILs. Partial RDFs show the strongest and closest peak in interaction between the $-CH_2F$ site of HFC-134a and the

https://doi.org/10.1021/acs.chemrev.3c00276
Chem. Rev. XXXX, XXX, XXX−XXX

Table 14. Number of Times Molecular Simulations Have Been Investigated for Different Anion and Cation Combinations with Different FC Refrigerants Excluding Diffusion Coefficients

	Anion: [Cl]	[BF4]-	[PF6]-	[SCN]-	[Tf2N]-	[Pf2N]-	[TCM]-
	3	7	5	5	10	8	12
Cation							
4 [C2C1im]+					1		3
19 [C4C1im]+		5	5	5	1		3
8 [C6C1im]+	3	2					3
11 [C8C1im]+					4	4	3
8 [C8H4F13C1im]+					4	4	

nitrogen of $[TCM]^-$ among all interactions between HFC-134a and $[C_2C_1im][TCM]$. The corresponding CN showed that each $-CH_2F$ site has approximately one nitrogen atom of the anion around because of the formation of the hydrogen bond. Quantum calculations confirmed the observation from RDFs of these three refrigerants, which implies HFC-134a, HFO-1234yf, and HFO-1234ze(E) interact with ILs through van der Waals interactions. It was also realized that the larger solubility of HFO-1234ze(E) than HFO-1234yf is caused by different charge distributions of the atom sites of refrigerants. By knowing the facts that a longer alkyl chain of the cation leads to the high solubility of all these three gases in ILs and that solubility differences arise mainly from anion−solute interactions, a new direction of IL design was proposed to separate these three refrigerants by focusing on the length of the alkyl chain of the cation and the choice of the anion.

Wang et al.[181] applied a molecular-dynamics-based simulation procedure that combines alchemical free energy simulations with Hamiltonian replica exchange moves to predict the solubility isotherms of HFC-32 and HFC-125 in $[C_4C_1im][BF_4]$, $[C_4C_1im][PF_6]$, $[C_4C_1im][SCN]$, and $[C_6C_1im][BF_4]$. Their approach successfully addresses the challenges related to accurate sampling and equilibration that often plague researchers. Predicted solubility isotherms were compared against both experiment and more conventional biased Monte Carlo simulations. Their approach matches experimental data and provides more accurate results in a significantly shorter time frame than more standard biased Monte Carlo. Their method is generally applicable to any system where insertions into the liquid phase make free energy calculations or open ensemble simulations challenging.

Table 13 and Table 14 summarize the studied IL/refrigerant combination in the literature.

4.3. Analytic Models for IL−FC Refrigerant Phase Equilibrium

Once either experimental or molecular simulation data is generated for IL−FC refrigerant phase equilibrium, it is important to have a way of modeling the data with analytic expressions. This serves at least three purposes. First, analytic models provide a convenient way of interpolating between data points, and even predicting phase behavior outside the range where the data is available. Second, when the models have a sound thermodynamic basis, the fitting procedure can provide a means for checking the reasonableness of the data and can also identify data that is thermodynamically inconsistent. Finally, analytic equations are needed when performing process engineering calculations, such as in the design of separation processes. Many different approaches have been used in the literature to model IL−FC refrigerant phase equilibrium; an excellent review on the topic may be found elsewhere.[182] Here, we focus on the three most widely used approaches: Henry's constant correlation approaches such as the Krichevsky−Kasarnovsky (KK) model, excess Gibbs energy/activity coefficient models, and equation of state (EOS) models.

Much of the experimental IL−FC refrigerant solubility data in the literature is in the form of Henry's law constants. The thermodynamic definition of the Henry's law constant for species i (in this case, the HFC) is

$$H_i \equiv \lim_{x_i \to 0} \frac{f_i^L}{x_i} \tag{3}$$

where x_i is the mole fraction of the HFC in the IL, f_i^L is the fugacity of the HFC in the IL phase, and temperature is constant. Note that eq 3 only applies to the limit of very low solubility (i.e., low pressure), where isotherms are linear. Often the pressures are low enough so that the ideal gas assumption is valid, such that the HFC pressure can be substituted for the fugacity.

The pressure dependence of f_i^L depends on the partial molar volume of species i in the liquid phase.[183] Exploiting this and

https://doi.org/10.1021/acs.chemrev.3c00276
Chem. Rev. XXXX, XXX, XXX−XXX

Table 15. FC Refrigerant and IL Combinations with Analytical Models[a]

Ionic Liquid / Refrigerant	$[C_2C_1im][Tf_2N]$	$[C_2C_1im][Pf_2N]$		$[C_2C_1im][BF_4]$		$[C_2C_1im][OTf]$		$[C_2C_1im][PF_6]$	$[C_2C_1im][SCN]$	$[C_2C_1im][Tf_2N]$				$[C_2C_1im][TFES]$	
CFC-11															
CFC-113													71		
CFC-113a													71		
HCFC-123													71		
HCFC-123a													71		
HCFC-22													77		77
CFC-114										71			186		
CFC-114a										71					
HCFC-124a										71					
HCFC-124										71,189			186		
HCC-20															
HCC-20-d															
HFC-32	188	192	39		85	192	98		68	188	73	86	39,99	192	39
HFC-125									68	72,189					
HFC-134										71,189			99		
HFC-134a			59		85		85		68	71,189	73		99,186		
HFC-152a						192	98								
HFC-245fa															
HFC-143a										72					
HFC-227ea															
HFC-41										86					
HFC-23								90		55,86,189		73			
HFC-161															
HFC-134															
HFC-236fa															
HFO-1234yf					64		85		68				85		
HFO-1234ze(E)				188	80,187				68						
HCFO-1233zd(E)															
PFC-14										73					
HC-50															
HC-290				189											
HFC-E143a										72					
HFC-E125										72					
HFC-22B1													87		

https://doi.org/10.1021/acs.chemrev.3c00276
Chem. Rev. XXXX, XXX, XXX−XXX

Table 15. continued

Ionic Liquid / Refrigerant	$[C_2C_1im][C_1CO_2]$	$[C_4C_1im][C_1CO_2]$		$[C_4C_1im][BF_4]$			$[C_4C_1im][FS]$	$[C_4C_1im][HFPS]$		$[C_4C_1im][C_2SO_4]$	$[C_4C_1im][C_1SO_4]$	$[C_4C_1im][OTf]$	
CFC-11													
CFC-113													
CFC-113a													
HCFC-123													
HCFC-123a													
HCFC-22				77									
CFC-114													
CFC-114a													
HCFC-124a													
HCFC-124													
HCC-20													
HCC-20-d													
HFC-32		81	39	24	81,192	39,99,186	39	192	39		39	192	98
HFC-125		81			81								
HFC-134													
HFC-134a									59				
HFC-152a												192	98
HFC-245fa													
HFC-143a													
HFC-227ea													
HFC-41													
HFC-23													
HFC-161													
HFC-134													
HFC-236fa													
HFO-1234yf	65	65											
HFO-1234ze(E)													
HCFO-1233zd(E)													
PFC-14													
HC-50										189	189		
HC-290				189									
HFC-E143a													
HFC-E125													
HFC-22B1				87									

https://doi.org/10.1021/acs.chemrev.3c00276
Chem. Rev. XXXX, XXX, XXX−XXX

Table 15. continued

Refrigerant \ Ionic Liquid	[C_4C_1im][PF_6]			[C_4C_1im][SCN]		[C4C1im][TTES]		[C_4C_1im][Tf_2N]	[C_4C_1im][TPES]	[C_4C_1im][TFES]		[C4C1im][NO_3]	[C_6C_1im][BF_4]		
CFC-11	107														
CFC-113	107														
CFC-113a															
HCFC-123	107														
HCFC-123a															
HCFC-22	77														
CFC-114															
CFC-114a															
HCFC-124a															
HCFC-124															
HCC-20	107														
HCC-20-d	107														
HFC-32	24	191,192	39,99,186	81	39	192	39		39	192	39				
HFC-125	24	109,189,191,192	99,186	81											
HFC-134	99	189													
HFC-134a	24	109,189,191,192	58,59,99,186				59		59					99,186	97,189,192
HFC-152a	24	109,191,192	99,186												
HFC-245fa															42
HFC-143a	24	109,191,192	99,186												
HFC-227ea															42
HFC-41	58,187	109,189													
HFC-23	24	57,109,189,192	99												
HFC-161	58,187	109,189													
HFC-134	58														
HFC-236fa															42
HFO-1234yf	76														62,64
HFO-1234ze(E)	75												188	75	80,187
HCFO-1233zd(E)															91
PFC-14															
HC-50								189							
HC-290								189				189			
HFC-E143a															
HFC-E125															
HFC-22B1	87														

https://doi.org/10.1021/acs.chemrev.3c00276
Chem. Rev. XXXX, XXX, XXX−XXX

Table 15. continued

Refrigerant \ Ionic Liquid	[C_6C_1im][Cl]	[C_6C_1im][OTf]	[C_6C_1im][FAP]	[C_6C_1im][PF_6]		[C_6C_1im][Tf_2N]		[C_7C_1im][TFES]	[C_8C_1im][BF_4]			[C_8C_1im][PF_6]	[$C_{12}C_1$im][TFES]	[$(C_1)_2C_3$im][Tf_2N]
CFC-11														
CFC-113														
CFC-113a														
HCFC-123														
HCFC-123a														
HCFC-22														
CFC-114														
CFC-114a														
HCFC-124a														
HCFC-124														
HCC-20														
HCC-20-d														
HFC-32	81		81			67		39					39	39
HFC-125	81		81			67								
HFC-134														
HFC-134a				97,190,192	99,186	99,186	97,189,190,192							
HFC-152a						67								
HFC-245fa														
HFC-143a						51								
HFC-227ea														
HFC-41														
HFC-23														
HFC-161						51								
HFC-134														
HFC-236fa														
HFO-1234yf		62			62,76		83			64		76		
HFO-1234ze(E)						83	187		188	80,187	75			
HCFO-1233zd(E)		91					91							
PFC-14						56,189								
HC-50						189								
HC-290						189			189					
HFC-E143a														
HFC-E125														
HFC-22B1														

https://doi.org/10.1021/acs.chemrev.3c00276
Chem. Rev. XXXX, XXX, XXX−XXX

Table 15. continued

Ionic Liquid / Refrigerant	$[(C_1)_2C_3im][TMeM]$		$[P_{4,4,4,1}][C_1SO_4]$	$[P_{4,4,4,2}][(C_2)_2PO_4]$	$[P_{4,4,4,14}][HFPS]$	$[P_{6,6,6,14}][Cl]$	$[P_{6,6,6,14}][Tf_2N]$	$[P_{6,6,6,14}][TMPP]$		$[P_{6,6,6,14}][TPES]$	$[C_3C_1py][Tf_2N]$		$[C_4C_1py][Tf_2N]$	$[m\text{-}2\text{-}HEA][C_2CO_2]$	$[m\text{-}2\text{-}HEA][C_4CO_2]$
CFC-11															
CFC-113															
CFC-113a															
HCFC-123															
HCFC-123a															
HCFC-22															
CFC-114															
CFC-114a															
HCFC-124a															
HCFC-124															
HCC-20															
HCC-20-d															
HFC-32	188	39	92	92		92	86	66			39	188	39	86	86
HFC-125									46						
HFC-134															
HFC-134a					59			46	188	59					
HFC-152a								46	188						
HFC-245fa								66	188						
HFC-143a								46	188						
HFC-227ea								66	188						
HFC-41			92	92		92	86							86	86
HFC-23			92	92		92	86							86	86
HFC-161								46	188						
HFC-134															
HFC-236fa								66							
HFO-1234yf						65									
HFO-1234ze(E)															
HCFO-1233zd(E)															
PFC-14															
HC-50															
HC-290															
HFC-E143a															
HFC-E125															
HFC-22B1															

[a]The data available is represented by different colors: NRTL, Wilson, Margules (red), NRTL (dark green), NRTL LLE (light green), KK (blue), NRTL and KK (purple), e-NRTL (yellow), EOS(RK, CPA, VDW, PR, or Sanchez–Lacombe) (orange), and soft-SAFT (pink).

making some additional assumptions, one obtains the following expression

$$\ln \frac{f_i^{L}}{x_i} = \ln H_i + \frac{V_i^{\infty} P}{RT} \tag{4}$$

https://doi.org/10.1021/acs.chemrev.3c00276
Chem. Rev. XXXX, XXX, XXX−XXX

Table 16. Number of Times Analytical Models Were Used for Different Anion and Cation Combinations with FC Refrigerants

	Anion	[Cl]⁻	[BF4]⁻	[PF6]⁻	[FAP]⁻	[SCN]⁻	[Tf2N]⁻	[Pf2N]⁻	[OTf]⁻	[TFES]⁻	[C1CO2]⁻	[FS]⁻	[HFPS]⁻	[C2SO4]⁻	[C1SO4]⁻	[TTES]⁻	[TPES]⁻	[NO3]⁻	[TMeM]⁻	[(C2)2PO4]⁻	[TMPP]⁻	[C2CO2]⁻	[C4CO2]⁻
		6	38	69	2	8	66	3	12	7	5	1	4	1	5	3	3	1	2	3	15	3	3
64	Cation [C2C1im]⁺		7	1		5	38	3	6	3	1												
98	[C4C1im]⁺		10	60		3	2		4	2	4	1	3	1	2	3	2	1					
47	[C6C1im]⁺	2	15	7	2		19		2														
1	[C7C1im]⁺									1													
7	[C8C1im]⁺		6	1																			
1	[C12C1im]⁺									1													
3	[(C1)2C3im]⁺						1												2				
3	[P4,4,4,1]⁺														3								
3	[P4,4,4,2]⁺																			3			
1	[P4,4,4,14]⁺												1										
23	[P6,6,6,14]⁺	4					3										1				15		
6	[m-2-HEA]⁺																					3	3
2	[C3C1py]⁺						2																
1	[C4C1py]⁺						1																

where V_i^∞ is the partial molar volume of species i at infinite dilution. Equation 4 is known as the Krichevsky−Kasarnovsky (KK) equation.[184] The vapor pressure of the IL is assumed to be zero. By fitting solubility data to eq 4, one can obtain estimates of both H_i and V_i^∞. This is helpful because, when there is a limited amount of low-pressure data, it can be difficult to estimate the linear portion of an isotherm and thus determine H directly from eq 3. The quality of fits is generally good as long as HFC compositions are not high such that the isotherms are only slightly curved. This is often the case, and therefore, the simple KK functional form is effective for correlating data and determining Henry's law constants. Liu and co-workers have applied the KK equation to fit experimental data for a number of FC refrigerants in imidazolium-based and phosphonium-based ILs.[46,51,67,83] An empirical extension was also used to the normal KK equation to obtain better data fits.[83] Table 15 shows the specific systems modeled by the KK equation.

The most common way people have modeled IL−FC refrigerant phase behavior is through the use of excess Gibbs energy models, which enable one to compute the activity coefficients of the HFC in the IL phase. Because activity coefficients are well-defined thermodynamic quantities, the temperature and pressure dependence enable one to derive other thermodynamic properties such as partial molar excess enthalpies and volumes. One can also check thermodynamic consistency with these models, which helps identify potential problems with a data set. The molar excess Gibbs energy, G^E, is related to the activity coefficient of species i in the mixture, γ_i, via the following expression

$$\left(\frac{G_i^E}{\partial n_i}\right)_{T,P,n_j} = \bar{G}^E = RT \ln \gamma_i \tag{5}$$

where G_i^E is the partial molar excess Gibbs energy of species i. Given a model for G^E, one can evaluate the activity coefficient of a given species in the mixture by applying eq 5.

Several models for G^E have been proposed. It appears that the earliest use of excess Gibbs energy models to treat IL−FC refrigerant data was that of Shiflett and Yokozeki in 2006.[24] The Margules, Wilson, and non-random two liquid (NRTL) models were tested and found that, for a range of refrigerants dissolved in $[C_4C_1im][PF_6]$, the quality of the fit was comparable. Due to its flexibility and perceived accuracy, most authors subsequently have used the NRTL model to correlate experimental data and have followed the Shiflett and Yokozeki formulation. Briefly, one starts with the general expression for vapor−liquid equilibrium for a species i

$$y_i P \Phi_i = x_i \gamma_i P_i^s \tag{6}$$

where y_i is the gas phase mole fraction of species i, Φ_i is the vapor phase fugacity coefficient of species i, and P^s is the vapor pressure of species i. By assuming the gas phase is well-represented by the virial equation of state truncated after the second term, one can write

$$\Phi_i = \exp\left[\frac{(B_i - V_i^L)(P - P_i^s)}{RT}\right] \tag{7}$$

where B_i is the second virial coefficient for species i (usually obtained from external sources such as REFPROP),[185] V^L is the

https://doi.org/10.1021/acs.chemrev.3c00276
Chem. Rev. XXXX, XXX, XXX−XXX

saturated molar liquid volume of species i at temperature T, and the IL is assumed to be non-volatile so that $y_i = 1$.

The different excess Gibbs energy models provide different expressions for γ_i, which are then fit to the data using an optimization procedure. For example, the NRTL equation for the excess Gibbs energy of a binary mixture is

$$\frac{G^E}{RT} = x_1 x_2 \left[\frac{\tau_{21} G_{21}}{x_1 + x_2 G_{21}} + \frac{\tau_{12} G_{12}}{x_2 + x_1 G_{12}} \right] \quad (8)$$

Through a combination of parameters, there are actually only three adjustable parameters in eq 8 that must be fit to experimental data. For moderately non-ideal systems, it is probably unnecessary to use the NRTL model, as simpler models like the KK equation are sufficient. However, for more non-ideal systems, NRTL provides the flexibility to fit most IL−FC refrigerant data sets that have been published. For example, Shiflett and co-workers showed that the solubility of HFC-32 can be fit using NRTL for 19 different ILs.[39] Kim et al., on the other hand, showed that NRTL can model a wide range of HFCs in a handful of different ILs.[186] NRTL can also predict liquid−liquid equilibrium[24] and has been used to predict immiscibility regions.[85] Extensive testing of the NRTL model has been done by many different groups, with generally good fits to the data.[42, 58, 59, 62, 64, 65, 68, 71, 75−77, 80, 83, 85, 87, 91, 98, 99, 107, and 186−188] Table 15 provides a listing of the systems that have been investigated.

It is also possible to model the phase behavior of HFCs with ILs using equations of state. The most commonly used EOSs are cubic equations of state such as the van der Waals, Peng−Robinson, or Redlich−Kwong. In this approach, the pressure−volume−temperature properties of the pure fluids are determined from pure component properties. These are used along with "binary interaction parameters" to develop analytic expressions for the fugacity coefficients, which are then be used to solve the phase equilibrium problem. Parameter estimation is a key challenge, especially for ILs which do not have a critical point. Various methods for estimating pure component parameters have been reported in the literature.

Perhaps the earliest example of IL−FC refrigerant phase behavior modeling with a cubic equation of state was reported by Shariati and Peters.[90] High-pressure vapor−liquid equilibria for fluoroform (HFC-23) + $[C_2C_1im][PF_6]$ were measured beyond the critical point of fluoroform. The data was modeled using the Peng−Robinson EOS. Interestingly, a very high concentration of fluoroform in the liquid phase was observed, and some of the IL was present in the supercritical fluid phase. Soon after, Shiflett and Yokozeki reported vapor−liquid and vapor−liquid−liquid equilibrium results for several HFCs in $[C_4C_1im][PF_6]$, which were well-modeled with the Redlich−Kwong EOS. A key advantage of the EOS modeling approach is that predictions of phase equilibria beyond the measured data can be made. Ren and Scurto[97] modeled experimental vapor−liquid−liquid equilibria data for HFC-134a in various imidazolium-based ILs using the Peng−Robinson EOS with a van der Waals 2-parameter mixing rule. The model matched the vapor−liquid equilibrium and vapor−liquid−liquid equilibrium data very well. There have been many other studies in which different EOSs have been used to model IL−FC refrigerant data, as detailed in Table 15 and Table 16.[55−57,71,72,81,86,92,109,189−191]

EOS models enable rigorous tests for thermodynamic consistency. For example, Faúndez and co-workers[192] performed thermodynamic consistency tests on a wide range of previously published solubility data. It was found that 38 out of 48 data sets were thermodynamically consistent, 9 sets were not fully consistent, and one data set was not thermodynamically consistent. A best practice is to ensure thermodynamic consistency of data before submitting it for publication, whether by use of an EOS or other thermodynamic tests.

Many different models are capable of fitting IL−FC refrigerant solubility data. Only a few are highlighted here, but there are many others including statistical-mechanical-based models such as SAFT[73,193] and machine learning methods.[194] This is not surprising, as much of the HFC solubility data is only moderately non-linear when plotted versus pressure. It is much more challenging to predict new phase behavior (like vapor−liquid−liquid equilibrium) that is outside the range of where data was taken. It was shown that excess Gibbs energy models and EOSs can both do this. The choice of the model one uses is often an ad hoc decision guided by previous literature, prior experience, and convenience. Several fairly sophisticated EOS models with specially derived parameters have been used to model IL−FC refrigerant phase equilibrium,[195] but more complexity is not always better. Often times simpler models with fewer parameters can perform as well as more heavily parametrized models. Using methods such as uncertainty analysis, it is possible to identify parameter correlation in EOS models, suggesting the possibility of similarly accurate, reduced parameter thermodynamic models. For example, Dowling and co-workers showed that a two-parameter Peng−Robinson EOS with a classical van der Waals mixing rule did an excellent job fitting four new IL−FC refrigerant systems.[78]

4.4. Equation of State Modeling and Molecular Simulation General Trends

Imidazolium-based ILs and refrigerants HFC-32 and HFC-125 are most commonly investigated in molecular simulation studies of refrigerant/IL mixtures. The most commonly used cation is $[C_4C_1im]^+$, while $[TCM]^-$ and $[Tf_2N]^-$ were the most studied anions. Limited literature was found on molecular simulation studies of HFC/IL mixtures, while analytical models explored a broader range of refrigerant and IL combinations. This trend arises from the higher computational expense associated with molecular simulation compared to analytical modeling. Among analytical models, imidazolium-based ILs are also frequently examined, with the cation $[C_4C_1im]^+$ and anions $[PF_6]^-$ and $[Tf_2N]^-$ appearing most in these studies.

The accuracy of molecular simulation greatly relies on the selection of sampling methods and the precision of the force field utilized. The development of refrigerant force fields has progressed from simplified united atom models to more precise all-atom models. In certain cases,[158,161] machine-learning-assisted models have been employed to better align with experimental data. Studied properties mainly involve VLE properties, dynamic properties, and structural properties. Future investigations involve the development of the generalized force field of HFCs and HFOs and the polarizable force field[253] of ionic liquids. At the same time, more advanced sampling methods, like Hamiltonian replica exchange[181] and the Widom insertion method,[196] have been employed to efficiently predict solubility isotherms of HFCs in ILs and underway to fast-screen the optimal candidate to separate azeotropic HFC mixtures. The combination of molecular simulations and machine learning techniques can accelerate the progress on the discovery of novel green refrigerant.

https://doi.org/10.1021/acs.chemrev.3c00276
Chem. Rev. XXXX, XXX, XXX−XXX

5. IONIC LIQUIDS AS ENTRAINERS FOR REFRIGERANT SEPARATIONS

Due to the azeotropic behavior of most refrigerant blends, conventional distillation is not an effective way to separate the mixtures. Because of this, ionic liquids are commonly used as an entrainer in order to trap the more volatile component. A rate-based and an equilibrium model for four refrigerant mixtures, R-404A, R-407C, and R-410A + HCFC-22, were designed in Aspen Plus. Vapor-equilibrium data was available for the following refrigerants: HFC-32, HCFC-22, HFC-125, HFC-143a, HFC-134a, $[C_2C_1im][Tf_2N]$, and $[C_4C_1im][PF_6]$. Additionally, each refrigerant was regressed according to the method mentioned previously. From this point, structured packing columns were compared by testing under conventional distillation, extractive distillation, and a flash unit. Constraints and heuristics were examined in order to optimize the process. A height was set to be a maximum of 15 m based on the area in which the pilot column was to be built on the University of Kansas campus. Temperature, complete separation, feed rate, and feed stage were all optimized based on the Aspen rate-based model. In this model both the volume of the packing material as well as the feed column diameter are taken into consideration.

From the modeling, pilot scale model steps have been made to construct a pilot scale model column at the University of Kansas' engineering campus. This column is the first step toward commercialization and provides insight into steps moving forward. Modeling can be compared to real data in order to analyze accuracy.[40,104]

5.1. Aspen Modeling

Aspen Plus software can be used to determine which refrigerants are most soluble in a particular ionic liquid. If, for a given refrigerant mixture, one of the refrigerants is much more soluble in a given ionic liquid than the other, that IL may be a suitable entrainer for extractive distillation. While Aspen Plus contains data for most refrigerants, it does not have preloaded data for the ionic liquids used, so data including critical properties, ideal gas heat capacities, and binary interaction parameters (BIPs) for each IL is required. Unfortunately, ILs cannot be observed as supercritical fluids, or boiled, so the critical properties and ideal gas heat capacities must be estimated using the Group Contribution Method (GCM). Table 17 and Table 18 summarize the systems investigated using Aspen modeling.

By developing an EOS model (as described above), Aspen Plus can accurately model the phase behavior of various refrigerants in different ionic liquids. By comparing the solubilities of the refrigerants, the most suitable ionic liquids are those that allow for the greatest difference in solubilities between the refrigerants. It is important to conduct such simulations, as these can be compared to any experimental solubility data that has been found, increasing the validity of the simulations. The simulations can also be used to find multiple suitable ionic liquids for extractive distillation; while one ionic liquid might display a higher difference in solubilities than another, the former may be unstable or expensive, so finding multiple suitable entrainers is ideal.

Many refrigerant mixtures (R-404A, R-507, R-410A) that have an azeotrope, making the recycling of HFCs difficult. However, if the azeotorpic mixtures are separated, lower GWP HFCs (for example, HFC-32) can be used in new refrigerant mixtures like R-454 blends (HFC-32 and HFO-1234yf) and higher GWP HFCs (for example, HFC-125 and HFC-143a) can be used as feedstocks or fluorinated polymers.[104]

Extractive distillation is the most common method used to separate azeotropic mixtures and utilizes a solvent (the entrainer) to change the properties of the liquid phase and the volatilities of the components, enabling more efficient separation. One component is absorbed by the entrainer which is then carried to the bottom of the column, while the other is distilled from the top. The dissolved component (solute) and entrainer are fed to another unit operation (flash or stripping column) to purify the solute; entrainers typically have lower volatility than the solute, facilitating this purification. While organic liquid solvents are a common choice, ILs are also attractive for being more selective than the organic liquids in some processes. In addition, ILs have negligible vapor pressures (leading to purer solutes) and are highly customizable (composed of a cation and an anion). Finberg et al. analyzed the separation of low boiling components in R-410A (binary mixture) and R-404A, R-407C, and R-410A mixed with 10 wt % HCFC-22 (ternary mixtures).[40,104] The group simulated process designs with Aspen Plus in an attempt to achieve 99.5% purity, using $[C_2C_1im][Tf_2N]$ and $[C_4C_1im][PF_6]$ as entrainers in both equilibrium and rate-based models.

The researchers used the Peng–Robinson EOS and Boston–Mathias mixing parameters in the regression of VLE data.[40,104] This also required the knowledge of physical properties (e.g., boiling temperature and molecular weight), critical properties (e.g., critical temperature, critical pressure, critical volume, critical compressibility factor, and acentric factor), and ideal gas heat capacity of ILs.[104] The critical properties and ideal gas heat capacities were estimated using a group contribution method, as many of these properties cannot be measured. The group created *PTx* diagrams for HFC-32, HFC-125, HFC-134a, and HFC-143a in $[C_4C_1im][PF_6]$ and for HFC-32, HFC-125, and HFC-134a in $[C_2C_1im][Tf_2N]$. There was no literature data of HFC-143a in $[C_2C_1im][Tf_2N]$, so the refrigerant was assumed to have the same behavior that it had in $[C_4C_1im][PF_6]$. It was noted that HFC-125 had similar solubilities in both ionic liquids, so it was assumed that HFC-143a would exhibit similar behavior as well, especially at lower solubilities. LLE was observed in all refrigerants except HFC-32.

The equilibrium models were based on MESH (Material balances, Equilibrium, Summation equations, and Heat Balances) equations to compute flow rates, compositions, temperatures, and pressures at each stage of the process. This model assumed all stages were in equilibrium with the inlet and outlet streams to approximate how many stages would be required. Efficiencies were used to account for the fact that real trays are almost never at equilibrium.

Table 17. Cations and Anions Investigated in Aspen Modeling for Separating FC Refrigerants

		Anion	$[PF_6]^-$	$[Tf_2N]^-$	$[C_4F_9CO_2]^-$
			11	3	1
4	Cation	$[C_2C_1im]^+$		3	1
11		$[C_4C_1im]^+$	11		

https://doi.org/10.1021/acs.chemrev.3c00276
Chem. Rev. XXXX, XXX, XXX−XXX

Table 18. Refrigerant Mixtures and ILs Investigated Using Aspen Modeling

Refrigerant Mixture \ Ionic Liquid	$[C_2C_1im][C_4F_9CO_2]$	$[C_2C_1im][Tf_2N]$	$[C_4C_1im][PF_6]$
HFC-32, HFC-125, HCFC-22			40
HFC-32, HCFC-22			40
HFC-32, HFC-125, HFC-134a, HFC-143a, HCFC-22, HC-290, HC-600a			40
HFC-32, HFC-134a, HCFC-22			40
HFC-32, HFC-125, HFC-134a, HFC-143a, HCFC-22, HC-290, HC-600a			40
HFC-32, HFC-125, HFC-134a, HCFC-22, HC-290			40
HFC-32, HFC-125, HFC-134a, HCFC-22			40
HFC-125, HFC-134a, HFC-143a		104	
HFC-125, HFC-143a		104	
HFC-32, HFC-125, HF-134a			104
HFC-32, HFC-134a, HCFC-22			104
HFC-32, HFC-125, HCFC-22			104
HFC-32, HFC-125		197	104
HFC-32, HFC-125, HFC-134a	198		

The rate-based models, however, can be applied to non-equilibrium systems, as estimations of column or tray efficiency are not required. These models instead calculate column performance using rate equations and transfer coefficients for mass and energy transfer through the gas−liquid interface and do not assume each tray is in equilibrium. Unlike MESH, rate-based models use balances in gas and liquid phases separately and consider mass and heat transfer resistances using film theory, better accounting for temperature gradients in both gas and liquid phases. The rate-based models also account for geometry and sizing of trays or packings to determine effective interfacial area, pressure drops, and flooding/weeping phenomena. The rate-based models can even be used to predict the column geometry necessary to achieve the desired purity of outlet streams. It should be noted, however, that the higher viscosities of ILs can decrease mass transfer efficiency, leading column sizing predictions to be less accurate.

For both ionic liquids used, the group tabulated several temperature-dependent physical properties (density, viscosity, surface tension, and liquid heat capacity) needed for Aspen Plus to run the rate-based models. Correlations were used to predict these properties, which were then compared to literature data. The group then proceeded to begin simulating extractive distillation processes.

The group simulated a flash separation, conventional distillation, and extractive distillation process for the separation of the refrigerant mixtures (R-404A, R-410A, R-407C).[104] Heuristics were developed prior to the simulations to efficiently optimize the many variables in these simulations. The reboiler temperature was set between 288 and 408 K to avoid the need of a low temperature thermostat and prevent IL decomposition. To improve purity, the refrigerant was fed as a liquid at a low temperature of 293 K, and the feed entered the unit at the top of the packing due to the IL's lack of appreciable vapor pressure. For better separation, the distillate rate was set equal to either the mass fraction of one component multiplied by the feed (component leaves in distillate) or the mass fraction sum of the other components multiplied by the feed (component leaves in bottoms). The simulations used a feed of 10 kg/h and a column diameter of 10 cm. A Sulzer-structured packing (750Y Mellapak) was used for pilot scale simulations. The remaining variables that were optimized were pressure, feed stage, reflux ratio, solvent-to-feed ratio, and number of theoretical stages.

The R-407C separation was able to achieve 99.9 wt % purity of HFC-134a with a conventional distillation column and 99.7 wt % purity for both HFC-125 and HFC-32 using extractive distillation with $[C_4C_1im][PF_6]$ as the entrainer. The same separation could only achieve 95.9 wt % purity with an entrainer of $[C_2C_1im][Tf_2N]$. The R-410A separation was able to achieve 99.6 wt % purity for both HFC-125 and HFC-32 using extractive distillation using $[C_4C_1im][PF_6]$ as the entrainer. The same separation using $[C_2C_1im][Tf_2N]$ as the entrainer only resulted in a separation purity of 95.5 wt %.[104] The R-404A separation achieved 99.5 wt % purity for HFC-134a using conventional distillation but was not able to achieve the same purity for separating the azeotropic mixture of HFC-125 and HFC-143a using extractive distillation and entrainers $[C_2C_1im][Tf_2N]$ and $[C_4C_1im][PF_6]$.

https://doi.org/10.1021/acs.chemrev.3c00276
Chem. Rev. XXXX, XXX, XXX−XXX

For the separation of a mixture containing R-410A and 10 wt % HCFC-22, purities of 99.5 and 99.7 wt % were obtained for HFC-32 and HCFC-22, respectively. However, only 90 and 99.7% of the original HFC-32 and HCFC-22, respectively, were able to be recovered. Extractive distillation would be required for separating such a mixture, and conventional distillation required a packing height of 54 m and very low condenser and reboiler temperatures.[40,104]

To prevent the incineration or venting of complex multicomponent HFC mixtures, Finberg et al. showed that azeotropic refrigerant mixtures could be separated via extractive distillation.[40] The group conducted research on seven common refrigerants and regressed BIPs for various refrigerant and ionic liquid mixtures to predict VLE and LLE data.

The Peng−Robinson equation of state and the van der Waals 1-parameter (vdW1) mixing rule were used along with Aspen Plus software to regress mixing parameters for various refrigerant mixtures. To calculate the critical properties of ionic liquids necessary for the Peng−Robinson EOS, a group contribution method was utilized; since these properties occur at a critical temperature higher than the ionic liquids' decomposition temperature, these critical properties were considered pseudocritical properties. For non-ideal systems, the Boston−Mathias (B−M) correction was added to the vdW1 mixing rule. For the regression of experimental data, the maximum likelihood technique was utilized. Error in the four experimental variables was analyzed using the absolute average deviation, as relative deviation analyses are inconsistent and become large as experimental values approach zero. For refrigerant and ionic liquid systems with more than one set of data, each set was analyzed individually, as one may be less consistent or accurate than the other. In addition, for systems with data at only one temperature, the temperature dependent parameter k_{ij}^2 was set equal to zero.

The group first regressed data for azeotropic refrigerant systems and found that most of the models fit the experimental data well. The group then used the regressions to simulate where the azeotropes would occur at normalized pressures for each refrigerant mixture. The group continued by regressing the solubilities of seven refrigerants in $[C_4C_1im][PF_6]$ using the vdW1 mixing rule with B−M correction, though some solubility data had to be assumed due to a lack of data. The refrigerant−ionic liquid systems were found to have an average AAD in composition of 1.048 mol %, about 0.357 mol % larger than that of binary refrigerant systems. The average AAD for deviations in temperature was 0.4 K, about the same as binary refrigerant systems, and the average AAD for all pressure deviations was 3.326×10^{-4} MPa, approximately 2 orders of magnitude smaller than those of binary refrigerant systems. These solubilities were then compared in a *PTx* diagram to determine which refrigerants were most soluble in $[C_4C_1im][PF_6]$.

Prior to developing process designs for the extractive distillation, the group defined heuristics to reduce the number of variables that needed to be optimized. All feed temperatures were set at 293.15 K so streams did not need to be cooled. The feed pressure was fixed at 2.0 MPa, higher than the operating pressure of the column, to ensure the feed was in the liquid phase. The ionic liquid stream entered the column near the top (solvent feed stage $N_S = 2$), as ionic liquids have immeasurably small vapor pressures, and feed stage depends on a component's volatility. The distillate rate was set equal to the feed rate of the light key component (or sum thereof) to achieve the desired purity of a given component. Since determining which component(s) is/are the light key or heavy key component(s) proves difficult in multicomponent mixtures where multiple azeotropes exist, the group established a novel method to test if conventional distillation could be used for multicomponent mixtures. This was done using mass distilled versus distillate rate diagrams. In doing so, the group confirmed that the multicomponent azeotropic mixtures did not follow the order of boiling point, which is typically used to determine the LK and HK components. Using these diagrams, a complete separation would be possible if one component has about 0% mass distilled while all others reached 100%. If such a feature did not appear, extractive distillation was considered.

In either case, the group first optimized the distillate rate and then proceeded to optimize other design variables to obtain a separation purity of 99.5 wt %. If such a separation was not possible, the group would iterate again. If a system was initially predicted to be separable via conventional distillation but the purity was too low or the number of trays exceeded 50, extractive distillation was recommended for more efficient separation.

The group determined that 8 of the 21 binary refrigerant mixtures were zeotropic and could be separated via conventional distillation and simulated the separation of each mixture with 50/50 wt % to achieve 99.5 wt % purity of each component.[40] The group then proceeded to utilize Aspen Plus software to simulate process designs for the separation of three azeotropic refrigerant mixtures. All of these separations involved using $[C_4C_1im][PF_6]$ as an entrainer. The first simulation was a separation of HCFC-22 contaminated with 10 wt % R-410A. Both a conventional distillation and extractive distillation process design were simulated. The maximum amount of HCFC-22 that could be recovered had a purity of 99.5 wt % and a flow rate of 21 kg/h, with an overall recovery of 78 wt % of HCFC-22. However, the process was able to recover 100% of HFC-125.

A second simulation was conducted to determine if separating HCFC-22 from a multicomponent refrigerant mixture was feasible. The multicomponent mixture had a composition based on market trends, with a total of seven components: HFC-32, HFC-125, HFC-134a, HFC-143a, HCFC-22, HC-290, HC-600a.[40] However, even with two conventional distillation columns, a separation purity of 99.5 wt % was not able to be realized; only 10 kg of HCFC-22 was able to be recovered, while 20 kg of the other refrigerants would require disposing of or repurposing as fluorinated feedstock for other products. The overall recovery of HCFC-22 was 63.6 wt %.

The third simulation was conducted to determine if it was possible to separate a mixture of HFC-32, HFC-125, HFC-134a, HCFC-22, and HC-290 into its individual components, each with a purity of 99.5 wt %.[40] This simulation utilized one extractive distillation column followed by two conventional distillation columns. The desired purity for HFC-32, HCFC-22, and HFC-134a of 99.5 wt % could be obtained, and approximately 75% of the mixture could be recovered; however, this process required a high reflux ratio.[40]

5.2. Efficiency

In addition to developing a simulation for the separation of R-410A, Monjur et al. utilized Synthesis and Process Intensification of Chemical Enterprises Involving Extractive Distillation (SPICE_ED) to further optimize the process simulation in terms of minimizing energy, ensuring sustainability, and the economics of the design.[199] This software can find the best design solution without prior knowledge of possible config-

https://doi.org/10.1021/acs.chemrev.3c00276
Chem. Rev. XXXX, XXX, XXX−XXX

urations. The simulation from SPICE_ED was then compared to simulations developed using Aspen Plus software for validity, with the group finding similarities between the main design variables in both simulations.

SPICE_ED is based off an earlier simulator, SPICE, but has additional rigorous phenomena and thermodynamic property models that make it specially tailored for extractive distillation. Among the variables that can be optimized are theoretical stages, reflux ratios, feed stages of solvent, amount of makeup solvent, minimum energy consumption, minimum CO_2 equivalent, and minimum cost of separation. Using these, along with sensitivity, techno-economic, and life-cycle analyses, theoretical bounds on the process simulation variables can be determined.

Using SPICE_ED, the group represents the process of design simulation via building-blocks, where each block represents a design element and its interior and boundaries are used to accommodate physicochemical phenomena. Blocks can represent either a reactor or adsorber, or its interior may be empty; blocks also allow streams of mass or heat to enter or exit. The blocks' boundary type can be either unrestricted, semirestricted, or completely restricted. The unrestricted and completely restricted boundaries are akin to open and closed systems, respectively. Semirestricted boundaries allow mass transfer, but streams passing through may experience a change in composition; these can be determined via equilibrium models, as equilibrium-based separation depends on this. For these simulations, the group used the Gamma-Phi model for phase equilibrium.

For thermodynamic data, saturation pressures of the refrigerants were estimated using the Antione equation. The second virial coefficients for refrigerants were obtained from an outside source.[200] Specific enthalpies of the ionic liquids were estimated as being linearly dependent on temperature, and Aspen Plus was used to estimate the specific enthalpies of refrigerants. (For the liquid phase of refrigerants, a piecewise polynomial from SPICE_ED was used to estimate the specific enthalpy and was compared to values obtained in Aspen Plus.)

The group then developed several objective functions, for energy consumption, process sustainability, and process economics. These functions were developed using cited data for the costs and other relevant data of several pieces of equipment. The group then analyzed a previously developed process using $[C_4C_1][PF_6]$ to separate R-410A, first transferring the process design from classical representation to the building-block representation. Utilizing SPICE-ED, the group was able to obtain at least 99.5 wt % purity of both refrigerants, consuming 659 kJ/s for 0.3 kg/s R-410A, costing $0.081/kg R-410A, and emitting 0.058 kg CO_2-eqv/kg; these results were compared to simulations developed by Shiflett and Yokozeki,[200] with some assumptions due to missing energy data. The simulation developed with SPICE_ED was recreated in Aspen Plus to verify the results; both simulations were found to have similar values for the variables, suggesting the SPICE_ED simulation was accurate.

After this simulation was completed, the group expanded on the work to optimize more general cases of extractive distillation, this time fixing the R-410A feed to 100 kg/h and a minimum separation purity of 99.5% for both HFC-125 and HFC-32.[199]

5.3. Life Cycle Analysis

In addition to performing simulations with Aspen Plus, Jovell et al. conducted life cycle analysis (LCA) to determine the economic feasibility and environmental impact of new separation units.[198] The group focused on the separation of HFC-32 from a mixture of R-407F (HFC-32, HFC-125, R-134a) and $[C_2C_1im][C_4F_9CO_2]$. The absorption process was modeled using Aspen Plus and the COSMO-SAC (conductor-like screening model with segment activity coefficient) property model, used for polarizable species to model electric fields on the molecular surface. The activity coefficient model was based on individual atoms instead of functional groups. Because it was not preloaded in Aspen Plus, the ionic liquid was entered as a pseudocomponent, with its molecular weight, normal boiling point, and density at 273 K specified, with remaining properties estimated using the API procedure and the previous works of Lydersen−Joback−Reid and Valderrama et al.[201−203] The group based the data regression on the Least Absolute Residuals (LAR) method and the Levenberg−Marquadt algorithm.

For this process simulation, an absorption column followed by a flash tank was used to separate HFC-32 from the refrigerant mixture and regenerate the ionic liquid, respectively. The stream containing the ionic liquid to be regenerated was then sent to a pump and heat exchanger to cool the ionic liquid before feeding it back to the absorption column. The R-407F was assumed to be fed at 8 bar and 298 K and was heated to 318.15 K and fed counter-currently at 1000 kg/h into the absorption column with ionic liquid at 287.15 K and 8 bar. In the absorption column, the ionic liquid was used as an absorber of both HFC-125 and HFC-134a, enabling for a gas stream rich in HFC-32 to emerge from the top. The ionic liquid, HFC-125, and HFC-134a mixture was then fed to a flash drum, with the ionic liquid regenerated via a pressure swing to 0.001 MPa. The ionic liquid was then cooled to 287.15 K prior to being recycled in the absorption column. For this design, a minimum 98 wt % purity for HFC-32 was set as a specification.

For the LCA, the group based the method used on the work of Wu et al.[204] SimaPro software was used to calculate the cradle-to-gate life cycle environmental impacts of HFC-32 recovery (circular economy) with ionic liquid and HFC-32 industrial production (Benchmark). The group conducted the LCA using 3 steps—defining the goal and scope, analyzing the Life Cycle Inventory (LCI), and conducting a Life Cycle Impact Assessment (LCIA)—and interpreted the results. The group sought to develop a framework for the LCA, comparing life cycle impacts on the environment for HFC-32 recovery from the simulated process. The group constructed a life cycle framework and LCI analysis for both HFC-32 recovery and HFC-32 production and then compared the LCIA of both processes. The Monte Carlo methodology was used to perform an uncertainty analysis and verify the results' validity. A sensitivity analysis was also performed to find the factors most greatly affecting environmental impacts. To simplify the LCA, allocation procedures for burdens associated with avoiding production of HFC-32 or its incineration were not considered.

The LCI for HFC-32 recovery included all mass and energy inputs and outputs, as well as emissions from precursor production, IL production, separation of refrigerants, and IL regeneration. For precursors and IL production, upstream feedstock, auxiliary materials (such as catalysts), and energy consumption were considered in the LCI. HFC-32 separation's LCI considered IL inputs, losses, and energy consumption. Ecoinvent 3 was utilized to obtain data for thermal energy (natural gas), electricity (electricity mix grid), chemical plants (chemical factory, organics), transportation (freight, lorry 16−32 tons), and EoL of wasted IL due to incineration. LCI databases did not contain precursor or used IL data, so the data

https://doi.org/10.1021/acs.chemrev.3c00276
Chem. Rev. XXXX, XXX, XXX−XXX

was obtained via literature or process simulations. A 0.2% emission into the air of input materials was assumed, except for the IL with its negligible vapor pressure. The theoretical energy needed for the precursors' production was scaled up using conversion factors. For endothermic reactions, the theoretical heat needed was multiplied by 4.2 as the heat was obtained from natural gas. For exothermic reactions, the theoretical heat generated was multiplied by 3.2 and was assumed to be cooled via electricity from the Spanish electricity mix.

CML-IA methodology was used to perform the LCIA of HFC-32 absorption, including global warming potential (GWP), abiotic element depletion and fossil fuels, ultimate reserves, ozone depletion potential (ODP), human toxicity potential (HTP), freshwater aquatic ecotoxicity potential (FAETP), marine aquatic ecotoxicology potential (MAETP), terrestrial ecotoxicity potential (TETP), photochemical oxidation potential (POCP), acidification potential (AP), and eutrophication potential (EP). To convert these into dimensionless scores, normalization with European normalization factors (EU25) was used.

COSMO-RS simulation results of experimental solubility were compared to those in Aspen Plus, and the predictions were deemed able to sufficiently predict experimental solubility. From Aspen Plus simulations, a minimum of 38 theoretical stages are necessary to achieve the desired 98 wt % purity of HFC-32. The process was determined to have modest energy consumption with its low operation flows and moderate temperature range. 30.3% of HFC-32 was recovered using 5774 kg/h of the IL, which is also recovered and recycled.

A material flow analysis (MFA) was conducted considering the separation of 1 kg of HFC-32 from R-407F blend with a purity greater than 98 wt % to understand the use of materials and the transformation in HFC-32 recovery. From the MFA, the IL is completely regenerated for further reuse, though it may lose separation efficiency with continued use. The group determined that the IL would need to be replaced annually, the consequences of which were analyzed in the LCA. Using these assumptions, the simulation predicted that 0.008 kg of IL is needed to separate 1 kg of HFC-32. To produce 0.008 kg of IL, 0.036 kg of raw materials is needed (calculated from cation and anion precursors). The total waste emission is 0.013 kg, or 36.4 wt % of raw materials. Water was also used in IL production, contributing 33.5 wt % of the total waste emissions from IL production. In the IL use stage, 0.008 kg of waste related to IL replacement is produced, contributing 22.9 wt % to total waste emission. HCl and H_2 were byproducts of the creation of the IL and could be considered "avoided products", contributing 3.2 wt % of raw materials introduced to the system.

An energy flow analysis (EFA) for the recovery of 1 kg of HFC-32 was also performed. The electricity consumption was 69.8% in HFC-32 recovery, 30.0% in IL precursor production, and 0.2% in IL production. For heat consumption, 60.9% was used for HFC-32 recovery, 21.6% was used for IL precursor production, and 17.5% was used for IL production. From these, it was determined that reducing electricity and heat production would be an effective means of reducing the total life cycle energy consumption.

From the environmental impact analysis, the production of IL precursors had the largest contribution to all impact categories (between 85% and 100%). These also contributed most to ADP (elements) and HTP. The emission of HF in the production of one of these precursors contributes 94.3% to the MAETP. The high HTP contributions come from ethylene oxide emissions. Process energy and transportation processes were found not to contribute as significantly, the latter of which was considered negligible regarding life cycle impacts. The use of the IL in the separation process contributed the most to the majority of impact categories, with the exception of GWP, whose impact was largely comprised of fugitive emissions. The construction of the chemical plant itself contributed less than 3% to environmental impact categories.

The benchmark scenario was selected to be the current HFC-32 production scenario. The patent of Yuichi et al.[205] was used for the LCA of HFC-32 production. For the production of 1 kg of HFC-32, it was determined that, with the exception of MAETP and HTP, the highest impact in most categories was due to HF and CH_2Cl_2 raw materials. Fugitive emissions caused most important impacts in HTP and MAETP, mostly due to HF emissions. The circular economy recovery scenario was observed to have significantly lower environmental loads in all impact categories than the benchmark production scenario. The highest impact is MAETP in both benchmark and circular economy scenarios. The results demonstrated the environmental benefits of recycling HFC-32 rather than producing new refrigerant.

For the sensitivity analysis, it was assumed from previous works that the negligible vapor pressures of ILs could be used to assume that ILs could be regenerated in the absorption processes without losing efficiency.[200,206] However, experience with other regenerable IL absorbents used to capture CO_2 did lose separation efficiency due to degradation or the presence of impurities. From the sensitivity analysis, it was found that IL replacement was not a critical factor for the sustainability of the circular economy scenario. While decreasing the time of IL replacement significantly impacted the ADP (elements) and HTP categories, the impacts were generally lower than those of the HFC-32 production scenario in most categories.[197,198,207]

Additionally, the Spain group investigated modeling the separation of R-410A. For this, the phase behavior was examined via the soft-SAFT equation of state. Previous work had verified the accuracy of this EOS.[208−210] The phase behavior and parameters were then able to be calculated. This data was then used to design an extractive distillation column utilizing $[C_2C_1im][Tf_2N]$ as an entrainer. The results revealed a high yield of recovery.[197]

5.4. General Trends of Ionic Liquids as Entrainers for Separating Refrigerant Mixtures

Aspen modeling of extractive distillation with ILs as entrainers for the separation of refrigerant mixtures investigated the separation of 14 different FC mixtures. The mixtures investigated range from two-component to seven-component mixtures. The IL investigated as an entrainer for the majority of mixtures was $[C_4C_1im][PF_6]$. Nearly all mixtures investigated were HFC mixtures with some including HCFC-22, HC-290, and HC-600a which commonly form azeotropes with HFCs. These initial results from the Aspen modeling indicate that separating azeotropic refrigerant mixtures with ionic liquids will allow for the refrigerants to be separated with a purity of 99.5 wt % or greater for the individual components. This level of separation is necessary for the refrigerants to meet AHRI-700 purity standards for refrigerant resale.

Beyond looking at the separation feasibility, process efficiency and life cycle analysis have also been investigated for the proposed separation process. SPICE_ED was shown to be an effective way to make process design decisions by optimizing

https://doi.org/10.1021/acs.chemrev.3c00276
Chem. Rev. XXXX, XXX, XXX−XXX

energy consumption, cost of separation, and CO_2 equivalency with key design decisions such as number of theoretical stages, reflux ratios, solvent to feed ratios, and solvent amount. By optimizing efficiency and understanding the LCA for these materials, better design decisions can be made early on to create the most efficient process.

6. PROMISING IONIC-LIQUID-BASED MATERIALS

6.1. Mixed Matrix Membranes

The incorporation of ILs into membranes creates a great possibility for more efficient separations due to both entities having separation potential. Although ionic liquid membranes (ILMs) have not been thoroughly explored for refrigerant separation, the potential to create a composite membrane harnessing the characteristics of both the polymer and the ionic liquid is attractive for this separation. Table 19 summarizes the literature that has been published for ILM use for refrigerant separation. Two types of ILMs have been tested for refrigerant separation: ionic liquid mixed matrix membranes (ILMMMs) and composite ionic liquid polymer membranes (ILPMs). An ILMMM is a polymer membrane incorporated with ionic liquid and inorganic filler. The ionic liquid and filler allow for a tunable separation, while the polymer adds durability. ILMMMs show promise for a wide range of separations; however, fabrication can be hard to replicate due to inconsistencies in how the inorganic filler is distributed within the matrix. ILPMs are polymer membranes in which IL is encapsulated within the polymer matrix as shown in Figure 9.

Table 19. Summary of ILs Studied for ILMMMs Used in Fluorocarbon Refrigerant Separation Applications[a]

		8	8	8	8	3
	Anion / Cation	$[BF_4]^-$	$[SCN]^-$	$[Tf_2N]^-$	$[OTf]^-$	$[C_4F_9SO_3]^-$
32	$[C_2C_1im]^+$	8	8	8	8	
3	$[C_2C_1py]^+$					3

[a]The intersections indicate the number of references in which the IL is reported.

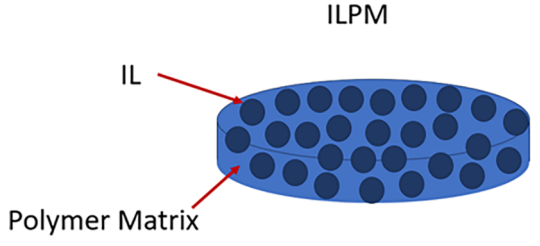

Figure 9. Schematic of an ionic liquid polymer membrane.

ILPMs exhibit good mechanical stability and are easier to reproduce in comparison to ILMMMs.[211] ILMMMs and ILPMs have been demonstrated for use with a number of separations, such as CO_2/N_2 separation,[212] pervaporation dehydration of isopropanol,[213] and acid gas separation.[214]

Minimal literature is available on the use of ILMMMs and ILPMs for refrigerant separation. A summary of the ionic liquids and refrigerants that have been tested are shown in Table 20.

Table 20. Summary of ILs Used in ILMMMs Studied for Fluorocarbon Refrigerant Adsorption[a]

Refrigerant / Ionic Liquid	$[C_2C_1im][BF_4]$	$[C_2C_1im][OTf]$	$[C_2C_1im][SCN]$	$[C_2C_1im][Tf_2N]$	$[C_2C_1py][C_4F_9SO_3]$
HFC-32	216,217	216,217	216,217	216,217	215
HFC-125	216	216	216	216	215
HFC-134a	217	217	217	217	
HFO-1234yf	217	217	217	217	
R-410A	216	216	216	216	215
R-513A	217	217	217	217	
R-454B	217	217	217	217	

[a]The intersections provide the reference(s) in which the ILMMMs were studied.

Pardo et al. reported on the use of ILMMMs consisting of Pebax1657, 1-ethyl-3-methylpyridinium perfluorobutanesulfonate ($[C_2C_1py][C_4F_9SO_3]$), and exfoliated graphene nanoplatelets (xGnPs). This study investigated the use of the prepared ILMMM for separating R-410A into its components: HFC-32 and HFC-125.[5] The xGnPs were combined with the IL to create ioNanofluids (IoNFs) that would later be combined with the polymer and formed into a film using a solvent evaporation method. The study reported the permeability of HFC-32 and HFC-125 with six different ILMMMs consisting of different ratios of inorganic filler and IL. The first three ILMMMs were 20 wt % IoNF to polymer, containing 1, 10, and 20 wt % xGnP to IL. The next three were 40 wt % IoNF to polymer, containing 1, 10, and 20 wt % xGnP to IL. A neat Pebax1657 membrane was also tested. Results indicated that the highest permeability of HFC-32 and HFC-125 could be achieved with the film containing the highest amount of IL and filler 40 wt % IoNF containing 20 wt % xGnP to IL. Two ILPMs consisting of 20 and 40 wt % IL were also tested and showed lower permeability in comparison to the ILMMMs of the same IL weight percent.[215]

The pure membrane had the highest selectivity, while selectivity with the ILMMMs decreased as the weight percent of IL or IoNF was increased. This trend agrees with previous data seen for ILPMs containing highly fluorinated ILs. The addition of IL increases permeability for both fluorinated gases while simultaneously decreasing selectivity indicating the well-known trade-off between permeability and selectivity. The neat Pebax1657 membrane, 40 wt % IL ILPM, and 40 wt % IL with 10 wt % xGnP ILMMM were tested for gas sorption of HFC-32 and HFC-125. The ILPM had the highest sorption, followed by the

https://doi.org/10.1021/acs.chemrev.3c00276
Chem. Rev. XXXX, XXX, XXX−XXX

ILMMM, and the lowest was the pure polymer membrane. It can be concluded that the xGnP filler acted as a solubility blocker in comparison to the ILPMs. Overall, for these ILMMMs to become more successful for R-410A separation, the packing of xGnPs would need to be studied further, and ILs that are more selective toward HFC-32 or HFC-125 would need to be considered.[215] Uncertainties are included for the mixed-gas permeability and separation factor values, although the manuscript lacks a description on how they are obtained.

Additional studies have focused on the use of ILPMs for separating R-410A. The same polymer as the previous study (Pebax1657) was combined with $[C_2C_1im][SCN]$, $[C_2C_1im][BF_4]$, $[C_2C_1im][OTf]$, and $[C_2C_1im][Tf_2N]$ to form ILPMs via a solvent evaporation method. Various IL to polymer ratios of each ILPM were tested for mixed gas permeability, selectivity, pressure change effect on permeability and selectivity, and long-term stability and separation performance of R-410A.[215] Mixed gas permeability tests were carried out on 20, 40, and 60 wt % IL ILPMs. No data was obtained for 60 wt % $[C_2C_1im][SCN]$ or $[C_2C_1im][Tf_2N]$ because the membranes were not mechanically stable enough to withstand the testing conditions. For each sample, as the IL weight percent increased, the permeability also increased. This is due to increased polymer chain mobility caused by the addition of IL. For HFC-32, the ILPMs did not exhibit a strong trend in which IL yielded the highest permeability values, but the results depended greatly on which weight percent was being analyzed. The greatest permeability was exhibited by the 60 wt % IL ILPMs. As for HFC-125, the permeability for each gas increased as the molar volume of the IL increased, resulting in permeabilities with the ILPMs of the following order: $[C_2C_1im][Tf_2N]$ > $[C_2C_1im][OTf]$ > $[C_2C_1im][BF_4]$ > $[C_2C_1im][SCN]$. The selectivity results show the opposite trend from permeability, with the $[C_2C_1im][SCN]$ ILPM having the largest selectivity and the $[C_2C_1im][Tf_2N]$ having the lowest. The presence of $[C_2C_1im][SCN]$ and $[C_2C_1im][BF_4]$ greatly improved both selectivity and permeability compared to the pure polymer membrane and illustrates the potential of ionic liquids to overcome the trade-off between permeability and selectivity in membrane separations by imparting a solubility-driven separation.[215] Although the presence of these ILs improved membrane performance in this study, it should be noted that the ILPMs were more prone to decreases in selectivity with increasing pressure than the neat polymer, due to ILPMs exhibiting higher chain mobility. Uncertainties are included for the mixed-gas permeability, although the manuscript lacks a description of how the uncertainty is obtained.

Additional work has been conducted with ILPMs for the separation of HFC/HFO blends such as R-513A and R-454B. The polymer used for these experiments was Pebax1657, which was combined with $[C_2C_1im][SCN]$, $[C_2C_1im][BF_4]$, $[C_2C_1im][OTf]$, and $[C_2C_1im][Tf_2N]$ and fabricated into films using the solvent evaporation method.[217] Single gas permeability tests were carried out on 20, 40, and 60 wt % IL ILPMs for each IL. The gases used were HFC-32, HFC-134a, and HFO-1234yf. As reported previously, no data was obtained for 60 wt % $[C_2C_1im][SCN]$ or $[C_2C_1im][Tf_2N]$ because the membranes were not mechanically stable enough to withstand the testing conditions. Results showed that the permeability of all gases increased with the amount of IL due to higher chain mobility. Permeability in all samples correlated to penetrant size, with HFC-32 being the greatest, then HFC-134a, and finally HFO-1234yf. Moreover, permeability for each gas increased as the molar volume of the IL increased, yielding an order of $[C_2C_1im][Tf_2N]$ > $[C_2C_1im][OTf]$ > $[C_2C_1im][BF_4]$ > $[C_2C_1im][SCN]$. HFC-32 presented an exception to this trend, with $[C_2C_1im][BF_4]$ having the greatest permeability.[217] This exception is likely due to the large solubility of HFC-32 in this fluorinated IL. In terms of selectivity analyses, two HFC/HFO mixtures were considered in this experiment: R-454B (68.9 wt% HFC-32 and 31.3 wt% HFO-1234yf) and R-513A (56 wt% HFO-1234yf and 44 wt% HFC-134a). For both gas mixtures, membranes containing $[C_2C_1im][SCN]$ and $[C_2C_1im][BF_4]$ showed significantly high selectivity in comparison to the neat polymer. This was especially evident for R-513A, where both 40 wt % ILPMs had a selectivity of about 23 and the neat polymer had a selectivity of 10. Solubility measurements were conducted for the 40 wt % $[C_2C_1im][SCN]$ and $[C_2C_1im][BF_4]$ ILPMs due to the promising selectivity and permeability results. Solubility in the neat polymer membrane was also tested. Due to a solubility blockage phenomenon, $[C_2C_1im][SCN]$ decreased the sorption from that of the pure polymer membrane for every gas. Solubility in the $[C_2C_1im][BF_4]$ ILPM compared to the pure polymer membrane showed higher values for HFC-32, the same or slightly decreased for HFC-134a, and decreased for HFO-1234yf. Uncertainties are included for the mixed-gas permeability, although the manuscript lacks a description of how the uncertainty is obtained.

Although there are minimal studies investigating ILMs for refrigerant separation, with all of them focusing on the same polymer, the published results indicate that the presence of ionic liquid in polymeric membranes can improve permeability and selectivity for a given mixture due to the solubility tunability of the IL. In general, permeability tends to increase as a function of IL content in the composite membrane. Moreover, ILPMs exhibit higher permeabilities with ILs containing larger molar volumes. Some barriers to this technology are the negative impact that the IL imparts on selectivity resistance to pressure, which could be an issue in industrial separation processes occurring under high pressure. Further studies are needed to explore the use of ILMs for separation on a larger scale and to investigate additional IL + polymer combinations.

6.2. Adsorbent/IL Composite Materials

It is clear from previous sections that ILs are excellent solvents for fluorocarbon refrigerant absorption and separation processes. Previous sections additionally provided instances in which ILs absorbed other species. Although ILs possess excellent absorption capacities, diffusion limitations can inhibit use in applications that are sensitive to absorption rates. Transport properties in ILs can increase by increasing contact area. One method of doing this is by synthesizing adsorbent/IL composite materials in which the IL is coated on the adsorbent surface. An example of this is shown in Figure 10.

Adsorbent/IL composites are reported for CO_2 capture and separation,[218−222] NH_3 capture,[223] desulfurization of fuels,[224,225] and water purification.[226,227] Few studies involving adsorbent/IL composites with fluorochemicals are reported. One group reported the synthesis of a clay/IL composite for PFOA and PFOS capture,[228] whereas two groups reported adsorbent/IL composites in fluorocarbon refrigerant applications.[229−231] In most cases, adsorbents with large surface areas, such as metal−organic frameworks (MOFs) and large-pore silicas, were used to provide larger contact areas for the IL and the species of interest. Instances of fluorocarbon refrigerant sorption using adsorbent/IL composites will now be discussed

https://doi.org/10.1021/acs.chemrev.3c00276
Chem. Rev. XXXX, XXX, XXX−XXX

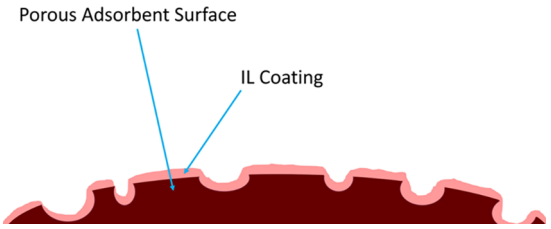

Figure 10. An adsorbent/IL composite material. A porous adsorbent (e.g., activated carbon and silica) is coated with an IL to increase the surface area and enhance the transport properties of the IL.

in detail. The refrigerants that were studied with adsorbent/IL composites are summarized in Table 21, and the ILs that were used to modify the adsorbents are summarized in Table 22.

A series of studies were performed by Yagnamurthy et al.[229−232] that investigated various composites for adsorption-cooling application with HFC-32. Previous studies showed that the Maxsorb III/HFC-32 working pair was promising for adsorption-cooling processes;[233,234] however, some adsorbent properties decrease the efficiency of the cooling cycle including low thermal conductivity and bulk density. This results in bulky heat exchangers needed for good cooling performance. To address the limitations, Yagnamurthy et al. synthesized five composite materials that contained varying compositions of Maxsorb III activated carbon, H25 graphene nanoplatelets (GNPs), poly(vinyl alcohol) (PVA), and $[C_6C_1im][Tf_2N]$.

Measurements showed that composite 4, which contains 40:40:10:10 of Maxsorb III:H25:$[C_6C_1im][Tf_2N]$:PVA, provided the largest thermal conductivity, whereas composite 1, which contains 80:0:10:10 of Maxsorb III:H25:$[C_6C_1im][Tf_2N]$:PVA, provided the largest volumetric cooling energy (VCE). The thermal conductivity in the perpendicular plane of composite 4 was 4.331 W/mK compared with 0.066 W/mK for Maxsorb III alone, whereas a 78% increase in VCE from Maxsorb III alone to composite 1 was reported. The uncertainty of the aforementioned values was not provided directly by the authors but could be investigated by understanding the experimental techniques used to acquire the data as outlined in the original text. The group concluded that composite 4 was ideal for adsorption-refrigerant cycles in which the surface area is the metric for heat exchanger design, whereas composite 1 was ideal when the volume of the heat exchanger was emphasized.

Through kinetic studies, cooling performance studies, and numerical modeling to optimize heat exchanger design, Yagnamurthy et al. later found that, for a comparable cooling power output, using composite 4 required 81% less surface area for heat exchange compared to composite 1. Furthermore, the ideal heat exchanger design when using composite 4 is an annular finned tube, whereas a longitudinal finned tube design is optimal when using composite 1 in adsorption-cooling application. The former design has a 25.5% larger volume and 40.9% lower heat exchanger mass compared to the latter design.

While investigating fluorocarbon refrigerant separation for repurposing and recycling, Sosa et al. studied sorption behavior between nine different silica/IL composites, HFC-32, HFC-125, and HFC-134a.[232] The group noted that ILs had the capability to absorb the HFCs but that diffusion limitations existed, which result from low contact areas. The following composites were synthesized and sorption capacities were measured using gravimetry at different temperatures: $SiO_2/[C_2C_1im][C_1CO_2]$, $SiO_2/[C_2C_1im][OTf]$, $SiO_2/[C_2C_1im][Tf_2N]$, $SiO_2/[C_2C_1im][PFP]$, $SiO_2/[C_2C_1im][PFBS]$, $SiO_2/[C_2C_1py][PFBS]$, $SiO_2/[C_2C_1im][Pf_2N]$, $SiO_2/[C_2C_1im][Nf_2N]$, $SiO_2/[C_2C_1im][PFOS]$.

Isotherm measurements showed that the composite materials had lower uptake capacities than the pure ILs and silica, and that the same sorption capacity trends existed with both the composites and pure ILs. Furthermore, the silica/IL composite isotherm data was corrected to only account for IL (i.e., a correction factor of 0.4 was applied to the data since 40% of the composite was IL) and the results were comparable to pure IL data. The group concluded that the IL properties control sorption behavior in the silica/IL composites. Sosa et al. further applied Ideal Adsorbed Solution Theory (IAST) using isotherm data for the silica/IL composites. At low pressures, selectivity for HFC-32 over HFC-125 increased, selectivity for HFC-134a over HFC-32 decreased, and selectivity for HFC-134a over HFC-125 decreased when using the composites with respect to pure silica. For HFC-134a/HFC-32 and HFC-134a/HFC-125, the selectivity was generally weaker for the composites (i.e., closer to 1) in the low-pressure region compared to pure silica. For HFC-32/HFC-125, the selectivity was either weaker or comparable in magnitude to that of pure silica.

Studies with adsorbent/IL composites and fluorocarbon refrigerants show that the composites can increase efficiency for refrigeration cycles in some cases, whereas supporting ILs on silicas decreases sorption capacity and can lead to weaker selectivity based on IAST predictions. In the latter case, the properties of the adsorbent surface for HFC interactions are lost, and the IL properties dictate sorption and separation outcome. Although sorption capacity decreases with the composites due to less IL, contact area between the HFCs and ILs increases, which decreases possible gas separation times relative to using

Table 21. Summary of Adsorbent/IL Composite Studies for Fluorocarbon Refrigerant Adsorption[a]

Refrigerant \ Ionic Liquid	$[C_6C_1im][Tf_2N]$	$[C_2C_1im][C_1CO_2]$	$[C_2C_1im][OTf]$	$[C_2C_1im][Pf_2N]$	$[C_2C_1im][PFP]$	$[C_2C_1im][PFBS]$	$[C_2C_1py][PFBS]$	$[C_2C_1im][Tf_2N]$	$[C_2C_1im][Nf_2N]$	$[C_2C_1im][PFOS]$	Adsorbent
HFC-32	229–231										Maxsorb III composites
		232	232	232	232	232	232	232	232	232	Silica
HFC-125		232	232	232	232	232	232	232	232	232	
HFC-134a		232	232	232	232	232	232	232	232	232	

[a]The intersections provide the reference(s) in which the adsorbent/IL materials were studied.

https://doi.org/10.1021/acs.chemrev.3c00276
Chem. Rev. XXXX, XXX, XXX−XXX

Table 22. Summary of ILs Studied for Modifying Adsorbents to Use in Fluorocarbon Refrigerant Adsorption Applications[a]

		3	3	3	3	3	6	3	3	3
	Anion / Cation	$[Tf_2N]^-$	$[C_1CO_2]^-$	$[CF_3SO_3]^-$	$[N(CF_3SO_2)_2]^-$	$[C_4F_9CO_2]^-$	$[C_4F_9SO_3]^-$	$[N(C_2F_5SO_2)_2]^-$	$[N(C_4F_9SO_2)_2]^-$	$[C_8F_{17}SO_3]^-$
24	$[C_2C_1im]^+$		3	3	3	3	3	3	3	3
33	$[C_6C_1im]^+$	3								
3	$[C_2C_1py]^+$						3			

[a]The intersections indicate the number of references in which the IL is reported.

pure ILs. Since Sosa et al. determined that the sorption behavior of the composites was identical to that for pure ILs, IAST predictions may not be an appropriate method for determining selectivity (i.e., *ab*sorption is taking place instead of *ad*sorption and so the thermodynamic description of the system is incorrect when using IAST). As a result, selectivity trends predicted by equation of state modeling for VLE might be more appropriate for adsorbent/IL composites.

6.3. Supported Ionic Liquid Phase Materials

One potential method of increasing the efficiency of ionic liquids as a gas separation medium are Supported Ionic Liquid Phase materials, also known as SILPs.[235] In a supported ionic liquid phase material, a thin film of ionic liquid is immobilized onto a solid support.[236] Typically, the thin film of IL is placed on a high surface area support, thus increasing the effective surface area.[235] This improves the mass transfer rate and decreases the viscosity which could make the process of gas absorption and desorption more efficient for industrial applications. Due to the various supports available to make SILPs, the success of a SILP is dependent on the chemical nature and porosity of the support used.[236] Supported ionic liquids take advantage of IL properties such as tunability as well as various characteristics of different solid supports such as a large surface area or high absorption capacity.[236,237] Other methods of increasing surface area of ILs such as stirring to create droplets are energy intensive due to the high viscosity.[238] The formation of SILPs requires less energy to increase the mass transfer rate while also decreasing the amount of IL needed. These advantages make SILPs a possible approach to the separation of refrigerant mixtures including R-410A.

SILPs materials have been tested for their ability to absorb many gases including ammonia, carbon monoxide, hydrogen, and fluorinated greenhouse gases.[232,237,239] In a study done for the absorption of ammonia, three metal ionic liquids (MILs) were placed on supports of porous silica gel, and all three of the MIL and silica composites showed higher NH_3 capacity and selectivity than regular silica gel, as well as faster NH_3 absorption rate compared to neat IL.[237] Both the IL and support had improved abilities when used together in the SILP. SILPs were also tested in a study on recovering H_2 and CO gas from N_2 gas streams.[239] The SILM was successful in separating H_2 and CO from an N_2 rich gas stream through improved permeability of CO but not N_2.[239] This selectivity could aid in the separation of the HFC-32 and HFC-125, the two components of R410-A, which also have diffusion coefficients similar to N_2 and CO. SILPs have also been tested on fluorinated greenhouse gases using fluorinated ionic liquids on silica supports.[232] The selectivity for the refrigerants, HFC-32, HFC-125, and HFC-134, was highly dependent on the fluorination of the IL as well as anion and cation groups on the IL.[232] In another study, the selectivity of the SILM was largely determined by the temperature and concentration of copper salt in the IL.[239,240] For the separation of R-410A, different ILs could be tested on more types of supports to continue improving the selectivity and absorption of the composite materials. As for the stability of SILPs, the thermal stability of supported ionic liquids is dependent on the type of support, with non-polar surfaces generally being more stable.[237] Additionally, SILPs in a study done with CO and N_2 gas were far more stable at lower pressures.[239] A SILP with copper containing ILs experienced enhanced CO permeability and did not undergo oxidation when kept under stable conditions for 2 weeks.[240] This means that SILPs displayed reusability for multiple absorption cycles. SILPs exhibited multiple advantages such as increased gas absorption capacity and absorption rates, selectivity for certain gases, and stability from supports, making them a promising technology for the separation of refrigerant mixtures.

6.4. Encapsulated Ionic Liquids

An emerging technology that holds potential for aiding in the separation of gaseous refrigerant mixtures such as R-410A is encapsulated ionic liquids, or ENILs.[241−249] Although ILs are great solvents due to properties including low vapor pressure and thermal stability, ILs typically have high viscosities and surface tensions.[241] This creates barriers for using ILs as a favorable separation media for filtration and extraction purposes. One proposed method to overcome the limiting mass transfer rate is by dispersing the IL into small droplets within microcapsules.[241] As a smaller droplet of IL, the active surface area available for gas absorption and desorption is increased which then improves the mass transfer rate. The four main methods of encapsulation are emulsion polymerization, solvent evaporation, pickering emulsion, and impregnation.[241] A more detailed explanation of how ILs are encapsulated is available in the previous source. Figure 11 shows a visualization of a single ENIL capsule. Since ILs are generally expensive materials to work with, encapsulation takes advantage of the properties of ILs while also being cost-effective.[243]

https://doi.org/10.1021/acs.chemrev.3c00276
Chem. Rev. XXXX, XXX, XXX−XXX

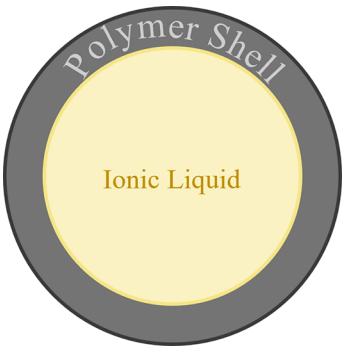

Figure 11. Visualization of an ENIL.

ENILs are being tested for CO_2 and ammonia capture. In a study done on ammonia capture, a gas stream of N_2 and NH_3 fed through ENILs experienced a rate of NH_3 absorption four times faster than that of neat IL while still maintaining the same absorption capacity.[244] By increasing the surface area and the mass transfer rate, the ENILs were able to speed up the absorption and desorption process. This could improve the cost-effectiveness and industrial applications of using ILs. In another study done on CO_2 capture, samples of used ENILs were regenerated using an ultrahigh vacuum.[245] The ENILs experienced no degradation, and the sorption capacity was stable upon multiple cycles.[245] Similarly, ENILs used for ammonia capture were easily regenerated under mild conditions and used in successive absorptions without loss of efficiency.[242] The recyclability of ENILs is another advantage, as the gas absorbed can be easily extracted without affecting the properties of the IL. Due to the high volume of R-410A and other HFC refrigerants that need to be recycled, ENILs could offer a faster, cheaper, and improved separation method. However, another study on CO_2 capture observed that some ILs had poorer thermal stability after encapsulation compared to neat IL.[243] This poses challenges for the separation of gases that may need to occur at a higher temperature. However, more experimentation with different ILs may yield improved thermal stabilities, especially if tested with ILs selective for HFC-32 and HFC-125. The following studies also used ENILs for gas separation.[242,243,248,250] Since multiple studies done with ENILs on other gases showed increased gas capture rates and selectivity for certain gases, ENILs could be applied to the separation of refrigerant mixtures.

The first paper investigating ENILs with FC refrigerants studied HFC-32 and HFC-125 sorption in ENILs made of a polyurea shell with three different ILs ($[C_4C_1im][PF_6]$, $[C_6C_1im][Cl]$, $[C_2C_1im][Tf_2N]$).[251] The results showed that the ENILs have very similar solubility trends compared to the neat ILs. However, they have significantly faster uptake of the HFC and slightly smaller sorption capacities on a mass basis when compared to the neat ILs. The absorption and desorption experiments showed the sorption was physical, where the diffusion was dominated by the polyurea shell and the solubility of the HFCs was dominated by the IL core.[251] These initial results show that ENILs have potential for use for FC refrigerants, though there is significantly more work to be done to better understand the shell/IL interactions and multicomponent sorption behavior.

6.5. Ionic-Liquid-Based Materials General Trends

Novel, IL-based materials including mixed matric membranes, absorbent/IL composite materials, supported IL phase materials, and encapsulated ionic liquids have shown promise for utilizing key IL properties to separate FC refrigerant mixtures with methods beyond extractive distillation. Nearly all ILs investigated with ILMMMs used a $[C_2C_1im]+$ cation with a variety of common anions with a single polymer type. The results showed that the incorporation of ILs can improve permeability and selectivity; however, the IL can negatively impact the selectivity resistance to pressure. The absorbent/IL composite tests also used a $[C_2C_1im]+$ cation with a variety of common anions with silica being the absorbent. The IL/absorbent composites showed increased efficiency in some cases; however, the sorption capacity is decreased in the composites compared to neat IL. The ENIL sorption of HFCs was shown with three common ILs. The ENILs allowed for an order of magnitude faster sorption due to increased surface area with only small decreases in sorption capacity compared to neat IL.

The use of IL-based materials for FC refrigerant separations shows initial promise; however, there is still significant work needed to fully understand the materials and if they have potential to be a commercial refrigerant separation technology. In particular lab scale and pilot scale testing would be required as well as methods for producing the IL-based materials at a large scale. These materials could allow for the separation of refrigerant mixtures at higher purities or lower energy usage than what can be achieved using extractive distillation.

7. CONCLUSIONS

Refrigeration is an essential technology that is relied upon daily and whose usage is increasing at a significant rate. Additionally, due to the environmental cost of many of the refrigerants used, each new generation of refrigerants is a set of more complex refrigerant mixtures. This and the fact that many refrigerant components form azeotropes with one another or have near azeotropic behavior lead to an enormous barrier for being able to reuse and recycle refrigerants at the end-of-life stage. ILs are being investigated as entrainers in extractive distillation and in other technologies to facilitate the separation of complex mixtures. This review summarized the studies completed on ILs and FC refrigerants including phase equilibria, transport and thermodynamic properties, molecular simulation and equation of state modeling, modeling and design of extractive distillation processes, material incorporating ILs, and other promising uses of ILs for this separation process.

The amount of research on this topic has significantly increased since its start in the early 2000s, and to the authors' knowledge, there have been at least 89 unique ILs investigated for this application with over 900 studies with a FC refrigerant in one of the areas discussed in this review. Even with this significant amount of work it is important to note that the top three cations, $[C_2C_1im]^+$, $[C_4C_1im]^+$, and $[C_6C_1im]^+$, make up over 75% of the investigations and the top three anions, $[BF_4]^-$, $[PF_6]^-$, and $[Tf_2N]^-$, make up over 45% of the investigations. This indicates both how much progress has been made and how much more opportunity there is for additional research. In particular, there are large gaps in transport and thermodynamic property measurements, the need to develop predictive molecular simulations, and additional experimental and modeling required of materials incorporating ionic liquids for refrigerant separations.

Studies on the thermodynamic and transport properties of FC refrigerant/IL mixtures have continued to increase gradually over the past decade. Yet, several properties that are vital to

https://doi.org/10.1021/acs.chemrev.3c00276
Chem. Rev. XXXX, XXX, XXX−XXX

process feasibility assessment and design such as calorimetric properties and surface/interfacial tension are scarce. The explored transport properties, mainly viscosity and thermal conductivity, can be used to estimate various design parameters and process viability. However, proper overall assessment would require further investigations into other thermodynamic and transport properties such as heat capacity, excess heat, and surface/interfacial tensions of mixtures.

Development of more robust screening processes that integrate the multitude of facets involved in IL selection such as the wide array of thermophysical properties governing two-phase unit design is vital. A better understanding of the molecular interactions in mixtures of ILs and fluorinated solutes through a combination of molecular dynamics simulations and experimental investigations would allow for better predictions and modeling of mixture behaviors. Ultimately, proper characterization of governing phenomena can decrease the dependency on costly experimental work and increase the viability of predictive selection criteria. Continued work on measuring the thermodynamic and transport properties of FC refrigerant/IL mixtures is key to high accuracy modeling and design work.

The improvement in force field accuracy and advanced sampling techniques facilitate rapid computer-aided screening of optimal entrainers for the separation of HFC mixtures. However, the manual calibration of force fields is a labor-intensive and time-consuming task that heavily relies on human expertise. While machine learning techniques have emerged as valuable tools to expedite this process, they often yield force fields that are customized for specific molecules. Thus, a more generalized force field of HFCs and HFOs that can accurately capture the diverse interactions and behaviors of these compounds is urgently required. Moreover, as computer technology continues to advance, it has become increasingly important to account for the polarization effect in molecular simulations to achieve higher levels of accuracy. At the same time, efforts to improve the efficiency of solubility calculations of HFCs in ILs are underway to enable faster screening of ideal candidates for HFC separations.

The results show that ILs have the selectivity and tunability to separate azeotropic refrigerant mixtures. This is supported by a growing amount of thermophysical property measurements of the mixtures and significant improvement in molecular simulation of these system. Finally, the initial modeling results of extractive distillation processes using ionic liquids as entrainers show the promise of this separation process. Improvements in screening capabilities and mixture properties for both experimental and simulation results will be used together to produce high-quality data faster while leading to more in-depth understanding of FC refrigerant/IL systems. This will result in higher accuracy separation process modeling and design that will soon be able to be compared to pilot scale separation data.

8. FUTURE WORK

As discussed in this review, current ILs in the literature are focused on the separation of refrigerant mixtures that are non-azeotropic and azeotropic. Although there has been significant progress in understanding FC refrigerant/IL systems, there is still work to be done investigating more cation types beyond imidazolium and measuring FC/IL mixture thermodynamic and transport properties. One major breakthrough in the future would be the design and synthesis of chiral ILs for the separation of refrigerant diastereomers and enantiomers. Beyond synthesis and experimental results, simulations have significantly improved in both time scale and accuracy. However, universal force fields that are transferable across classes of refrigerants such as HFCs, HFOs, HCFCs, and HCFOs are still needed. The development of novel materials poses an opportunity to utilize key properties of ILs in non-traditional applications such as packed beds and membrane modules. Another opportunity for ILs with refrigerant applications is the development of ILs as potential new lubricants for cooling systems.

The development of refrigerant separation technology is a key part of a circular refrigerant economy. However, today the refrigerant market is not circular, with less than 3% of refrigerants recycled. A significant philosophy shift is needed to evaluate the total equivalent warming impact of refrigerants (TEWI, which accounts for both direct and indirect emissions) rather than only refrigerant global warming potentials (GWP, direct emissions).

The combination of technology advancement and a philosophy shift will allow for the creation of a circular refrigerant economy, allowing for a significant increase in the recovery, recycling, and ultimate reuse of the fluorocarbon refrigerants (critical materials) both in refrigerant blends and as fluorinated feedstocks for new materials.

ASSOCIATED CONTENT

Supporting Information

The Supporting Information is available free of charge at https://pubs.acs.org/doi/10.1021/acs.chemrev.3c00276.

Abbreviations used throughout the manuscript; nomenclature, designations, and chemical formulas for single-component refrigerants and refrigerant mixtures; and nomenclature and abbreviations for ionic liquid anions and cations (PDF)

AUTHOR INFORMATION

Corresponding Author

Mark B. Shiflett − *Wonderful Institute for Sustainable Engineering, Lawrence, Kansas 66045, United States; Department of Chemical and Petroleum Engineering, University of Kansas, Lawrence, Kansas 66045, United States;* orcid.org/0000-0002-8934-6192; Email: mark.b.shiflett@ku.edu

Authors

Kalin R. Baca − *Wonderful Institute for Sustainable Engineering, Lawrence, Kansas 66045, United States; Department of Chemical and Petroleum Engineering, University of Kansas, Lawrence, Kansas 66045, United States;* orcid.org/0000-0002-7292-8698

Karim Al-Barghouti − *Wonderful Institute for Sustainable Engineering, Lawrence, Kansas 66045, United States; Department of Chemical and Petroleum Engineering, University of Kansas, Lawrence, Kansas 66045, United States;* orcid.org/0000-0002-6167-1516

Ning Wang − *Department of Chemical & Biomolecular Engineering, University of Notre Dame, Notre Dame, Indiana 46556, United States;* orcid.org/0000-0002-5515-6198

Madelyn G. Bennett − *Wonderful Institute for Sustainable Engineering, Lawrence, Kansas 66045, United States; Department of Chemical and Petroleum Engineering,*

https://doi.org/10.1021/acs.chemrev.3c00276
Chem. Rev. XXXX, XXX, XXX−XXX

University of Kansas, Lawrence, Kansas 66045, United States; orcid.org/0000-0002-0698-7518

Lucia Matamoros Valenciano − *Wonderful Institute for Sustainable Engineering, Lawrence, Kansas 66045, United States; Department of Chemical and Petroleum Engineering, University of Kansas, Lawrence, Kansas 66045, United States;* orcid.org/0000-0002-4964-9148

Tessie L. May − *Wonderful Institute for Sustainable Engineering, Lawrence, Kansas 66045, United States; Department of Chemical and Petroleum Engineering, University of Kansas, Lawrence, Kansas 66045, United States;* orcid.org/0000-0002-3000-9765

Irene V. Xu − *Wonderful Institute for Sustainable Engineering, Lawrence, Kansas 66045, United States; Department of Chemical and Petroleum Engineering, University of Kansas, Lawrence, Kansas 66045, United States*

Max Cordry − *Wonderful Institute for Sustainable Engineering, Lawrence, Kansas 66045, United States; Department of Chemical and Petroleum Engineering, University of Kansas, Lawrence, Kansas 66045, United States*

Dorothy M. Haggard − *Wonderful Institute for Sustainable Engineering, Lawrence, Kansas 66045, United States; Department of Chemical and Petroleum Engineering, University of Kansas, Lawrence, Kansas 66045, United States;* orcid.org/0000-0001-5575-1651

Abigail G. Haas − *Wonderful Institute for Sustainable Engineering, Lawrence, Kansas 66045, United States; Department of Chemical and Petroleum Engineering, University of Kansas, Lawrence, Kansas 66045, United States*

Ashley Heimann − *Wonderful Institute for Sustainable Engineering, Lawrence, Kansas 66045, United States; Department of Chemical and Petroleum Engineering, University of Kansas, Lawrence, Kansas 66045, United States*

Abby N. Harders − *Wonderful Institute for Sustainable Engineering, Lawrence, Kansas 66045, United States; Department of Chemical and Petroleum Engineering, University of Kansas, Lawrence, Kansas 66045, United States;* orcid.org/0000-0003-0311-3855

Hannah G. Uhl − *Wonderful Institute for Sustainable Engineering, Lawrence, Kansas 66045, United States; Department of Chemical and Petroleum Engineering, University of Kansas, Lawrence, Kansas 66045, United States*

Diego T. Melfi − *Wonderful Institute for Sustainable Engineering, Lawrence, Kansas 66045, United States; Department of Chemical and Petroleum Engineering, University of Kansas, Lawrence, Kansas 66045, United States*

Andrew D. Yancey − *Wonderful Institute for Sustainable Engineering, Lawrence, Kansas 66045, United States; Department of Chemical and Petroleum Engineering, University of Kansas, Lawrence, Kansas 66045, United States;* orcid.org/0000-0003-4910-1294

Rajkumar Kore − *Wonderful Institute for Sustainable Engineering, Lawrence, Kansas 66045, United States; Department of Chemical and Petroleum Engineering, University of Kansas, Lawrence, Kansas 66045, United States;* orcid.org/0000-0002-3361-1188

Edward J. Maginn − *Department of Chemical & Biomolecular Engineering, University of Notre Dame, Notre Dame, Indiana 46556, United States;* orcid.org/0000-0002-6309-1347

Aaron M. Scurto − *Wonderful Institute for Sustainable Engineering, Lawrence, Kansas 66045, United States; Department of Chemical and Petroleum Engineering, University of Kansas, Lawrence, Kansas 66045, United States;* orcid.org/0000-0001-7214-1871

Complete contact information is available at: https://pubs.acs.org/10.1021/acs.chemrev.3c00276

Author Contributions

CRediT: **Kalin R. Baca** writing-review & editing; **Karim S. Al-Barghouti** writing-review & editing; **Ning Wang** writing-review & editing; **Madelyn G. Bennett** writing-review & editing; **Lucia Matamoros Valenciano** writing-review & editing; **Tessie L. May** writing-review & editing; **Irene Xu** writing-review & editing; **Max Cordry** writing-review & editing; **Dorothy M Haggard** writing-review & editing; **Abigail Haas** writing-review & editing; **Ashley Heimann** writing-review & editing; **Abby N Harders** writing-review & editing; **Hannah Uhl** writing-review & editing; **Diego Melfi** writing-review & editing; **Andrew D. Yancey** writing-review & editing; **Rajkumar Kore** writing-review & editing; **Edward J. Maginn** writing-review & editing; **Aaron M Scurto** writing-review & editing; **Mark B. Shiflett** writing-review & editing.

Notes

The authors declare the following competing financial interest(s): Baca and Shiflett are co-founders of a startup company that works with refrigerants.

Biographies

Kalin R. Baca is the Chief Operating Officer and Co-founder of Icorium Engineering Company. Dr. Baca graduated with honors from the University of Kansas (KU) with a Ph.D. in Chemical Engineering, is an entrepreneur, and is an advocate for sustainable engineering practices. Her doctoral dissertation focused on investigating the role of ionic liquids for separating azeotropic refrigerant mixtures using extractive distillation, and her impactful research has resulted in over 15 technical presentations and 7 publications. Prior to her time at KU, she earned her M.S. in Chemical Engineering, B.S. in Chemical Engineering, and MBA from the University of New Mexico. Kalin's career also includes a position at Sandia National Laboratories, where she contributed to an R&D 100 Award-winning team for a groundbreaking 3D X-Ray Phase Contrast Imaging System. Kalin is a committed advocate for diversity, equity, and inclusivity in communities of innovation and the advancement of women in STEM and entrepreneurship. At KU, Kalin served as President of the Graduate Engineering Association, was a member of the SoE diversity, equity, and inclusion committee, and was a participant in KU's prestigious Self Graduate Fellows program for promising graduate student leaders.

Karim Al-Barghouti is a Chemical Engineering Ph.D. candidate working in Prof. Aaron Scurto's lab group at the University of Kansas. Mr. Al-Barghouti received his B.S. in Chemical Engineering with a minor in Biomedical Engineering from the University of South Florida in 2020. He is currently a member of project EARTH (Environmentally Applied Research Towards Hydrofluorocarbons), a multidisciplinary, multi-university (Univ. Kansas, Univ. Notre Dame, and Texas A&M Univ.) effort focused on the separation of azeotropic/near-azeotropic HFC blends. His work focuses on measurements and modeling of thermophysical properties of ionic liquids and HFC mixtures.

Ning Wang is a Ph.D. candidate in Chemical Engineering at the University of Notre Dame under the supervision of Dr. Edward Maginn and an Editorial Board Member of *Journal of Ionic Liquids*. She holds an M.S.E. in Materials Science and Engineering from the University of Pennsylvania and a B.E. in Polymer Materials and Engineering from Beijing University of Chemical Technology. Her expertise lies in

molecular modeling and simulations, free energy calculations, machine learning techniques, and force field development with an emphasis on ionic liquid and hydrofluorocarbon systems. She has received awards that include a National Scholarship from the Ministry of Education of China (2015), a Master's Scholar Award from Univ Pennsylvania (2019), and a Student Speaker Award from Univ. Notre Dame (2023). She works extensively on the National Science Foundation project, EFRI DChem: Next-generation Low Global Warming Refrigerants, Award no. EFRI-2029354. Her academic success was reflected in her impressive publication records, active participation in conferences, and commitment to professional growth through summer internships.

Madelyn G. Bennett is a Ph.D. student at the University of Colorado (CU) Boulder. She graduated from KU in 2023 with a B.S. in Chemical Engineering with distinction. She worked at KU as an undergraduate researcher for Project EARTH (Environmentally Applied Research Towards Hydrofluorocarbons) and focused on phase equilibria on ionic liquids and hydrofluorocarbons. Madelyn is a National Science Foundation (NSF) Graduate Research Fellow. Her doctoral research at CU is focused on high temperature energy storage.

Lucia Matamoros Valenciano is a chemical engineer in the chemical feed group for water and wastewater treatment at Black & Veatch. She graduated from KU in 2023 with a B.S. in Chemical Engineering with an environmental emphasis. She worked at KU as an undergraduate researcher for Project EARTH (Environmentally Applied Research Toward Hydrofluorocarbons). She was part of the University Honors Program and a member of the Society of Hispanic Professional Engineers (SHPE).

Tessie L. May is a class of 2024 undergraduate, studying chemical engineering at KU. Ms. May worked as an undergraduate researcher in the Wonderful Institute for Sustainable Engineering at KU (WISE-KU) working on Project EARTH (Environmentally Applied Research Toward Hydrofluorocarbons). Ms. May is also an executive member for KU's Engineering Student Council. Upon graduation, she will work at John Zink Hamworthy Combustion - A Koch Engineered Solutions Company as a Process Engineer.

Irene V. Xu is an undergraduate researcher, class of 2026, SELF Fellow studying chemical engineering at KU. Ms. Xu worked as an undergraduate researcher at WISE-KU (Wonderful Institute for Sustainable Engineering) working on Project EARTH (Environmentally Applied Research Towards Hydrofluorocarbons) and is currently an undergraduate R&D Engineering intern with Icorium Engineering Company. Ms. Xu also serves as the Community Relations Coordinator for The Big Event and an active member of the Engineers Without Borders (EWB) student chapter at KU.

Max Cordry is an undergraduate, class of 2024, studying chemical engineering at KU. He served as an undergraduate researcher for the Shiflett research group from 2022 to 2023, analyzing data for Project EARTH (Environmentally Applied Research Towards Hydrofluorocarbons) that is currently being used to design and scale-up extractive distillation using ionic liquids for refrigerant separations. He has interned for Kansas State University's PPI (Pollution Prevention Institute) to identify areas where a host company can reduce environmental emissions. He is also an officer for Tau Beta Pi's Kansas Alpha Chapter.

Dorothy M. Haggard is an undergraduate, class of 2024, chemical engineering student at KU. Dorothy has been a researcher in the Wonderful Institute for Sustainable Engineering at KU (WISE-KU) since 2021, studying the physical properties and solubilities of ionic liquids for the extractive distillation of refrigerant blends. She was granted the Undergraduate Research Fellowship within KU Engineering for this work. In addition, Dorothy is a business analyst at KU Innovation Park and is the co-president of KU's Society of Women Engineers.

Abigail G. Haas graduated with her B.S. in chemical engineering with an environmental emphasis in 2023. Ms. Haas worked on analyzing thermal properties of refrigerants and ionic liquid mixtures at KU. Ms. Haas served on the philanthropy committee and as service chair for Alpha Sigma Kappa-Women in Technical Studies. Ms. Haas worked on a greenhouse gas emission reduction program during her environmental engineering internship at Scout Energy Partners and transitioned to a full-time position shortly after graduation.

Ashley Heimann is a chemical engineering student, class of 2024, at KU. Ms. Heimann worked as an undergraduate research assistant at the Wonderful Institute for Sustainable Engineering at KU (WISE-KU) since the summer of 2022. She has worked on various projects such as Project EARTH (Environmentally Applied Research Towards Hydrofluorocarbons) and studying the dissolution of cellulose in ionic liquids. After graduation, Ms. Heimann plans to pursue a Ph.D. in Chemical Engineering at Iowa State University.

Abby N. Harders is a KU Chemical Engineering Ph.D. candidate and member of the Shiflett research group at KU. Harders graduated summa cum laude from Bethel College in 2020 with a B.A. in Chemistry and Mathematics. She is a member of Project EARTH (Enviromentally Applied Research Towards Hydrofluorocarbons), which is centered on developing sustainable processes for the selective separation of HFC refrigerant mixtures. Ms. Harders is a Chancellor's fellow at KU, a Phi Kappa Phi Scholar, and a student liaison and advocate for students and graduate students in the chemical engineering department at KU. Her doctoral research is focused on membrane separation using perfluoropolymers, and she is an author on 6 publications concerning the separation of azeotropic refrigerants.

Hannah G. Uhl is an undergraduate, class of 2024, chemical engineering student at KU. Ms. Uhl is an undergraduate researcher at the Wonderful Institute for Sustainable Engineering at KU (WISE-KU) working on Project EARTH (Environmentally Applied Research Towards Hydrofluorocarbons) researching sustainable refrigerant gas separation using membranes. Ms. Uhl has been an Analytical Intern at Crititech Particle Engineering Solutions and a Process Engineering Intern at Bayer Crop Science. She also is a School of Engineering Ambassador and an active member of the Chi Omega Sorority at KU.

Diego T. Melfi is a Ph.D. student at the University of Kansas. He received his B.S. (2018) and M.S (2021) in Chemical Engineering from the Federal University of Paraná (UFPR, Brazil). His Ph.D. focuses on separation processes that are relevant for plastics' upcycling and manufacturing of renewable polymers.

Andrew D. Yancey is a Ph.D. student in Chemical Engineering at KU. He graduated from Baylor University with a B.S. in Chemistry in 2019. His current research focuses on adsorption-based separation of refrigerant mixtures, which entails adsorbent characterization, pure and binary adsorption data collection, performing dynamic breakthrough experiments, pure and binary adsorption modeling, and process design and scale-up.

Rajkumar Kore is a Principal Investigator at the INVISTA Company since May 2023. Dr. Kore worked with the Shiflett research group at KU as an Associate Researcher from 2018 to 2023. Dr. Kore worked on multiple projects at KU that are based on the development of sustainable materials (e.g., ILs, polymers, etc.) for catalysis, extraction, and separation. Before KU, he worked with Prof. Robin Rogers at the University of Alabama as a Postdoctoral Research Scientist from 2014 to 2018. Dr. Kore received his Ph.D. from IIT Ropar in 2014 and his M.S. from the University of Pune in 2009. Prior to his Ph.D., he worked

https://doi.org/10.1021/acs.chemrev.3c00276
Chem. Rev. XXXX, XXX, XXX−XXX

at the National Chemical Laboratory in Pune for one year. Dr. Kore is an inventor of 10 U.S. patents and has published over 35 articles.

Edward J. Maginn is a Keough-Hesburgh Professor in the Department of Chemical and Biomolecular Engineering and Associate Vice President for Research at the University of Notre Dame. Professor Maginn was named a Fellow of the National Academy of Inventors (NAI) in 2023. Professor Maginn received his B.S. in Chemical Engineering from Iowa State University in 1987. Upon graduation he joined Procter and Gamble as an operations engineer. In 1990, he entered graduate school, and he received his Ph.D. in Chemical Engineering from the University of California at Berkeley in 1995. He joined the faculty of Notre Dame in 1995 as an Assistant Professor of Chemical Engineering and has remained at Notre Dame ever since. His research focuses on the development and application of molecular modeling techniques for understanding structure−property relationships in materials related to sustainable energy and environmental applications. He has over 240 refereed publications and 10 patents. He has consulted for a number of companies and is the recipient of the Dow Outstanding New Faculty Award from the American Society for Engineering Education, the Faculty Early Career Development (CAREER) Award from the National Science Foundation, and the Early Career Award from the Computational Molecular Science and Engineering Forum of the American Institute of Chemical Engineers. He has also received several teaching awards, including the BP Outstanding Teacher award for the Notre Dame College of Engineering, two John A. Kaneb Awards from the University of Notre Dame, and the American Institute of Chemical Engineers Student Chapter Outstanding Teaching Award.

Aaron M. Scurto is a Professor in the Department of Chemical & Petroleum Engineering at KU. He received his B.S. in Chemical Engineering from the University of Delaware and his Ph.D. from the University of Notre Dame, where he focused on metal chelates in supercritical fluids (SCFs) and ionic liquid separations. He then performed postdoctoral projects in technical chemistry at the RWTH-Aachen on homogeneous catalysis in ionic liquids and SCFs and in Chemistry and Bioengineering at MIT on biocatalysis in non-aqueous solvents. He joined KU in 2004 and is a member of the Wonderful Institute of Sustainable Engineering (WISE-KU) and Center for Environmentally Beneficial Catalysis (CEBC) at KU. In 2015, he became an Associate Editor for Industrial & Engineering Chemistry Research (IECR). Professor Scurto's current interests include ionic liquids for reactions, separations, and biomass processing; thermophysical property measurement and modeling at high pressures; and polymer upcycling separations.

Mark B. Shiflett is a Distinguished Foundation Professor in the Department of Chemical and Petroleum Engineering and Director of the Wonderful Institute for Sustainable Engineering at the University of Kansas (WISE-KU). Professor Shiflett joined KU as a Foundation Professor in August 2016 after retiring from the DuPont Company. Professor Shiflett worked for DuPont for 28 years and was a Technical Fellow in the Central Research and Development organization (Wilmington, Delaware). Professor Shiflett was also an adjunct professor at the University of Delaware in the Department of Chemical and Biomolecular Engineering. Professor Shiflett received his Ph.D. and M.S. in chemical engineering from the University of Delaware in 2001 and 1998. He received his B.S. in chemical engineering from N.C. State University in 1989. Professor Shiflett is an inventor on 46 U.S. patents and has published 140 articles on his research in both academia and DuPont. He was awarded the DuPont Bolton Carothers award in 2005, the ACS Hero of Chemistry award in 2006, and the University of Delaware presidential citation in 2007 for his development of hydrofluorocarbon refrigerant mixtures to replace chlorofluorocarbons, which were linked to the depletion of the Earth's ozone layer. Professor Shiflett was elected in 2014 to be a Fellow in the American Institute of Chemical Engineers, in 2016 to be a Division Fellow in the American Chemical Society, and in 2018 to be a Fellow in the National Academy of Inventors for his significant professional accomplishments and contributions to the chemical engineering profession. Professor Shiflett received the American Institute of Chemical Engineers Institute award for Industrial Research in 2016 for the development of non-ozone-depleting refrigerants, which have led to the healing of the Earth's ozone layer, new applications using ionic liquids, an environmentally friendly TiO_2 process, and mentoring and educating chemical engineers. Professor Shiflett is a licensed professional engineer in the State of Delaware, and his research at KU focuses on developing environmentally friendly, energy efficient processes and products for the chemical industry.

ACKNOWLEDGMENTS

The project was funded by the National Science Foundation, Grant Award 2029354 and 1917480.

REFERENCES

(1) Evans, O. *Transcribed Classic Text: The Abortion of the Young Steam Engineer's Guide*; University of Rochester Steam Collection, The Hopkin Thomas Project, 1805. https://www.thehopkinthomasproject.com/TheHopkinThomasProject/TimeLine/Wales/Steam/URochesterCollection/Evans/Evans%20Combined.htm (accessed April 16, 2023).

(2) Nagengast, B. *Air Conditioning and Refrigeration Timeline*; ASHRAE. https://www.ashrae.org/about/mission-and-vision/ashrae-industry-history/air-conditioning-and-refrigeration-timeline (accessed April 16, 2023).

(3) Perkins Vapor-Compression Cycle for Refrigeration: A Historical Mechanical Engineering Landmark; 2020. https://www.asme.org/getmedia/cb9bea09-6d23-425e-bfe5-5f6d786919fb/274-perkins-vapor-comp-refrig.pdf (accessed April 16, 2023).

(4) Calm, J. M. The next Generation of Refrigerants − Historical Review, Considerations, and Outlook. *International Journal of Refrigeration* **2008**, *31* (7), 1123−1133.

(5) Sicard, A. J.; Baker, R. T. Fluorocarbon Refrigerants and Their Syntheses: Past to Present. *Chem. Rev.* **2020**, *120* (17), 9164−9303.

(6) Montreal Protocol. *Article 2F: Hydrochlorofluorocarbons*. UN Environmental Program, Ozone Secretariat. https://ozone.unep.org/treaties/montreal-protocol/articles/article-2f-hydrochlorofluorocarbons (accessed April 16, 2023).

(7) Montreal Protocol. *Article 2A: CFCs*. UN Environmental Program, Ozone Secretariat. https://ozone.unep.org/treaties/montreal-protocol/articles/article-2a-cfcs (accessed April 16, 2023).

(8) Asensio-Delgado, S.; Pardo, F.; Zarca, G.; Urtiaga, A. Absorption Separation of Fluorinated Refrigerant Gases with Ionic Liquids: Equilibrium, Mass Transport, and Process Design. *Sep Purif Technol.* **2021**, *276*, 119363.

(9) Montreal Protocol. *The Kigali Amendment (2016): The amendment to the Montreal Protocol agreed by the Twenty-Eighth Meeting of the Parties (Kigali, 10−15 October 2016)*. UN Environmental Program, Ozone Secretariat. https://ozone.unep.org/treaties/montreal-protocol/amendments/kigali-amendment-2016-amendment-montreal-protocol-agreed (accessed April 16, 2023).

(10) Air Pollution Prevention and Control. In *United States Code Title 42 - The Public Heath and Welfare*; U.S. Government Publishing Office: 2013.

(11) California Air Resources Board. *AB 32 Global Warming Solutions Act of 2006*. https://ww2.arb.ca.gov/resources/fact-sheets/ab-32-global-warming-solutions-act-2006 (accessed April 16, 2023).

(12) European Parliament. *Regulation (EC) No 842/2006 on certain fluorinated greenhouse gases — European Environment Agency*. https://

https://doi.org/10.1021/acs.chemrev.3c00276
Chem. Rev. XXXX, XXX, XXX−XXX

www.eea.europa.eu/policy-documents/regulation-ec-no-842-2006 (accessed April 16, 2023).
(13) Booten, C.; Nicholson, S.; Mann, M.; Abdelaziz, O. *Refrigerants: Market Trends and Supply Chain Assessment*; 2020. DOI: 10.2172/1599577.
(14) Asensio-Delgado, S.; Viar, M.; Pardo, F.; Zarca, G.; Urtiaga, A. Gas Solubility and Diffusivity of Hydrofluorocarbons and Hydrofluoroolefins in Cyanide-Based Ionic Liquids for the Separation of Refrigerant Mixtures. *Fluid Phase Equilib.* **2021**, *549*, 113210.
(15) *ASHRAE Refrigerant Designations*. ANSI/ASHRAE 34-2022, Designation and Safety Classification of Refrigerants. https://www.ashrae.org/technical-resources/standards-and-guidelines/ashrae-refrigerant-designations (accessed April 18, 2023).
(16) ASHRAE Standards Committee; ASHRAE Technology Council; American National Standards Institute. *Designation and Safety Classification of Refrigerants*; 1997. www.ashrae.org (accessed April 16, 2023).
(17) ASHRAE Technical Committee. *ASHRAE Terminology Database*. https://terminology.ashrae.org/ (accessed April 18, 2023).
(18) Yancey, A. D.; Terian, S. J.; Shaw, B. J.; Bish, T. M.; Corbin, D. R.; Shiflett, M. B. A Review of Fluorocarbon Sorption on Porous Materials. *Microporous Mesoporous Mater.* **2022**, *331*, 111654.
(19) Pardo, F.; Gutiérrez-Hernández, S. V.; Zarca, G.; Urtiaga, A. Toward the Recycling of Low-GWP Hydrofluorocarbon/Hydrofluoroolefin Refrigerant Mixtures Using Composite Ionic Liquid-Polymer Membranes. *ACS Sustain Chem. Eng.* **2021**, *9* (20), 7012−7021.
(20) Zhao, L.; Zeng, W.; Yuan, Z. Reduction of Potential Greenhouse Gas Emissions of Room Air-Conditioner Refrigerants: A Life Cycle Carbon Footprint Analysis. *J. Clean Prod* **2015**, *100*, 262−268.
(21) Jovell Hidalgo, D. Design and Optimization of the Recovery and Recycling of Fluorinated Working Fluids Using a Multiscale Simulation Approach; Universitat Ramon Llull: 2023. https://www.tdx.cat/handle/10803/687654 (accessed April 18, 2023).
(22) Zhao, Y.; Li, Z.; Zhang, X.; Wang, X.; Dong, X.; Gao, B.; Gong, M.; Shen, J. Azeotropic Refrigerants and Its Application in Vapor Compression Refrigeration Cycle. *International Journal of Refrigeration* **2019**, *108*, 1−13.
(23) Holbrey, J. D.; Seddon, K. R. Ionic Liquids. *Clean Products and Processes* **1999**, *1* (4), 223−236.
(24) Shiflett, M. B.; Yokozeki, A. Solubility and Diffusivity of Hydrofluorocarbons in Room-Temperature Ionic Liquids. *AIChE J.* **2006**, *52* (3), 1205−1219.
(25) Hallett, J. P.; Welton, T. Room-Temperature Ionic Liquids: Solvents for Synthesis and Catalysis. 2. *Chem. Rev.* **2011**, *111* (5), 3508−3576.
(26) Welton, T. Room-Temperature Ionic Liquids. Solvents for Synthesis and Catalysis. *Chem. Rev.* **1999**, *99* (8), 2071−2083.
(27) *1-Hexyl-3-methylimidazolium chloride, >98% | IoLiTec*. https://iolitec.de/en/node/118 (accessed March 12, 2023).
(28) Gómez, E.; González, B.; Domínguez, Á.; Tojo, E.; Tojo, J. Dynamic Viscosities of a Series of 1-Alkyl-3-Methylimidazolium Chloride Ionic Liquids and Their Binary Mixtures with Water at Several Temperatures. *J. Chem. Eng. Data* **2006**, *51* (2), 696−701.
(29) Klomfar, J.; Součková, M.; Pátek, J. Experimental Densities and Surface Tension and Models Generating the Best-Current-Knowledge Values of Them for Members of 1-Cn-3-Methylimidazolium Bromide Homologous Series. *J. Chem. Thermodyn.* **2018**, *118*, 225−234.
(30) Li, J. G.; Hu, Y. F.; Sun, S. F.; Liu, Y. S.; Liu, Z. C. Densities and Dynamic Viscosities of the Binary System (Water + 1-Hexyl-3-Methylimidazolium Bromide) at Different Temperatures. *J. Chem. Thermodyn.* **2010**, *42* (7), 904−908.
(31) McAtee, Z. P.; Heitz, M. P. Density, Viscosity and Excess Properties in the Trihexyltetradecylphosphonium Chloride Ionic Liquid/Methanol Cosolvent System. *J. Chem. Thermodyn* **2016**, *93*, 34−44.
(32) *1-Butyl-3-methylimidazolium hexafluorophosphate, 99% | IoLiTec*. https://iolitec.de/en/products/ionic_liquids/catalogue/imidazolium-based/il-0011-hp (accessed March 12, 2023).
(33) Kumełan, J.; Kamps, Á. P. S.; Tuma, D.; Maurer, G. Solubility of CO in the Ionic Liquid [Bmim][PF6]. *Fluid Phase Equilib.* **2005**, *228*−*229*, 207−211.
(34) Salgado, J.; Regueira, T.; Lugo, L.; Vijande, J.; Fernández, J.; García, J. Density and Viscosity of Three (2,2,2-Trifluoroethanol + 1-Butyl-3-Methylimidazolium) Ionic Liquid Binary Systems. *J. Chem. Thermodyn* **2014**, *70*, 101−110.
(35) 1-Ethyl-3-methylimidazolium Bis(trifluoromethylsulfonyl) imide, 99% | IoLiTec. https://iolitec.de/en/node/455 (accessed 2023-03-12).
(36) Jacquemin, J.; Husson, P.; Majer, V.; Costa Gomes, M. F. Influence of the Cation on the Solubility of CO2 and H 2 in Ionic Liquids Based on the Bis(Trifluoromethylsulfonyl)Imide Anion. *J. Solution Chem.* **2007**, *36* (8), 967−979.
(37) Tariq, M.; Carvalho, P. J.; Coutinho, J. A. P.; Marrucho, I. M.; Lopes, J. N. C.; Rebelo, L. P. N. Viscosity of (C2−C14) 1-Alkyl-3-Methylimidazolium Bis(Trifluoromethylsulfonyl)Amide Ionic Liquids in an Extended Temperature Range. *Fluid Phase Equilib.* **2011**, *301* (1), 22−32.
(38) Walden, P. Molecular Weights and Electrical Conductivity of Several Fused Salts. *Bull. Acad. Imper. Sci. (St. Petersburg)* **1914**, *8*, 405−422.
(39) Shiflett, M. B.; Harmer, M. A.; Junk, C. P.; Yokozeki, A. Solubility and Diffusivity of Difluoromethane in Room-Temperature Ionic Liquids. *J. Chem. Eng. Data* **2006**, *51* (2), 483−495.
(40) Finberg, E. A.; May, T. L.; Shiflett, M. B. Multicomponent Refrigerant Separation Using Extractive Distillation with Ionic Liquids. *Ind. Eng. Chem. Res.* **2022**, *61* (27), 9795−9812.
(41) Shiflett, M. B.; Yokozeki, A.; Schiller, M. Utilizing Ionic Liquids for Hydrofluorocarbon Separation. US8628644, 2014.
(42) Liu, X.; Nguyen, M. Q.; Xue, S.; Song, C.; He, M. Vapor−Liquid Equilibria and Inter-Diffusion Coefficients for Working Pairs for Absorption Refrigeration Systems Composed of [HMIM][BF4] and Fluorinated Propanes. *International Journal of Refrigeration* **2019**, *104*, 34−41.
(43) Lepre, L. F.; Andre, D.; Denis-Quanquin, S.; Gautier, A.; Pádua, A. A. H.; Costa Gomes, M. Ionic Liquids Can Enable the Recycling of Fluorinated Greenhouse Gases. *ACS Sustain Chem. Eng.* **2019**, *7* (19), 16900−16906.
(44) Jacquemin, J.; Costa Gomes, M. F.; Husson, P.; Majer, V. Solubility of Carbon Dioxide, Ethane, Methane, Oxygen, Nitrogen, Hydrogen, Argon, and Carbon Monoxide in 1-Butyl-3-Methylimidazolium Tetrafluoroborate between Temperatures 283 and 343 K and at Pressures Close to Atmospheric. *J. Chem. Thermodyn* **2006**, *38* (4), 490−502.
(45) Shiflett, M. B.; Yokozeki, A. Solubilities and Diffusivities of Carbon Dioxide in Ionic Liquids: [Bmim][PF6] and [Bmim][BF4]. *Ind. Eng. Chem. Res.* **2005**, *44* (12), 4453−4464.
(46) Liu, X.; Qi, X.; Lv, N.; He, M. Gaseous Absorption of Fluorinated Ethanes by Ionic Liquids. *Fluid Phase Equilib.* **2015**, *405*, 1−6.
(47) Lepre, L. F.; Pison, L.; Otero, I.; Gautier, A.; Dévemy, J.; Husson, P.; Pádua, A. A. H.; Costa Gomes, M. Using Hydrogenated and Perfluorinated Gases to Probe the Interactions and Structure of Fluorinated Ionic Liquids. *Phys. Chem. Chem. Phys.* **2019**, *21* (17), 8865−8873.
(48) Shiflett, M. B.; Corbin, D. R.; Yokozeki, A. Comparison of the Sorption of Trifluoromethane (R-23) on Zeolites and in an Ionic Liquid. *Adsorpt. Sci. Technol.* **2013**, *31* (1), 59−83.
(49) Pison, L.; Canongia Lopes, J. N.; Rebelo, L. P. N.; Padua, A. A. H.; Costa Gomes, M. F. Interactions of Fluorinated Gases with Ionic Liquids: Solubility of CF4, C2F6, and C3F8 in Trihexyltetradecylphosphonium Bis(Trifluoromethylsulfonyl)Amide. *J. Phys. Chem. B* **2008**, *112* (39), 12394−12400.
(50) Liu, X.; Pan, P.; He, M. Vapor-Liquid Equilibrium and Diffusion Coefficients of R32 + [HMIM][FEP], R152a + [HMIM][FEP] and R161 + [HMIM][FEP]. *J. Mol. Liq.* **2018**, *253*, 28−35.
(51) Liu, X.; He, M.; Lv, N.; Qi, X.; Su, C. Solubilities of R-161 and R-143a in 1-Hexyl-3-Methylimidazolium Bis(Trifluoromethylsulfonyl)-Imide. *Fluid Phase Equilib.* **2015**, *388*, 37−42.

https://doi.org/10.1021/acs.chemrev.3c00276
Chem. Rev. XXXX, XXX, XXX−XXX

(52) Asensio-Delgado, J. M.; Asensio-Delgado, S.; Zarca, G.; Urtiaga, A. Analysis of Hybrid Compression Absorption Refrigeration Using Low-GWP HFC or HFO/Ionic Liquid Working Pairs. *International Journal of Refrigeration* **2022**, *134*, 232−241.
(53) Sosa, J. E.; Santiago, R.; Redondo, A. E.; Avila, J.; Lepre, L. F.; Gomes, M. C.; Araújo, J. M. M.; Palomar, J.; Pereiro, A. B. Design of Ionic Liquids for Fluorinated Gas Absorption: COSMO-RS Selection and Solubility Experiments. *Environ. Sci. Technol.* **2022**, *56* (9), 5898−5909.
(54) Liu, X.; Pan, P.; Yang, F.; He, M. Solubilities and Diffusivities of R227ea, R236fa and R245fa in 1-Hexyl-3-Methylimidazolium Bis-(Trifluoromethylsulfonyl)Imide. *J. Chem. Thermodyn* **2018**, *123*, 158−164.
(55) Shiflett, M. B.; Corbin, D. R.; Elliott, B. A.; Yokozeki, A. Sorption of Trifluoromethane in Zeolites and Ionic Liquid. *J. Chem. Thermodyn* **2013**, *64*, 40−49.
(56) Kumełan, J.; Kamps, A. P. S.; Tuma, D.; Yokozeki, A.; Shiflett, M. B.; Maurer, G. Solubility of Tetrafluoromethane in the Ionic Liquid [Hmim][Tf2N]. *J. Phys. Chem. B* **2008**, *112* (10), 3040−3047.
(57) Yokozeki, A.; Shiflett, M. B. Global Phase Behaviors of Trifluoromethane in Ionic Liquid [Bmim][PF6]. *AIChE J.* **2006**, *52* (11), 3952−3957.
(58) Shiflett, M. B.; Yokozeki, A. Gaseous Absorption of Fluoromethane, Fluoroethane, and 1,1,2,2-Tetrafluoroethane in 1-Butyl-3-Methylimidazolium Hexafluorophosphate. *Ind. Eng. Chem. Res.* **2006**, *45* (18), 6375−6382.
(59) Shiflett, M. B.; Harmer, M. A.; Junk, C. P.; Yokozeki, A. Solubility and Diffusivity of 1,1,1,2-Tetrafluoroethane in Room-Temperature Ionic Liquids. *Fluid Phase Equilib.* **2006**, *242* (2), 220−232.
(60) Shiflett, M. B.; Yokozeki, A. Phase Equilibria of Hydrofluorocarbon-4310mee Mixtures with Ionic Liquids: Miscibility of Threo- and Erythro-Diastereomers in Ionic Liquids. *Ind. Eng. Chem. Res.* **2008**, *47* (3), 926−934.
(61) Ahosseini, A.; Ren, W.; Weatherley, L. R.; Scurto, A. M. Viscosity and Self-Diffusivity of Ionic Liquids with Compressed Hydrofluorocarbons: 1-Hexyl-3-Methyl-Imidazolium Bis-(Trifluoromethylsulfonyl)Amide and 1,1,1,2-Tetrafluoroethane. *Fluid Phase Equilib.* **2017**, *437*, 34−42.
(62) Liu, X.; Ye, Z.; Bai, L.; He, M. Performance Comparison of Two Absorption-Compression Hybrid Refrigeration Systems Using R1234yf/Ionic Liquid as Working Pair. *Energy Convers Manag* **2019**, *181*, 319−330.
(63) Esaki, T.; Kobayashi, N. Experimental Absorption Solubility and Rate of Hydrofluoroolefin Refrigerant in Ionic Liquids for Absorption Chiller Cycles. *Chem. Eng. Res. Des.* **2021**, *171*, 340−348.
(64) Sun, Y.; Zhang, Y.; Wang, X.; Prausnitz, J. M.; Jin, L. Gaseous Absorption of 2,3,3,3-Tetrafluoroprop-1-Ene in Three Imidazolium-Based Ionic Liquids. *Fluid Phase Equilib.* **2017**, *450*, 65−74.
(65) Sun, Y.; Di, G.; Wang, J.; Hu, Y.; Wang, X.; He, M. Gaseous Solubility and Thermodynamic Performance of Absorption System Using R1234yf/IL Working Pairs. *Appl. Therm Eng.* **2020**, *172*, No. 115161.
(66) Liu, X.; Lv, N.; Su, C.; He, M. Solubilities of R32, R245fa, R227ea and R236fa in a Phosphonium-Based Ionic Liquid. *J. Mol. Liq.* **2016**, *218*, 525−530.
(67) Liu, X.; He, M.; Lv, N.; Qi, X.; Su, C. Vapor-Liquid Equilibrium of Three Hydrofluorocarbons with [HMIM][Tf2N]. *J. Chem. Eng. Data* **2015**, *60* (5), 1354−1361.
(68) Asensio-Delgado, S.; Pardo, F.; Zarca, G.; Urtiaga, A. Enhanced Absorption Separation of Hydrofluorocarbon/Hydrofluoroolefin Refrigerant Blends Using Ionic Liquids. *Sep Purif Technol.* **2020**, *249*, No. 117136.
(69) Shiflett, M. B.; Harmer, M. A.; Junk, C. P.; Yokozeki, A. Solubility and Diffusivity of Difluoromethane in Room-Temperature Ionic Liquids. *J. Chem. Eng. Data* **2006**, *51* (2), 483−495.
(70) Sosa, J. E.; Ribeiro, R. P. P. L.; Castro, P. J.; Mota, J. P. B.; Araújo, J. M. M.; Pereiro, A. B. Absorption of Fluorinated Greenhouse Gases Using Fluorinated Ionic Liquids. *Ind. Eng. Chem. Res.* **2019**, *58* (45), 20769−20778.
(71) Shiflett, M. B.; Yokozeki, A. Solubility Differences of Halocarbon Isomers in Ionic Liquid [Emim][Tf 2N]. *J. Chem. Eng. Data* **2007**, *52* (5), 2007−2015.
(72) Shiflett, M. B.; Yokozeki, A. Binary Vapor-Liquid and Vapor-Liquid-Liquid Equilibria of Hydrofluorocarbons (HFC-125 and HFC-143a) and Hydrofluoroethers (HFE-125 and HFE-143a) with Ionic Liquid [Emim][Tf2N]. *J. Chem. Eng. Data* **2008**, *53* (2), 492−497.
(73) Jovell, D.; Gómez, S. B.; Zakrzewska, M. E.; Nunes, A. V. M.; Araujo, J. M. M.; Pereiro, A. B.; Llovell, F. Insight on the Solubility of R134a in Fluorinated Ionic Liquids and Deep Eutectic Solvents. *J. Chem. Eng. Data* **2020**, *65* (10), 4956−4969.
(74) Ren, W.; Scurto, A. M. Global Phase Behavior of Imidazolium Ionic Liquids and Compressed 1,1,1,2-Tetrafluoroethane (R-134a). *AIChE J.* **2009**, *55* (2), 486−493.
(75) Sun, Y.; Zhang, Y.; Di, G.; Wang, X.; Prausnitz, J. M.; Jin, L. Vapor-Liquid Equilibria for R1234ze(E) and Three Imidazolium-Based Ionic Liquids as Working Pairs in Absorption-Refrigeration Cycle. *J. Chem. Eng. Data* **2018**, *63* (8), 3053−3060.
(76) Zhang, Y.; Yin, J.; Wang, X. Vapor-Liquid Equilibrium of 2,3,3,3-Tetrafluoroprop-1-Ene with 1-Butyl-3-Methylimidazolium Hexafluorophosphate, 1-Hexyl-3-Methyl Imidazolium Hexafluorophosphate, and 1-Octyl-3-Methylimidazolium Hexafluorophosphate. *J. Mol. Liq.* **2018**, *260*, 203−208.
(77) Minnick, D. L.; Shiflett, M. B. Solubility and Diffusivity of Chlorodifluoromethane in Imidazolium Ionic Liquids: [Emim][Tf2N], [Bmim][BF4], [Bmim][PF6], and [Emim][TFES]. *Ind. Eng. Chem. Res.* **2019**, *58* (25), 11072−11081.
(78) Baca, K. R.; Olsen, G. M.; Matamoros Valenciano, L.; Bennett, M. G.; Haggard, D. M.; Befort, B. J.; Garciadiego, A.; Dowling, A. W.; Maginn, E. J.; Shiflett, M. B. Phase Equilibria and Diffusivities of HFC-32 and HFC-125 in Ionic Liquids for the Separation of R-410A. *ACS Sustain Chem. Eng.* **2022**, *10* (2), 816−830.
(79) Kato, R.; Krummen, M.; Gmehling, J. Measurement and Correlation of Vapor−Liquid Equilibria and Excess Enthalpies of Binary Systems Containing Ionic Liquids and Hydrocarbons. *Fluid Phase Equilib.* **2004**, *224* (1), 47−54.
(80) Wang, X.; Zhang, Y.; Wang, D.; Sun, Y. Phase Equilibria of Trans-1,3,3,3-Tetrafluoropropene with Three Imidazolium Ionic Liquids. *J. Chem. Eng. Data* **2017**, *62* (6), 1825−1831.
(81) Morais, A. R. C.; Harders, A. N.; Baca, K. R.; Olsen, G. M.; Befort, B. J.; Dowling, A. W.; Maginn, E. J.; Shiflett, M. B. Phase Equilibria, Diffusivities, and Equation of State Modeling of HFC-32 and HFC-125 in Imidazolium-Based Ionic Liquids for the Separation of R-410A. *Ind. Eng. Chem. Res.* **2020**, *59* (40), 18222−18235.
(82) Kamiaka, T.; Dang, C.; Hihara, E. Vapor-Liquid Equilibrium Measurements for Binary Mixtures of R1234yf with R32, R125, and R134a. *International Journal of Refrigeration* **2013**, *36* (3), 965−971.
(83) Liu, X.; Bai, L.; Liu, S.; He, M. Vapor−liquid Equilibrium of R1234yf/[HMIM][Tf2N] and R1234ze(E)/ [HMIM][Tf2N] Working Pairs for the Absorption Refrigeration Cycle. *J. Chem. Eng. Data* **2016**, *61* (11), 3952−3957.
(84) Carvalho, P. J.; Khan, I.; Morais, A.; Granjo, J. F. O.; Oliveira, N. M. C.; Santos, L. M. N. B. F.; Coutinho, J. A. P. A New Microebulliometer for the Measurement of the Vapor−Liquid Equilibrium of Ionic Liquid Systems. *Fluid Phase Equilib.* **2013**, *354*, 156−165.
(85) Asensio-Delgado, S.; Pardo, F.; Zarca, G.; Urtiaga, A. Vapor-Liquid Equilibria and Diffusion Coefficients of Difluoromethane, 1,1,1,2-Tetrafluoroethane, and 2,3,3,3-Tetrafluoropropene in Low-Viscosity Ionic Liquids. *J. Chem. Eng. Data* **2020**, *65* (9), 4242−4251.
(86) Sousa, J. M. M. V.; Granjo, J. F. O.; Queimada, A. J.; Ferreira, A. G. M.; Oliveira, N. M. C.; Fonseca, I. M. A. Solubilities of Hydrofluorocarbons in Ionic Liquids: Experimental and Modelling Study. *J. Chem. Thermodyn* **2014**, *73*, 36−43.
(87) Minnick, D. L.; Shiflett, M. B. Solubility and Diffusivity of Bromodifluoromethane (Halon-1201) in Imidazolium Ionic Liquids: [C2C1im][Tf2N], [C4C1im][BF4], and [C4C1im][PF6]. *J. Chem. Eng. Data* **2020**, *65* (7), 3277−3286.

https://doi.org/10.1021/acs.chemrev.3c00276
Chem. Rev. XXXX, XXX, XXX−XXX

(88) Shiflett, M. B.; Harmer, M. A.; Junk, C. P.; Yokozeki, A. Solubility and Diffusivity of Difluoromethane in Room-Temperature Ionic Liquids. *J. Chem. Eng. Data* **2006**, *51* (2), 483−495.
(89) Liu, X.; Nguyen, M. Q.; Xue, S.; Song, C.; He, M. Vapor−Liquid Equilibria and Inter-Diffusion Coefficients for Working Pairs for Absorption Refrigeration Systems Composed of [HMIM][BF4] and Fluorinated Propanes. *International Journal of Refrigeration* **2019**, *104*, 34−41.
(90) Shariati, A.; Peters, C. J. High-Pressure Phase Behavior of Systems with Ionic Liquids: Measurements and Modeling of the Binary System Fluoroform+1-Ethyl-3-Methylimidazolium Hexafluorophosphate. *J. Supercrit. Fluids* **2003**, *25* (2), 109−117.
(91) He, M.; Pan, P.; Yang, F.; Wang, T.; Liu, X. Gaseous Absorption of Trans-1-Chloro-3,3,3-Trifluoropropene in Three Immidazolium-Based Ionic Liquids. *J. Chem. Eng. Data* **2018**, *63* (5), 1780−1788.
(92) Sousa, J. M. M. V.; Granjo, J. F. O.; Queimada, A. J.; Ferreira, A. G. M.; Oliveira, N. M. C.; Fonseca, I. M. A. Solubility of Hydrofluorocarbons in Phosphonium-Based Ionic Liquids: Experimental and Modelling Study. *J. Chem. Thermodyn* **2014**, *79*, 184−191.
(93) Shiflett, M. B.; Yokozeki, A.; Knapp, J. P. Process for the Separation of Fluorocarbons Using Ionic Liquids. US796476082, 2011.
(94) Shiflett, M.; Yokozeki, A. Absorption Cycle Utilizing Ionic Liquid as Working Fluid. US8715521B2, 2014.
(95) Asensio-Delgado, S.; Pardo, F.; Zarca, G.; Urtiaga, A. Absorption Separation of Fluorinated Refrigerant Gases with Ionic Liquids: Equilibrium, Mass Transport, and Process Design. *Sep Purif Technol.* **2021**, *276*, No. 119363.
(96) Minnick, D. L.; Turnaoglu, T.; Rocha, M. A.; Shiflett, M. B. Review Article: Gas and Vapor Sorption Measurements Using Electronic Beam Balances. *Journal of Vacuum Science & Technology A: Vacuum, Surfaces, and Films* **2018**, *36* (5), 050801.
(97) Ren, W.; Scurto, A. M. Phase Equilibria of Imidazolium Ionic Liquids and the Refrigerant Gas, 1,1,1,2-Tetrafluoroethane (R-134a). *Fluid Phase Equilib.* **2009**, *286* (1), 1−7.
(98) Dong, L.; Zheng, D.; Sun, G.; Wu, X. Vapor-Liquid Equilibrium Measurements of Difluoromethane + [Emim]OTf, Difluoromethane + [Bmim]OTf, Difluoroethane + [Emim]OTf, and Difluoroethane + [Bmim]OTf Systems. *J. Chem. Eng. Data* **2011**, *56* (9), 3663−3668.
(99) Dong, L.; Zheng, D.; Wu, X. Working Pair Selection of Compression and Absorption Hybrid Cycles through Predicting the Activity Coefficients of Hydrofluorocarbon + Ionic Liquid Systems by the UNIFAC Model. *Ind. Eng. Chem. Res.* **2012**, *51* (12), 4741−4747.
(100) He, M.; Peng, S.; Liu, X.; Pan, P.; He, Y. Diffusion Coefficients and Henry's Constants of Hydrofluorocarbons in [HMIM][Tf_2N], [HMIM][TfO], and [HMIM][BF_4]. *J. Chem. Thermodyn* **2017**, *112*, 43−51.
(101) Yu, G.; Jiang, Y.; Lei, Z. Pentafluoroethane Dehydration with Ionic Liquids. *Ind. Eng. Chem. Res.* **2018**, *57* (36), 12225−12234.
(102) Baca, K. R.; Broom, D. P.; Roper, M. G.; Benham, M. J.; Shiflett, M. B. First Measurements for the Simultaneous Sorption of Difluoromethane and Pentafluoroethane Mixtures in Ionic Liquids Using the Integral Mass Balance Method. *Ind. Eng. Chem. Res.* **2022**, *61* (27), 9774−9784.
(103) Leslie, E. H.; Carr, A. R. Vapor Pressure of Organic Solutions And Application of Dühring's Rule to Calculation of Equilibrium Diagrams. *Ind. Eng. Chem.* **1925**, *17* (8), 810−817.
(104) Finberg, E. A.; Shiflett, M. B. Process Designs for Separating R-410A, R-404A, and R-407C Using Extractive Distillation and Ionic Liquid Entrainers. *Ind. Eng. Chem. Res.* **2021**, *60* (44), 16054−16067.
(105) Ren, W.; Scurto, A. M.; Shiflett, M. B.; Yokozeki, A. Phase Behavior and Equilibria of Ionic Liquids and Refrigerants: 1-Ethyl-3-Methyl-Imidazolium Bis(Trifluoromethylsulfonyl)Imide ([EMIm]-[Tf_2N]) and R-134a. *ACS Symp. Ser.* **2009**, *1006*, 112−128.
(106) van Konynenburg, P. H.; Scott, R. L. Critical Lines and Phase Equilibria in Binary van Der Waals Mixtures. *Philosophical Transactions of the Royal Society of London. Series A, Mathematical and Physical Sciences* **1980**, *298* (1442), 495−540.
(107) Shiflett, M. B.; Yokozeki, A. Hydrogen Substitution Effect on the Solubility of Perhalogenated Compounds in Ionic Liquid [Bmim][PF6]. *Fluid Phase Equilib.* **2007**, *259* (2), 210−217.
(108) Shiflett, M. B.; Elliott, B. A.; Yokozeki, A. Phase Behavior of Vinyl Fluoride in Room-Temperature Ionic Liquids [Emim][Tf_2N], [Bmim][$N(CN)_2$], [Bmpy][BF_4], [Bmim][HFPS] and [Omim]-[TFES]. *Fluid Phase Equilib.* **2012**, *316*, 147−155.
(109) Shiflett, M. B.; Yokozeki, A. Vapor - Liquid - Liquid Equilibria of Hydrofluorocarbons + 1-Butyl-3-Methylimidazolium Hexafluorophosphate. *J. Chem. Eng. Data* **2006**, *51* (5), 1931−1939.
(110) Shiflett, M. B.; Yokozeki, A. Vapor-Liquid-Liquid Equilibria of Pentafluoroethane and Ionic Liquid [Bmim][PF_6] Mixtures Studied with the Volumetric Method. *J. Phys. Chem. B* **2006**, *110* (29), 14436−14443.
(111) Bolz, A.; Deiters, U. K.; Peters, C. J.; De Loos, T. W. Nomenclature for Phase Diagrams with Particular Reference to Vapour-Liquid and Liquid-Liquid Equilibria (Technical Report). *Pure Appl. Chem.* **1998**, *70* (11), 2233−2258.
(112) Ren, W.; Scurto, A. M. High-Pressure Phase Equilibria with Compressed Gases. *Rev. Sci. Instrum.* **2007**, *78* (12), 125104.
(113) Shariati, A.; Gutkowski, K.; Peters, C. J. Comparison of the Phase Behavior of Some Selected Binary Systems with Ionic Liquids. *AIChE J.* **2005**, *51* (5), 1532−1540.
(114) Al-Barghouti, K. S.; Scurto, A. M. Thermal Conductivity of 1-Alkyl-3-Methylimidazolium [Tf_2N] Ionic Liquids and Compressed 1,1,1,2-Tetrafluoroethane (R-134a). *J. Chem. Eng. Data* **2022**, *67* (8), 1796−1809.
(115) Currás, M. R.; Costa Gomes, M. F.; Husson, P.; Padua, A. A. H.; Garcia, J. Calorimetric and Volumetric Study on Binary Mixtures 2,2,2-Trifluoroethanol + (1-Butyl-3-Methylimidazolium Tetrafluoroborate or 1-Ethyl-3-Methylimidazolium Tetrafluoroborate)†. *J. Chem. Eng. Data* **2010**, *55* (12), 5504−5512.
(116) Zhang, Y.; Wang, X.; Yin, J. Viscosity of Saturated Mixtures of 1-Hexyl-3-Methyl-Imidazolium Bis(Trifluoromethylsulfonyl)Amide with R600a and R152a. *J. Chem. Thermodyn* **2020**, *141*, No. 105970.
(117) Wang, N.; Zhang, Y.; Al-Barghouti, K. S.; Kore, R.; Scurto, A. M.; Maginn, E. J. Structure and Dynamics of Hydrofluorocarbon/Ionic Liquid Mixtures: An Experimental and Molecular Dynamics Study. *J. Phys. Chem. B* **2022**, *126* (41), 8309−8321.
(118) Zhang, Y.; Jia, X.; Wang, X. Experimental Investigation on the Viscosity of [Hmim][Tf_2N] Saturated with R1234ze(E) or R1234yf. *International Journal of Refrigeration* **2020**, *117*, 338−345.
(119) Currás, M. R.; Husson, P.; Pádua, A. A. H.; Costa Gomes, M. F.; García, J. High-Pressure Densities of 2,2,2-Trifluoroethanol + Ionic Liquid Mixtures Useful for Possible Applications in Absorption Cycles. *Ind. Eng. Chem. Res.* **2014**, *53* (26), 10791−10802.
(120) Fatima, U.; Riyazuddeen; Dhakal, P.; Shah, J. K. Comparative Study of Influence of Ethanol and 2,2,2-Trifluoroethanol on Thermophysical Properties of 1-Ethyl-3-Methylimidazolium Dicyanamide in Binary Mixtures: Experimental and MD Simulations. *J. Chem. Eng. Data* **2021**, *66* (1), 101−115.
(121) Salgado, J.; Regueira, T.; Lugo, L.; Vijande, J.; Fernández, J.; García, J. Density and Viscosity of Three (2,2,2-Trifluoroethanol + 1-Butyl-3-Methylimidazolium) Ionic Liquid Binary Systems. *J. Chem. Thermodyn* **2014**, *70*, 101−110.
(122) Currás, M. R.; Vijande, J.; Pinẽiro, M. M.; Lugo, L.; Salgado, J.; Garciẽa, J. Behavior of the Environmentally Compatible Absorbent 1-Butyl-3-Methylimidazolium Tetrafluoroborate with 2,2,2-Trifluoroethanol: Experimental Densities at High Pressures and Modeling of PVT and Phase Equilibria Behavior with PC-SAFT EoS. *Ind. Eng. Chem. Res.* **2011**, *50* (7), 4065−4076.
(123) Currás, M. R.; Mato, M. M.; Sánchez, P. B.; García, J. Experimental Densities of 2,2,2-Trifluoroethanol with 1-Butyl-3-Methylimidazolium Hexafluorophosphate at High Pressures and Modelling with PC-SAFT. *J. Chem. Thermodyn* **2017**, *113*, 29−40.
(124) Matsuda, T.; Mishima, Y.; Azizian, S.; Matsubara, H.; Takiue, T.; Aratono, M. Interfacial Tension and Wetting Behavior of Air/Oil/Ionic Liquid Systems. *Colloid Polym. Sci.* **2007**, *285* (14), 1601−1605.

https://doi.org/10.1021/acs.chemrev.3c00276
Chem. Rev. XXXX, XXX, XXX−XXX

(125) Kim, K. S.; Shin, B. K.; Lee, H.; Ziegler, F. Refractive Index and Heat Capacity of 1-Butyl-3-Methylimidazolium Bromide and 1-Butyl-3-Methylimidazolium Tetrafluoroborate, and Vapor Pressure of Binary Systems for 1-Butyl-3-Methylimidazolium Bromide + Trifluoroethanol and 1-Butyl-3-Methylimidazolium Tetrafluoroborate + Trifluoroethanol. *Fluid Phase Equilib.* **2004**, *218* (2), 215−220.
(126) Al-Barghouti, K. S.; Scurto, A. M. Thermal Conductivity of the Ionic Liquid [HMIm][Tf_2N] with Compressed Carbon Dioxide. *AIChE J.* **2022**, *68* (6), No. e17635.
(127) Aspen Plus. *Aspen Plus User Guide*; Cambridge, 2003.
(128) Taylor, R.; Krishna, R. *Multicomponent Mass Transfer*; John Wiley & Sons: 1993; Vol. *2*.
(129) Darken, L.; Diffusion, S. Mobility and Their Interrelation through Free Energy in Binary Metallic Systems. *Trans. AIME* **1984**, *175*, 184−201.
(130) Krishna, R.; Van Baten, J. M. The Darken Relation for Multicomponent Diffusion in Liquid Mixtures of Linear Alkanes: An Investigation Using Molecular Dynamics (MD) Simulations. *Ind. Eng. Chem. Res.* **2005**, *44* (17), 6939−6947.
(131) Liu, X.; Vlugt, T. J. H.; Bardow, A. Predictive Darken Equation for Maxwell-Stefan Diffusivities in Multicomponent Mixtures. *Ind. Eng. Chem. Res.* **2011**, *50* (17), 10350−10358.
(132) Tyrrell, H. J. V.; Harris, K. R. *Diffusion in Liquids: A Theoretical and Experimental Study*; Butterworth-Heinemann: 1984.
(133) Keskin, S.; Sholl, D. S. Efficient Methods for Screening of Metal Organic Framework Membranes for Gas Separations Using Atomically Detailed Models. *Langmuir* **2009**, *25* (19), 11786−11795.
(134) Katsumata, R.; Dulaney, A. R.; Kim, C. B.; Ellison, C. J. Glass Transition and Self-Diffusion of Unentangled Polymer Melts Nanoconfined by Different Interfaces. *Macromolecules* **2018**, *51* (19), 7509−7517.
(135) Assael, M. J.; Goodwin, A. R.; Vesovic, V.; Wakeham, W. A. In *Experimental Thermodynamics: Advances in Transport Properties of Fluids*; Assael, M. J., Ed.; Royal Society of Chemistry: 2014; Vol. *IX*.
(136) Suárez-Iglesias, O.; Medina, I.; Sanz, M. D. L. Á.; Pizarro, C.; Bueno, J. L. Self-Diffusion in Molecular Fluids and Noble Gases: Available Data. *J. Chem. Eng. Data* **2015**, *60* (10), 2757−2817.
(137) Arnold, W. A.; Hartman, T. G.; McQuillen, J. Chemical Characterization and Thermal Stressing Studies of Perfluorohexane Fluids for Space-Based Applications. *J. Spacecr. Rockets* **2012**, *44* (1), 94−101.
(138) Chapman, W. G.; Gubbins, K. E.; Jackson, G.; Radosz, M. New Reference Equation of State for Associating Liquids. *I.& E. C. Res.* **1990**, *29* (8), 1709−1721.
(139) Wang, J.; Chen, D.; Zhu, L. Integrated Working Fluids and Process Optimization for Refrigeration Systems Using Polar PC-SAFT. *I.& E. C. Res.* **2021**, *60* (48), 17640−17649.
(140) Alam, Md.S.; Jeong, J. H. Thermodynamic Properties and Critical Parameters of HFO-1123 and Its Binary Blends with HFC-32 and HFC-134a Using Molecular Simulations. *Int. J. Refrig.* **2019**, *104*, 311−320.
(141) Mountain, R. D.; Morrison, G. Molecular Dynamics Study of Liquid CCl_2F_2 and $CClHF_2$. *Mol. Phys.* **1988**, *64* (1), 91−95.
(142) Lísal, M.; Budinsky, R.; Vacek, V.; Aim, K. Vapor−Liquid Equilibria of Alternative Refrigerants by Molecular Dynamics Simulations. *Int. J. Thermophys.* **1999**, *20*, 163−174.
(143) Stoll, J.; Vrabec, J.; Hasse, H. A Set of Molecular Models for Carbon Monoxide and Halogenated Hydrocarbons. *J. Chem. Phys.* **2003**, *119* (21), 11396−11407.
(144) Fernández, G. A.; Vrabec, J.; Hasse, H. Shear Viscosity and Thermal Conductivity of Dipolar Real Fluids from Equilibrium Molecular Dynamics Simulation. *Cryog.* **2006**, *46* (10), 711−717.
(145) Lin, F.-Y.; MacKerell, A. D., Jr. Polarizable Empirical Force Field for Halogen-Containing Compounds Based on the Classical Drude Oscillator. *J. Chem. Theory Comput.* **2018**, *14* (2), 1083−1098.
(146) Lísal, M.; Vacek, V. Effective Potentials for Liquid Simulation of the Alternative Refrigerants HFC-134a (CF_3CH_2F) and HFC-125 (CF_3CHF_2). *Fluid Phase Equilib.* **1997**, *127* (1), 83−102.
(147) Budinský, R.; Vacek, V.; Lísal, M. Vapor−Liquid Equilibria of Alternative Refrigerants and Their Binaries by Molecular Simulations Employing the Reaction Gibbs Ensemble Monte Carlo Method. *Fluid Phase Equilib.* **2004**, *222−223*, 213−220.
(148) Potter, S. C.; Tildesley, D. J.; Burgess, A. N.; Rogers, S. C. A Transferable Potential Model for the Liquid-Vapour Equilibria of Fluoromethanes. *Mol. Phys.* **1997**, *92* (5), 825−834.
(149) Lísal, M.; Vacek, V. Molecular Dynamics Simulations of Fluorinated Ethanes. *Mol. Phys.* **1996**, *87* (1), 167−187.
(150) Higashi, B. S.; Takada, A. Molecular Dynamics Study of Liquid CH2F2 (HFC-32). *Mol. Phys.* **1997**, *92* (4), 641−650.
(151) Lísal, M.; Smith, W. R.; Aim, K. Direct Molecular-Level Monte Carlo Simulation of Joule—Thomson Processes. *Mol. Phys.* **2003**, *101* (18), 2875−2884.
(152) Tillner-Roth, R.; Yokozeki, A. An International Standard Equation of State for Difluoromethane (R-32) for Temperatures from the Triple Point at 136.34 to 435 K and Pressures up to 70 MPa. *J. Phys. Chem. Ref. Data* **1997**, *26* (6), 1273−1328.
(153) Fermeglia, M.; Ferrone, M.; Pricl, S. Development of an All-Atoms Force Field from Ab Initio Calculations for Alternative Refrigerants. *Fluid Phase Equilib.* **2003**, *210* (1), 105−116.
(154) Peguin, R. P. S.; Kamath, G.; Potoff, J. J.; da Rocha, S. R. P. All-Atom Force Field for the Prediction of Vapor-Liquid Equilibria and Interfacial Properties of HFA134a. *J. Phys. Chem. B* **2009**, *113* (1), 178−187.
(155) Smith, W. R.; Figueroa-Gerstenmaier, S.; Skvorova, M. Molecular Simulation for Thermodynamic Properties and Process Modeling of Refrigerants. *J. Chem. Eng. Data* **2014**, *59* (10), 3258−3271.
(156) Figueroa-Gerstenmaier, S.; Lísal, M.; Nezbeda, I.; Smith, W. R.; Trejos, V. M. Prediction of Isoenthalps, Joule−Thomson Coefficients and Joule−Thomson Inversion Curves of Refrigerants by Molecular Simulation. *Fluid Phase Equilib.* **2014**, *375*, 143−151.
(157) Yang, Z.; Gong, M.; Dong, X.; Li, X.; Wu, J. Molecular Modeling and Simulation of Vapor−Liquid Equilibrium of the Refrigerant R152a and Its Mixture R152a+R32. *Fluid Phase Equilib.* **2015**, *394*, 93−100.
(158) Befort, B. J.; DeFever, R. S.; Tow, G. M.; Dowling, A. W.; Maginn, E. J. Machine Learning Directed Optimization of Classical Molecular Modeling Force Fields. *J. Chem. Inf. Model.* **2021**, *61* (9), 4400−4414.
(159) Raabe, G. Molecular Simulation Studies on the Vapor−Liquid Phase Equilibria of Binary Mixtures of R-1234yf and R-1234ze(E) with R-32 and CO_2. *J. Chem. Eng. Data* **2013**, *58* (6), 1867−1873.
(160) Raabe, G. Molecular Dynamics Studies on Liquid-Phase Dynamics and Structures of Four Different Fluoropropenes and Their Binary Mixtures with R-32 and CO_2. *J. Phys. Chem. B* **2014**, *118* (1), 240−254.
(161) Wang, N.; Carlozo, M. N.; Marin-Rimoldi, E.; Befort, B. J.; Dowling, A. W.; Maginn, E. J. Machine Learning-Enabled Development of Accurate Force Fields for Refrigerants. *J. Chem. Theory Comput* **2023**, *19*, 4546.
(162) Raabe, G.; Maginn, E. J. Molecular Modeling of the Vapor-Liquid Equilibrium Properties of the Alternative Refrigerant 2,3,3,3-Tetrafluoro-1-Propene (HFO-1234yf). *J. Phys. Chem. Lett.* **2010**, *1* (1), 93−96.
(163) Raabe, G.; Maginn, E. J. A Force Field for 3,3,3-Fluoro-1-Propenes, Including HFO-1234yf. *J. Phys. Chem. B* **2010**, *114* (31), 10133−10142.
(164) Paulechka, E.; Kazakov, A.; Frenkel, M. Monte Carlo Simulation of Vapor−Liquid Equilibria for Perfluoropropane (R-218) and 2, 3, 3, 3-Tetrafluoropropene (R-1234yf). *Int. J. Thermophys.* **2010**, *31*, 462−474.
(165) Raabe, G. Molecular Modeling of Fluoropropene Refrigerants. *J. Phys. Chem. B* **2012**, *116* (19), 5744−5751.
(166) Raabe, G. Molecular Simulation Studies on the Vapor−Liquid Equilibria of the Cis- and Trans-HCFO-1233zd and the Cis- and Trans-HFO-1336mzz. *J. Chem. Eng. Data* **2015**, *60* (8), 2412−2419.

https://doi.org/10.1021/acs.chemrev.3c00276
Chem. Rev. XXXX, XXX, XXX−XXX

(167) Raabe, G. Molecular Simulation Studies on the Thermophysical Properties of the Refrigerant Blend R-445A. *J. Chem. Eng. Data* **2013**, *58* (12), 3470−3476.
(168) Raabe, G. Molecular Simulation Studies in Hydrofluoroolefine (HFO) Working Fluids and Their Blends. *Sci. Technol. Built Environ* **2016**, *22* (8), 1077−1089.
(169) Raabe, G. Molecular Simulation Studies on Refrigerants Past − Present − Future. *Fluid Phase Equilib.* **2019**, *485*, 190−198.
(170) Paulechka, E.; Kroenlein, K.; Kazakov, A.; Frenkel, M. A Systematic Approach for Development of an OPLS-Like Force Field and Its Application to Hydrofluorocarbons. *J. Phys. Chem. B* **2012**, *116* (49), 14389−14397.
(171) Zhang, N.; Hu, P.; Chen, L.; Zhi, L. Molecular Modeling of Vapor-Liquid Equilibrium Properties of HFC-161 and Its Mixture HFC-161+HFO-1234yf. *J. Mol. Liq.* **2020**, *306*, No. 112896.
(172) Cao, Y.; Liu, C.; Zhang, H.; Xu, X.; Li, Q. Thermal Decomposition of HFO-1234yf through ReaxFF Molecular Dynamics Simulation. *Appl. Therm. Eng.* **2017**, *126*, 330−338.
(173) Huo, E.; Liu, C.; Xu, X.; Dang, C. A ReaxFF-Based Molecular Dynamics Study of the Pyrolysis Mechanism of HFO-1336mzz(Z). *Int. J. Refrig.* **2017**, *83*, 118−130.
(174) Wang, N.; Zhang, Y.; Maginn, E. J. Molecular Dynamics Study of the Ionic Liquid 1-n-Hexyl-3-Methylimidazolium Tris-(Pentafluoroethyl)Trifluorophosphate ($[C_6C_1im][FAP]$): Force Field Development and the Effect of $[FAP]^-$ Isomer Content on Properties. *J. Ionic Liq.* **2022**, *2* (2), No. 100040.
(175) Zhang, Y.; Maginn, E. J. The Effect of C2 Substitution on Melting Point and Liquid Phase Dynamics of Imidazolium Based-Ionic Liquids: Insights from Molecular Dynamics Simulations. *Phys. Chem. Chem. Phys.* **2012**, *14* (35), 12157−12164.
(176) Liu, H.; Maginn, E.; Visser, A. E.; Bridges, N. J.; Fox, E. B. Thermal and Transport Properties of Six Ionic Liquids: An Experimental and Molecular Dynamics Study. *Ind. Eng. Chem. Res.* **2012**, *51* (21), 7242−7254.
(177) Annapureddy, H. V. R.; Kashyap, H. K.; De Biase, P. M.; Margulis, C. J. What Is the Origin of the Prepeak in the X-Ray Scattering of Imidazolium-Based Room-Temperature Ionic Liquids? *J. Phys. Chem. B* **2010**, *114* (50), 16838−16846.
(178) Raabe, G.; Köhler, J. Thermodynamical and Structural Properties of Imidazolium Based Ionic Liquids from Molecular Simulation. *J. Chem. Phys.* **2008**, *128* (15), 154509.
(179) Wang, T.; Liu, X.; Chu, J.; Shi, Y.; Li, J.; He, M. Molecular Dynamics Simulation of Diffusion and Interaction of [Bmim][Tf2N] + HFO-1234yf Mixture. *J. Mol. Liq.* **2020**, *312*, No. 113390.
(180) Asensio-Delgado, S.; Viar, M.; Pádua, A. A. H.; Zarca, G.; Urtiaga, A. Understanding the Molecular Features Controlling the Solubility Differences of R-134a, R-1234ze(E), and R-1234yf in 1-Alkyl-3-Methylimidazolium Tricyanomethanide Ionic Liquids. *ACS Sustainable Chem. Eng.* **2022**, *10* (46), 15124−15134.
(181) Wang, N.; DeFever, R. S.; Maginn, E. J. Alchemical Free Energy and Hamiltonian Replica Exchange Molecular Dynamics to Compute Hydrofluorocarbon Isotherms in Imidazolium-Based Ionic Liquids. *J. Chem. Theory Comput* **2023**, *19*, 3324.
(182) Vega, L. F.; Vilaseca, O.; Llovell, F.; Andreu, J. S. Modeling Ionic Liquids and the Solubility of Gases in Them: Recent Advances and Perspectives. *Fluid Phase Equilib.* **2010**, *294* (1), 15−30.
(183) Prausnitz, J. M.; Lichtenthaler, R. N.; de Azevedo, E. G. *Molecular Thermodynamics of Fluid-Phase Equilibria*; Pearson Education: 1998.
(184) Krichevsky, I. R.; Kasarnovsky, J. S. Thermodynamical Calculations of Solubilities of Nitrogen and Hydrogen in Water at High Pressures. *J. Am. Chem. Soc.* **1935**, *57* (11), 2168−2171.
(185) Lemmon, E. W.; Bell, I. H.; Huber, M. L.; McLinden, M. O. *NIST Standard Reference Database 23: Reference Fluid Thermodynamic and Transport Properties-REFPROP, Version 10.0*; National Institute of Standards and Technology: 2018. DOI: 10.18434/T4/1502528.
(186) Kim, Y. J.; Kim, S.; Joshi, Y. K.; Fedorov, A. G.; Kohl, P. A. Thermodynamic Analysis of an Absorption Refrigeration System with Ionic-Liquid/Refrigerant Mixture as a Working Fluid. *Energy* **2012**, *44* (1), 1005−1016.
(187) Wu, W.; You, T.; Zhang, H.; Li, X. Comparisons of Different Ionic Liquids Combined with Trans-1,3,3,3-Tetrafluoropropene (R1234ze(E)) as Absorption Working Fluids. *Int. J. Refrig.* **2018**, *88*, 45−57.
(188) Bai, L.; He, M.; Liu, X.; Ye, Z. A New Activity Coefficient Model for the Solution of Molecular Solute + Ionic Liquid. *Fluid Phase Equilib.* **2019**, *493*, 144−152.
(189) Hekayati, J.; Roosta, A.; Javanmardi, J. Thermodynamic Modeling of Refrigerants Solubility in Ionic Liquids Using Original and E*-Modified Sanchez-Lacombe Equations of State. *Fluid Phase Equilib.* **2015**, *403*, 14−22.
(190) Kim, S.; Kohl, P. A. Analysis of $[Hmim][PF_6]$ and $[Hmim][Tf_2N]$ Ionic Liquids as Absorbents for an Absorption Refrigeration System. *Int. J. Refrig.* **2014**, *48*, 105−113.
(191) Kim, S.; Patel, N.; Kohl, P. A. Performance Simulation of Ionic Liquid and Hydrofluorocarbon Working Fluids for an Absorption Refrigeration System. *Ind. Eng. Chem. Res.* **2013**, *52* (19), 6329−6335.
(192) Faúndez, C. A.; Barrientos, L. A.; Valderrama, J. O. Modeling and Thermodynamic Consistency of Solubility Data of Refrigerants in Ionic Liquids. *Int. J. Refrig.* **2013**, *36* (8), 2242−2250.
(193) Albà, C. G.; Vega, L. F.; Llovell, F. Assessment on Separating Hydrofluoroolefins from Hydrofluorocarbons at the Azeotropic Mixture R513A by Using Fluorinated Ionic Liquids: A Soft-SAFT Study. *Ind. Eng. Chem. Res.* **2020**, *59* (29), 13315−13324.
(194) Asensio-Delgado, S.; Pardo, F.; Zarca, G.; Urtiaga, A. Machine Learning for Predicting the Solubility of High-GWP Fluorinated Refrigerants in Ionic Liquids. *J. Mol. Liq.* **2022**, *367*, 120472.
(195) Yokozeki, A.; Shiflett, M. B. Gas Solubilities in Ionic Liquids Using a Generic van Der Waals Equation of State. *J. Supercrit. Fluids* **2010**, *55* (2), 846−851.
(196) Smith, R. W.; Maginn, E. J. Rapid Screening of Gas Solubility in Ionic Liquids Using Biased Particle Insertions with Pre-Sampled Liquid Trajectories. *Mol. Simul* **2024**, *50*, 26.
(197) Asensio-Delgado, S.; Jovell, D.; Zarca, G.; Urtiaga, A.; Llovell, F. Thermodynamic and Process Modeling of the Recovery of R410A Compounds with Ionic Liquids. *International Journal of Refrigeration* **2020**, *118*, 365−375.
(198) Jovell, D.; Pou, J. O.; Llovell, F.; Gonzalez-Olmos, R. Life Cycle Assessment of the Separation and Recycling of Fluorinated Gases Using Ionic Liquids in a Circular Economy Framework. *ACS Sustain Chem. Eng.* **2022**, *10* (1), 71−80.
(199) Monjur, M. S.; Iftakher, A.; Hasan, M. M. F. Separation Process Synthesis for High-GWP Refrigerant Mixtures: Extractive Distillation Using Ionic Liquids. *Ind. Eng. Chem. Res.* **2022**, *61* (12), 4390−4406.
(200) Shiflett, M.; Yokozeki, A. Separation of Difluoromethane and Pentafluoroethane by Extractive Distillation Using Ionic Liquid. *Chim. Oggi* **2006**, *24*, 28−30.
(201) Valderrama, J. O.; Rojas, R. E. Critical Properties of Ionic Liquids. *Revisited. Ind. Eng. Chem. Res.* **2009**, *48* (14), 6890−6900.
(202) Valderrama, J. O.; Robles, P. A. Critical Properties, Normal Boiling Temperatures, and Acentric Factors of Fifty Ionic Liquids. *Ind. Eng. Chem. Res.* **2007**, *46* (4), 1338−1344.
(203) Valderrama, J. O.; Toro, A.; Rojas, R. E. Prediction of the Heat Capacity of Ionic Liquids Using the Mass Connectivity Index and a Group Contribution Method. *J. Chem. Thermodyn* **2011**, *43* (7), 1068−1073.
(204) Wu, B.; Dai, C.; Chen, B.; Yu, G.; Liu, N.; Xu, R. Ionic Liquid versus Traditional Volatile Organic Solvent in the Natural Gas Dehydration Process: A Comparison from a Life Cycle Perspective. *ACS Sustain Chem. Eng.* **2019**, *7* (23), 19194−19201.
(205) Yuichi, I.; Ji, H.; Cho, O. Method of Producing Difluoromethane. US20040102659A1, February 24, 2003.
(206) Sosa, J. E.; Santiago, R.; Hospital-Benito, D.; Costa Gomes, M.; Araújo, J. M. M.; Pereiro, A. B.; Palomar, J. Process Evaluation of Fluorinated Ionic Liquids as F-Gas Absorbents. *Environ. Sci. Technol.* **2020**, *54* (19), 12784−12794.

https://doi.org/10.1021/acs.chemrev.3c00276
Chem. Rev. XXXX, XXX, XXX−XXX

(207) Jovell, D.; Gómez, S. B.; Zakrzewska, M. E.; Nunes, A. V. M.; Araujo, J. M. M.; Pereiro, A. B.; Llovell, F. Insight on the Solubility of R134a in Fluorinated Ionic Liquids and Deep Eutectic Solvents. *J. Chem. Eng. Data* **2020**, *65* (10), 4956−4969.
(208) Vilaseca, O.; Llovell, F.; Yustos, J.; Marcos, R. M.; Vega, L. F. Phase Equilibria, Surface Tensions and Heat Capacities of Hydrofluorocarbons and Their Mixtures Including the Critical Region. *J. Supercrit. Fluids* **2010**, *55* (2), 755−768.
(209) Llovell, F.; Marcos, R. M.; Vega, L. F. Transport Properties of Mixtures by the Soft-SAFT + Free-Volume Theory: Application to Mixtures of n-Alkanes and Hydrofluorocarbons. *J. Phys. Chem. B* **2013**, *117* (17), 5195−5205.
(210) Albà, C. G.; Vega, L. F.; Llovell, F. A Consistent Thermodynamic Molecular Model of N-Hydrofluoroolefins and Blends for Refrigeration Applications. *International Journal of Refrigeration* **2020**, *113*, 145−155.
(211) Yan, X.; Anguille, S.; Bendahan, M.; Moulin, P. Ionic Liquids Combined with Membrane Separation Processes: A Review. *Sep Purif Technol.* **2019**, *222*, 230−253.
(212) Ahmad, N. N. R.; Leo, C. P.; Ahmad, A. L. Effects of Solvent and Ionic Liquid Properties on Ionic Liquid Enhanced Polysulfone/SAPO-34 Mixed Matrix Membrane for CO_2 Removal. *Microporous Mesoporous Mater.* **2019**, *283*, 64−72.
(213) Thorat, G. B.; Gupta, S.; Murthy, Z. V. P. Synthesis, Characterization and Application of PVA/Ionic Liquid Mixed Matrix Membranes for Pervaporation Dehydration of Isopropanol. *Chin J. Chem. Eng.* **2017**, *25* (10), 1402−1411.
(214) Bhattacharya, M.; Mandal, M. K. Synthesis and Characterization of Ionic Liquid Based Mixed Matrix Membrane for Acid Gas Separation. *J. Clean Prod* **2017**, *156*, 174−183.
(215) Pardo, F.; Gutiérrez-Hernández, S. V.; Hermida-Merino, C.; Araújo, J. M. M.; Piñeiro, M. M.; Pereiro, A. B.; Zarca, G.; Urtiaga, A. Integration of Stable Ionic Liquid-Based Nanofluids into Polymer Membranes. Part II: Gas Separation Properties toward Fluorinated Greenhouse Gases. *Nanomaterials 2021, Vol. 11, Page 582* **2021**, *11* (3), 582.
(216) Pardo, F.; Zarca, G.; Urtiaga, A. Effect of Feed Pressure and Long-Term Separation Performance of Pebax-Ionic Liquid Membranes for the Recovery of Difluoromethane (R32) from Refrigerant Mixture R410A. *J. Membr. Sci.* **2021**, *618*, 118744.
(217) Pardo, F.; Gutiérrez-Hernández, S. V.; Zarca, G.; Urtiaga, A. Toward the Recycling of Low-GWP Hydrofluorocarbon/Hydrofluoroolefin Refrigerant Mixtures Using Composite Ionic Liquid-Polymer Membranes. *ACS Sustain Chem. Eng.* **2021**, *9* (20), 7012−7021.
(218) Lian, S.; Song, C.; Liu, Q.; Duan, E.; Ren, H.; Kitamura, Y. Recent Advances in Ionic Liquids-Based Hybrid Processes for CO(2) Capture and Utilization. *J. Environ. Sci. (China)* **2021**, *99*, 281−295.
(219) Cota, I.; Fernandez Martinez, F. Recent Advances in the Synthesis and Applications of Metal Organic Frameworks Doped with Ionic Liquids for CO_2 Adsorption. *Coord. Chem. Rev.* **2017**, *351*, 189−204.
(220) Yin, M.; Wang, L.; Tang, S. Amino-Functionalized Ionic-Liquid-Grafted Covalent Organic Frameworks for High-Efficiency CO(2) Capture and Conversion. *ACS Appl. Mater. Interfaces* **2022**, *14* (50), 55674−55685.
(221) Philip, F. A.; Henni, A. Enhancement of Post-Combustion CO2 Capture Capacity by Incorporation of Task-Specific Ionic Liquid into ZIF-8. *Microporous Mesoporous Mater.* **2022**, *330*, 111580.
(222) Olajire, A. A. Synthesis of Bare and Functionalized Porous Adsorbent Materials for CO2capture. *Greenhouse Gases: Science and Technology* **2017**, *7* (3), 399−459.
(223) Zheng, S.; Xu, Q.; Zeng, S.; Li, G.; Jiang, H.; Sun, X.; Zhang, X. Porous Multi-Site Ionic Liquid Composites for Superior Selective and Reversible Adsorption of Ammonia. *Sep Purif Technol.* **2023**, *310*, 123161.
(224) Kaur, P.; Chopra, H. K. SBA-15 Supported Benzoxazolium-Based Ionic Liquids: Synthesis, Characterization, and Application in the Adsorptive Desulfurization. *Fuel Process. Technol.* **2022**, *238*, 107480.
(225) Kaur, P.; Kumar Chopra, H. MCM-41 Supported S-Alkyl/Aryl-Substituted 2-Mercaptobenzothiazolium-Based Ionic Liquids: Synthesis, Characterization, and Application in the Fuel Desulfurization. *Fuel* **2023**, *332*, 126009.
(226) Wu, H.; Kudo, T.; Kim, S.-Y.; Miwa, M.; Matsuyama, S. Recovery of Cesium Ions from Seawater Using a Porous Silica-Based Ionic Liquid Impregnated Adsorbent. *Nuclear Engineering and Technology* **2022**, *54* (5), 1597−1605.
(227) Zare, E. N.; Mudhoo, A.; Khan, M. A.; Otero, M.; Bundhoo, Z. M. A.; Navarathna, C.; Patel, M.; Srivastava, A.; Pittman, C. U.; Mlsna, T.; Mohan, D.; Makvandi, P.; Sillanpää, M. Water Decontamination Using Bio-Based, Chemically Functionalized, Doped, and Ionic Liquid-Enhanced Adsorbents: Review. *Environ. Chem. Lett.* **2021**, *19* (4), 3075−3114.
(228) Dong, Q.; Min, X.; Huo, J.; Wang, Y. Efficient Sorption of Perfluoroalkyl Acids by Ionic Liquid-Modified Natural Clay. *Chemical Engineering Journal Advances* **2021**, *7*, 100135.
(229) Yagnamurthy, S.; Rakshit, D.; Jain, S.; Saha, B. B. Compact Heat Exchanger Designs for Difluoromethane-Activated Carbon Composites Based Adsorption Cooling Systems. *International Communications in Heat and Mass Transfer* **2023**, *140*, 106549.
(230) Yagnamurthy, S.; Rakshit, D.; Jain, S.; Rocky, K. A.; Islam, M. A.; Saha, B. B. Adsorption of Difluoromethane onto Activated Carbon Based Composites: Adsorption Kinetics, Heat of Adsorption, Cooling Performance and Irreversibility Evaluation. *Appl. Therm Eng.* **2022**, *210*, 118359.
(231) Yagnamurthy, S.; Rakshit, D.; Jain, S.; Rocky, K. A.; Islam, M. A.; Saha, B. B. Adsorption of Difluoromethane onto Activated Carbon Based Composites: Thermophysical Properties and Adsorption Characterization. *Int. J. Heat Mass Transf* **2021**, *171*, 121112.
(232) Sosa, J. E.; Ribeiro, R. P. P. L.; Castro, P. J.; Mota, J. P. B.; Pereiro, A. B.; Araújo, J. M. M. Sorption of Fluorinated Greenhouse Gases in Silica-Supported Fluorinated Ionic Liquids. *J. Environ. Chem. Eng.* **2022**, *10* (6), 108580.
(233) Askalany, A. A.; Saha, B. B.; Uddin, K.; Miyzaki, T.; Koyama, S.; Srinivasan, K.; Ismail, I. M. Adsorption Isotherms and Heat of Adsorption of Difluoromethane on Activated Carbons. *J. Chem. Eng. Data* **2013**, *58* (10), 2828−2834.
(234) Askalany, A. A.; Saha, B. B. Experimental and Theoretical Study of Adsorption Kinetics of Difluoromethane onto Activated Carbons. *International Journal of Refrigeration* **2015**, *49*, 160−168.
(235) Riisager, A.; Fehrmann, R.; Haumann, M.; Wasserscheid, P. Supported Ionic Liquids: Versatile Reaction and Separation Media. *Top Catal* **2006**, *40* (1−4), 91−102.
(236) Lemus, J.; Palomar, J.; Gilarranz, M. A.; Rodriguez, J. J. Characterization of Supported Ionic Liquid Phase (SILP) Materials Prepared from Different Supports. *Adsorption* **2011**, *17* (3), 561−571.
(237) Zeng, S.; Wang, J.; Li, P.; Dong, H.; Wang, H.; Zhang, X.; Zhang, X. Efficient Adsorption of Ammonia by Incorporation of Metal Ionic Liquids into Silica Gels as Mesoporous Composites. *Chemical Engineering Journal* **2019**, *370*, 81−88.
(238) Riisager, A.; Fehrmann, R.; Haumann, M.; Wasserscheid, P. Supported Ionic Liquid Phase (SILP) Catalysis: An Innovative Concept for Homogeneous Catalysis in Continuous Fixed-Bed Reactors. *Eur. J. Inorg. Chem.* **2006**, *2006* (4), 695−706.
(239) Zarca, G.; Ortiz, I.; Urtiaga, A. Facilitated-Transport Supported Ionic Liquid Membranes for the Simultaneous Recovery of Hydrogen and Carbon Monoxide from Nitrogen-Enriched Gas Mixtures. *Chem. Eng. Res. Des.* **2014**, *92* (4), 764−768.
(240) Zarca, G.; Ortiz, I.; Urtiaga, A. Copper(I)-Containing Supported Ionic Liquid Membranes for Carbon Monoxide/Nitrogen Separation. *J. Membr. Sci.* **2013**, *438*, 38−45.
(241) Yan, J.; Mangolini, F. Engineering Encapsulated Ionic Liquids for Next-Generation Applications. *RSC Adv.* **2021**, *11* (57), 36273−36288.
(242) Lemus, J.; Bedia, J.; Moya, C.; Alonso-Morales, N.; Gilarranz, M. A.; Palomar, J.; Rodriguez, J. J. Ammonia Capture from the Gas Phase by Encapsulated Ionic Liquids (ENILs). *RSC Adv.* **2016**, *6* (66), 61650−61660.

https://doi.org/10.1021/acs.chemrev.3c00276
Chem. Rev. XXXX, XXX, XXX−XXX

(243) Lemus, J.; Da Silva, F. A.; Palomar, J.; Carvalho, P. J.; Coutinho, J. A.P. Solubility of carbon dioxide in encapsulated ionic liquids. *Sep Purif Technol.* **2018**, *196*, 41−46.
(244) Palomar, J.; Lemus, J.; Alonso-Morales, N.; Bedia, J.; Gilarranz, M. A.; Rodriguez, J. J. Encapsulated Ionic Liquids (ENILs): From Continuous to Discrete Liquid Phase. *Chem. Commun.* **2012**, *48* (80), 10046−10048.
(245) Song, T.; Avelar Bonilla, G. M.; Morales-Collazo, O.; Lubben, M. J.; Brennecke, J. F. Recyclability of Encapsulated Ionic Liquids for Post-Combustion CO_2 Capture. *Ind. Eng. Chem. Res.* **2019**, *58* (12), 4997−5007.
(246) Luo, Q.; Pentzer, E. Encapsulation of Ionic Liquids for Tailored Applications. *ACS Appl. Mater. Interfaces* **2020**, *12* (5), 5169−5176.
(247) Santiago, R.; Lemus, J.; Moya, C.; Moreno, D.; Alonso-Morales, N.; Palomar, J. Encapsulated Ionic Liquids to Enable the Practical Application of Amino Acid-Based Ionic Liquids in CO_2 Capture. *ACS Sustain Chem. Eng.* **2018**, *6* (11), 14178−14187.
(248) Lemus, J.; Paramio, C.; Hospital-Benito, D.; Moya, C.; Santiago, R.; Palomar, J. Selective CO2/CH4Separation by Fixed-Bed Technology Using Encapsulated Ionic Liquids. *ACS Sustain Chem. Eng.* **2022**, *10* (42), 13917−13926.
(249) Luo, Q.; Wang, Y.; Chen, Z.; Wei, P.; Yoo, E.; Pentzer, E. Pickering Emulsion-Templated Encapsulation of Ionic Liquids for Contaminant Removal. *ACS Appl. Mater. Interfaces* **2019**, *11* (9), 9612−9620.
(250) Yu, T.; Cai, Q.; Lian, G.; Bai, Y.; Zhang, X.; Zhang, X.; Liu, L.; Zhang, S. Mechanisms behind High CO2/CH4 Selectivity Using ZIF-8 Metal Organic Frameworks with Encapsulated Ionic Liquids: A Computational Study. *Chemical Engineering Journal* **2021**, *419*, 129638.
(251) Baca, K. R.; Harders, A. N.; Starvaggi, N.; Yancey, A. D.; Wang, Y.; Pentzer, E.; Shiflett, M. B. First Measurements of the Sorption of Difluoromethane and Pentafluoroethane in Encapsulated Ionic Liquids. *Ind. Eng. Chem. Res.* **2023**, *62* (36), 14522−14536.
(252) Skarmoutsos, I.; Hunt, P. A. Structural and Dynamic Properties of the New Alternative Refrigerant 2,3,3,3-Tetrafluoro-1-propene (HFO-1234yf) in the Liquid State. *J. Phys. Chem. B* **2010**, *114* (51), 17120−17127.
(253) Wang, N.; Maginn, E. J. GAFF-Based Polarizable Force Field Development and Validation for Ionic Liquids. *J. Phys. Chem. B* **2024**, *128* (3), 871−881.

https://doi.org/10.1021/acs.chemrev.3c00276
Chem. Rev. XXXX, XXX, XXX−XXX